COMPUTATIONAL MODELLING OF THE ELECTRONIC AND STRUCTURAL PROPERTIES OF CHALCOPYRITE-TYPE SEMICONDUCTORS AND PLATINUM GROUP METAL CHALCOGENIDES

By

Dennis Silungwe

A dissertation submitted in partial fulfillment of the requirements for the degree of Master of Science in Physics

The University of Zambia

2016

I solemnly declare that this dissertation represents original work which has not been submitted for a degree at this or any other university.

Signature: ……

ABSTRACT

An important aspect in the development of semiconducting devices for use in photovoltaic systems is the design of materials with appropriate band gaps. Electronic structure calculations based on Density Functional Theory (DFT) have been extensively used to study and to describe such properties of many condensed matter systems.

In this work, we have utilized DFT to study the electronic properties of eight chalcopyrite-type semiconductors which are transition-metal type and hence are strongly correlated materials.

For our chosen systems we first used the Local Density Approximation (LDA) and Generalized Gradient Approximation (GGA) energy exchange correlation functionals within DFT as implemented in the Quantum Espresso (QE) computer simulation package.

The results from these two functionals predicted band gaps which were greatly underestimated and thus predicted metallic behaviour for some of the materials.

These materials are termed as strongly correlated because they have incompletely filled d or f-orbitals and valence electrons in these materials have a complex influence on their neighbours.

To circumvent this challenge the DFT+U method, which uses orbital-dependent potentials, is applied. With the application of the DFT+U method the results obtained were a great improvement over those obtained by LDA and GGA. An empirical shift method was also employed.

Dedication

This work is dedicated to my girl Zevyanji C Nalungwe and my boy, Wanjivwa E Silungwe for sharing with me their childlike love and passion

ACKNOWLEDGEMENT

I wish to express my sincere gratitude to my supervisors Prof. R. O. Manyala and Dr. A. Habanyama for their guidance, encouragement and support throughout my M.Sc. dissertation work. It is not possible to completely list everything I got from them. I, however, must say that their knowledge, technical skills and human qualities have been a source of inspiration to me. Working with them has really been a very pleasant and memorable experience.

I gratefully thank my lecturers, Prof. P. N. Kaloyerou, Dr. H. V. Mweene, Dr. S. A. Hatwaambo and Dr. K. Hansingo for their patience with me during the challenging moments of the course and their commitment to work.

My special loving thanks go to my wife, Bwalya L. Y. Kaniki, who stood by me through testing times and provided me great moral and emotional courage. It would have been impossible to pursue my research work without her encouragement and support.

My special thanks to my course mates, Mbayoni Mwansa and Shupe Siame for all their kindness and constant encouragement during the rough times of the course and for providing light moments on those occasions.

I am also very grateful to my sponsors, the Solar Energy Materials Project, in the Department of Physics at the University of Zambia. Without their financial support this work would not have been possible.

May I also express my most special thanks to the Department of Physics at the University of Swaziland for affording me a unique opportunity to do part of my research using departmental computer software and hardware.

Certificate of Approval

This is to certify that this dissertation entitled: **COMPUTATIONAL MODELLING OF THE ELECTRONIC AND STRUCTURAL PROPERTIES OF CHALCOPYRITE-TYPE SEMICONDUCTORS AND PLATINUM GROUP METAL CHALCOGENIDES** carried out by **DENNIS SILUNGWE** has been approved as fulfilling in part the requirement for the award of the degree of Master of Science in Physics.

Signed: Date:

…… …….

…… ……..

…… ……..

TABLE OF CONTENTS

LIST OF FIGURES

CHAPTER 1 INTRODUCTION

Energy is one of the most important topics currently under discussion in the global community. Most of the energy supplied to the general public has its origin in fossil fuels and nuclear power. Indefinable risks as in the case of Japan's Fukushima Nuclear Power Plant disaster [57] come to mind when one thinks of nuclear energy supply. The radioactive repository problem of the nuclear power as well as the fast rate of depletion and global scarcity of fossil resources and their negative environmental effects have caused renewable energies to grow more important for achieving sustainability.

Currently, the main sources of renewable energy are wind, hydroelectric and solar. Solar energy relies on the efficiency of the photovoltaic cells. Different materials are competing as part of a variety of technologies on the photovoltaic (PV) market. At the moment, the largest contribution still comes from the wafer based crystalline silicon solar cells, accounting for about 95%, whereas the thin film solar cells only make a relatively small contribution to the general PV market although large capacities are now under construction. The application of PV systems on large and economical scales has been greatly constrained by the cost of production and their relatively low efficiencies [49]. A lot of research is going on in the field of thin film PVs because they show a number of advantages as compared to the wafer based solar cells. The two major advantages are economical use of material and production cost reduction [49]. This is because the thin film PVs do not use large quantities of material and in some cases the materials are more abundant, hence lowering the cost per unit PV cell.

Among the materials that have attracted considerable interest for use as optical absorbers in PV systems and in optoelectronic devices are the ternary chalcopyrites for the following reasons:

a. Good direct wide band gap of about 1.68 eV, which has been found to match the optimum value for terrestrial applications which is 1.5 eV, and allows for absorption of a large part of the solar spectrum. This property enables them to find application for efficient conversion of solar energy into electricity;
b. Extra-ordinary radiation hardness (the resistance of an electronic component to ionizing radiation and high-energy electronic radiations such as those encountered in outer space), because of which they can be utilized in space work;
c. Good theoretical efficiencies exceeding 25% for single junction cells;
d. Very large optical absorption coefficient for visible light of about $10^4 cm^{-1}$;
e. Ability to form electronically inactive defect complexes which enable these materials to withstand foreign impurities and deviations from ideal stoichiometry [1]**.**

Over the past several years much research has been devoted to trying to understand the efficiency limiting factors of solar cell devices fabricated from these compounds. Among the thin film solar cells in use today, PV devices built on ternary chalcopyrites have reached the highest known efficiencies and they continue to move on to being more economical to produce [2]. In the recent past, copper gallium di-sulphide ($CuGaS_2$) has caught the eye of researchers because the material has a direct energy band gap which lies in the range suitable for application in solid state lighting and high efficiency tandem

solar cells [3]. A solid state solution between the chalcopyrite-type semi-conductors of copper indium di-selenide, $CuInSe_2$ and copper gallium di-selenide, $CuGaSe_2$ with 28% gallium/gallium-indium (Ga/Ga-In) produces the highest achieved efficiency in thin film solar cells technology with values exceeding 20% in the laboratory [4]. The copper indium/gallium di-selenide, $Cu(In\text{-}Ga)Se_2$, or CIGS thin-film solar cell technology seems to be the technology best suited to compete with the current silicon based solar cell technology. This is as a result of the excellent optical and structural properties of CIGS, which have good stability under various operating conditions [3]. The incorporation of Ga into an absorber layer of materials improves different absorber properties by increasing the energy band gap *E*g, a process which enhances the absorption of light as well as the electrical properties of the absorber layer and the resultant solar cell [5].

Great interest was generated in the field of solar cells built on ternary chalcopyrites when one was produced with these compounds as absorbers and producing an efficiency of about 10% [6]. Currently, much research is devoted to trying to understand the properties of these materials and finding more suitable chalcopyrites with greater direct band gaps, which enhances their application in opto-electronic devices, light emitting diodes (LEDs) and other PV systems. Some researchers are trying to find chalcopyrite-type semiconducting materials with aluminium (Al) replacing Ga or In in the $I\text{-}III\text{-}VI_2$ type of chalcopyrites because Al is much more abundant than Ga and In [53]. This is an advantage where there is need to produce PV systems on a large scale.

Chalcopyrite is a copper iron di-sulphide ($CuFeS_2$) mineral that crystallizes in the tetragonal structure; compounds such as $CuInS_2$ (copper indium di-sulphide) have what is referred to as the chalcopyrite-type crystal structure. A tetragonal structure is formed

when the average number of valence electrons per atom equals four, according to the Grimm-Sommerfeld rule [2].

The chalcopyrites studied in this work are of the zinc-blende (diamond-like) structure. Most of these ternary chalcopyrites have been found to belong to I-III-VI_2 and II-IV-V_2 groups of chalcopyrites. The Roman numerals stand for the group numbers in the periodic table [7]. The chalcopyrites are now referred to as chalcopyrite-type semiconductors because they have been found to possess semiconducting properties [8].

In the early days, study of these compounds concentrated on their low thermal conductivities but now the attention has shifted due to the potential use of these compounds in LEDs, PVs, optical frequency conversion applications and in solid state based tunable laser systems [9].

In this work the main objective is to compute the electronic and structural properties of eight chalcopyrite-type materials, namely, silver gallium di-selenide ($AgGaSe_2$), silver gallium di-sulphide ($AgGaS_2$), silver gallium di-telluride ($AgGaTe_2$), copper gallium di-sulphide ($CuGaS_2$), copper indium di-selenide ($CuInS_2$), zinc silicon di-arsenide ($ZnSiAs_2$) and zinc tin di-arsenide ($ZnSnAs_2$) using DFT methods as implemented in the Quantum Espresso (QE) software package.

Another objective of this study is to determine the accuracy of DFT methods implemented in QE for the modelling of the energy band-gap structures, the density of states and the bulk modulus of the materials under investigation. This is achieved by comparing computed data with available experimental data.

Another objective of this study is to determine the energy of formation of the vacancy defect and doped chalcopyrites. These impurity properties find application in the emerging field of band-gap engineering.

In this work we also study the electronic and structural properties of chalcogenides. A chalcogenide is a chemical compound made up of at least one chalcogen anion and one more electropositive element. The term, however, exclusively refers to sulphides, selenides and tellurides and not oxides, even though all members of Group 16 of the periodic table can be called chalcogens [10].

Chalcogenides have special properties which make them important optical and electronic materials. For example, very fast, cheap and reliable computer memories can be made from them by changing the chalcogenide from crystal to glass and back again by using electrical heating. They have high optical non-linearities, which means they can be used in devices that process and switch light signals (non-linear optical devices), and they are essential to high speed optical communication which forms the backbone of today's telecommunications network. The theoretical study of semiconducting transition metal chalcogenides to date has been limited, hence the need for more investigative work.

The transition metals including rhodium (Rh), iridium (Ir), platinum (Pt), palladium (Pd), ruthenium (Ru) and osmium (Os) are collectively referred to as the Platinum Group Metals (PGMs). The transition metal chalcogenides of interest in this study are those of the PGMs. In particular this work will investigate the electronic and structural properties of palladium chalcogenides, namely palladium sulphide (PdS) and palladium selenide (PdSe). Some of these compounds exist in binary, pseudo-binary and ternary forms. In

nature, they occur as minerals such as laurite (RuS_2), braggite ($PdPt_3S_4$), and luberoite (Pt_5Se_4). Although there is extensive literature on the synthesis and structural aspects of bulk PGM chalcogenides, only relatively recently has there been research into their electronic properties. Several PGM sulphides such as PdS, PtS, Rh_2S_3, Ir_2S_3 and RuS_2 are semiconducting. That is one of the main reasons why research is being devoted to studying them.

Great interest has been generated in the study of PGM chalcogenides by the many possible applications in materials science due to their semiconducting properties and their use in catalysis. In the photochemical industry, PdS has been employed as a light image receiving material together with silver halides [11], [12]. In the manufacture of semiconductors and solar cells, PdS has been found to be very useful as an absorber material [13]. Other PGM chalcogenides such as those of tellurium are mostly used as optical disks, electronic devices and photovoltaic cells. Tellurium chalcogenides such as tellurium suboxide are used in the rewritable data layer of some CD-RW disks and DVD-RW disks. Cadmium telluride is used in the production of high-efficiency materials for photovoltaic panels [14].

A number of methods are used in computational materials science and condensed matter physics. However, Density Functional Theory (DFT) methods are among the most widely used *ab-initio* (first principle) methods because of their computational efficiency and good accuracy. DFT is the theory of the electronic structure of atoms, molecules and solids in their ground state, in which the electronic density distribution rather than the wave function plays the central role. This is implemented via the Hohenberg-Kohn (HK) [15] and Kohn-Sham (KS) theorems [16]. The Hohenberg-Kohn theorem shows that the

knowledge of the ground state electronic density is sufficient for determining all the physical properties of an electron system. In general, any observable of a quantum system can be obtained from the density of the system. The density of electrons is used as a physical variable in the derivation of DFT functionals (a rule which associates a function with a number). Unfortunately, it is very difficult to obtain the density of an interacting system. To circumvent this problem the Kohn-Sham theorem proposes a mapping of the interacting many-body system onto an auxiliary Kohn-Sham system of non-interacting electrons (called a jellium) moving in an effective Kohn-Sham potential. The dynamics of these electrons are governed by choosing the Kohn-Sham potential such that the non-interacting electrons have the same density as the interacting ones.

CHAPTER 2 DENSITY FUNCTIONAL THEORY (DFT)

The DFT is one of the many techniques that try to solve the many-body Schrödinger equation

$$H\psi_i(1,2,...N) = E_i\psi_i(1,2,...N) \ , \tag{1}$$

where

H is the Hamiltonian of a quantum mechanical system that is made up of N-particles, ψ_i is the i^{th} wave function and E_i is the energy eigenvalue of the i^{th} state. The particle degrees of freedom (1,2,…N) are mainly related to the position and spin coordinate. For a system which has no relativistic velocities the Hamiltonian for an N-electron system is given as

$$H = -\frac{\hbar^2}{2m}\sum_{i=1}^{N}\nabla_i^2 + \sum_{i>j}^{N}\frac{1}{|r_i - r_j|} + \sum_{i=1}^{N} v(r_i) \tag{2}$$

where, $v(r_i)$ is the external potential while r_i and r_j are electron positions whereas and $\hbar$ m are fundamental constants. The first term is the kinetic energy of electrons, the second term represents the complexity of the problem because it describes the interactions between electrons and does not allow to decouple the equation in the N one particle problem. The third term is the external potential dual to the ions in which the electrons are immersed.

2.1 BASIS OF DFT

To determine the ground state molecular properties of a system one needs to have knowledge of the electron density. Having knowledge of the exact electron density $n_o(\boldsymbol{r}_o)$

implies that this singular density would coincide with the locations of the nuclei. The Born-Oppenheiner approximation assumes that the nuclei are effectively stationary with respect to electron motion. Earlier approaches to solving the many-body Schrödinger equation tried to transform the full *N*-particle equation into *N* single-particle equations using the Hartree-Fock (HF) approximation.

2.1.1 HARTREE-FOCK APPROXIMATION

The disadvantage of the HF approximation is that it affects the accuracy with which the 'exchange-correlation' contribution to the total energy is calculated. The exchange contribution is due to the Pauli Exclusion Principle which does not permit two fermions to occupy the same quantum state. The consequence of this is the reduction of the probability of one electron being near another electron of the same spin.

The other setback of the HF approximation is that it lowers the probability of the correlation contribution of a third electron being near the electron-electron Coulomb repulsion between two electrons. The only correlation contributions allowed by HF approximation are those of similar spin electrons, which arising from the contribution of opposite spin electrons are completely neglected. In the HF approximation, the part of the exchange-correlation included is known as the exchange contribution and the part not accepted is known as the correlation contribution. To improve the accuracy of the electron density or many-electron wave function, the Hohenberg-Kohn (HK) theorems were developed.

2.1.2 HOHENBERG-KOHN THEOREMS

The HK theorems deal with any system made up of electrons that are moving under the influence of an external potential $V_{ext}(\boldsymbol{r})$, where $\boldsymbol{r}$ is the electron nucleus-distance. These theorems are the basis of DFT and they are given as:

Theorem I

The external potential $V_{ext}(\boldsymbol{r})$ and hence the total energy is a unique functional of the electron density $n(\boldsymbol{r})$**.**

The energy functional $E[n(\boldsymbol{r})]$ mentioned in Theorem I above can be written in terms of the external potential $V_{ext}(\boldsymbol{r})$ as

$$E[n(\boldsymbol{r})] = \int n(\boldsymbol{r}) V_{ext}(\boldsymbol{r}) d\boldsymbol{r} + F[n(\boldsymbol{r})] \tag{3}$$

where $F[n(\boldsymbol{r})]$ is an unknown, but universal functional of the electron density $n(\boldsymbol{r})$only.

Theorem II

The ground state energy can be obtained variationally: the density that minimizes the total energy is the exact ground state density.

The functional $E[n(\boldsymbol{r})]$ has its minimum when the electron density is at the equilibrium electron density $n_0(\boldsymbol{r}_0)$. The minimum of the energy E_0 is exactly equal the true ground-state energy,

$$E_0 \equiv \min E[n(\boldsymbol{r})] = E[n_0(\boldsymbol{r_0})] \tag{4}$$

The Hohenberg-Kohn theorems are powerful but they have some limitations in that they do not provide a way of computing the ground-state density of a system in practice. Kohn and Sham came up with a simpler method of performing DFT calculations as a result [16].

2.1.3 KOHN-SHAM FORMULATION

The Hamiltonian is

$$\hat{\mathrm{H}} = \hat{F} + \hat{V}_{ext}, \tag{5}$$

while the energy functional is

$$E[n(\boldsymbol{r})] = \int n(\boldsymbol{r}) V_{ext}(\boldsymbol{r}) d\boldsymbol{r} + F[n(\boldsymbol{r})] \tag{6}$$

According to the variational problem in the second Hohenberg-Kohn Theorem, the ground-state energy of a many-electron system can be attained by making the energy functional $E[n(\boldsymbol{r})]$ minimal as long as the number of electrons, *N*, does not change. Kohn and Sham attempted to set up a system in which the kinetic energy could be evaluated exactly. They did this by utilizing a non-interacting system of electrons. The universal functional $F[n(\boldsymbol{r})]$ was then divided into three terms; the first two terms which are known exactly make up the majority of the energy. The last part is a small unknown quantity. The universal functional is given by

$$F[n(\boldsymbol{r})] = T_s[n(\boldsymbol{r})] + E_H[n(\boldsymbol{r})] + E_{XC}[n(\boldsymbol{r})] \tag{7}$$

where

$T_s[n(\boldsymbol{r})]$ is the kinetic energy of a non-interacting electron gas of density $n(\boldsymbol{r})$;

$E_H[n(\boldsymbol{r})]$ is the classical electrostatic (Hartree) energy of the electrons given by,

$$E_H[n(\boldsymbol{r})] = \frac{1}{2}\iint \frac{n(\boldsymbol{r})n(\boldsymbol{r}')}{|\boldsymbol{r}-\boldsymbol{r}'|} d\boldsymbol{r}d\boldsymbol{r}' \quad (8)$$

where $n(\boldsymbol{r})$and $n(\boldsymbol{r}')$ are electron densities at regions $\boldsymbol{r}$ and $\boldsymbol{r}'$ respectively.

$E_{XC}[n(\boldsymbol{r})]$ is the exchange-correlation energy, which contains the difference between the exact and non-interacting kinetic energies and also the non-classical contribution to the electron-electron interactions, of which the exchange energy is part.

The Kohn-Sham potential V_{KS}, also known as the effective potential V_{eff}, is given as

$$V_{eff} = V_{ext}(\boldsymbol{r}) + V_H(\boldsymbol{r}) + V_{XC}(\boldsymbol{r}) \quad (9)$$

where:

$V_{ext}(\boldsymbol{r}) = V_{nuc}(\boldsymbol{r})$ is the external potential to the electron system due to the nuclei; $V_H[n(\boldsymbol{r})]$ is the Hartree potential which accounts for the *classical average* electrostatic interaction between electrons, $V_{XC}[n(\boldsymbol{r})]$ is the exchange-correlation potential which comprises all the quantum many-body effects. This potential is not known. The approximations of this potential that are of interest in this work are the Local Density Approximation (LDA) and the Generalized Gradient Approximation (GGA) as implemented in the Quantum Espresso package.

We note that $V_H[n(\boldsymbol{r})$ and $V_{XC}[n(\boldsymbol{r})]$ are direct functionals of the electron density function, $n(\boldsymbol{r})$. This is what gives the name "Density Functional Theory" to this method.

The Hartree potential $V_H[n(\boldsymbol{r})$ is

$$V_H[n(\boldsymbol{r})] = \frac{\delta E_H[n(\boldsymbol{r})]}{\delta n(\boldsymbol{r})} = \int \frac{n(\boldsymbol{r}')}{|\boldsymbol{r}-\boldsymbol{r}'|} d\boldsymbol{r}' \quad (10)$$

while the exchange-correlation potential $V_{XC}[n(\boldsymbol{r})]$ is

$$V_{XC}[n(\boldsymbol{r}) = \frac{\delta E_{XC}[n(\boldsymbol{r})]}{\delta n(\boldsymbol{r})}. \quad (11)$$

The ground-state density is found by solving the *N* one-electron Schrödinger equation

$$\left[-\frac{\hbar^2}{2m}\nabla^2 + V_{eff}(\boldsymbol{r})\right]\psi_{\boldsymbol{i}} = \varepsilon_i \psi_i(\boldsymbol{r}) \quad (12)$$

Here ε_i are eigenvalues of the orthonormal *N* single-particle states ψ_i and ħ and *m* are taken as 1.

2.1.4 THE LOCAL DENSITY APPROXIMATION (LDA)

Due to the physical complexity of the exchange-correlation term of the universal constant $F[n(\boldsymbol{r})]$, an approximation has to be made at some point. One such approximation is known as the Local Density Approximation LDA. In this approximation, the charge density is assumed to vary slowly with each small volume (local density) which is modeled as a homogeneous electron gas known as jellium. The exchange-correlation energy $E_{XC}[n(\boldsymbol{r})]$ can be found by means of the equation below

$$E_{XC}^{LDA}[n(\boldsymbol{r})] = \int n(\boldsymbol{r})\varepsilon_{xc}(n)d^3\boldsymbol{r} \quad (13)$$

where

ε_{xc} is the exchange-correlation energy per electron in a homogeneous electron gas at a density *n,* which can be determined.

Though simple, LDA is successful in producing some good results but like many other approaches it has its own limitations. Among them are the following:

i. It is poor at determining eigenvalues;
ii. It lacks derivative continuity;
iii. It fails when dealing with excited states and can only predict for the ground-state situations;
iv. It has self-interaction problems;
v. It fails to accurately make predictions for metal oxides;
vi. The spin and orbital momentum are not large enough;
vii. The band-gaps in semiconductors and insulators are always underestimated and
viii. It usually gives too-large cohesive energies and bulk moduli.

2.1.5 THE GENERALISED GRADIENT APPROXIMATION

The LDA is too simple to allow meaningful work to be carried out for some real systems. Hohenberg and Kohn came up with an extension of the LDA known as the Gradient Expansion Approximation (GEA) [17]**.** Even though the GEA did not work as expected, it provided a platform for the development of the Generalized Gradient Approximation, GGA. At the moment, the GGA is one of the most popular exchange-correlation functionals in Solid State Physics. The GGA is a density gradient expansion. One takes

the density at each point as well as the magnitude of the gradient of the density. It is normally written in terms of an analytical function known as the enhancement factor $F_{XC}[n(\boldsymbol{r})], \nabla n(\boldsymbol{r})]$, which directly changes the LDA energy density to give:

$$E_{XC}^{GGA}[n(\boldsymbol{r})] = \int n(\boldsymbol{r}) \varepsilon_{xc}^{homo} F_{XC}[n(\boldsymbol{r}), \nabla_n(\boldsymbol{r})] d^3\boldsymbol{r} \tag{14}$$

2.2 PSEUDO-POTENTIALS

The fact that electrons experience a Coulomb potential due to the nuclei given by

$$V_{nuc} = -\frac{Ze}{r}, \tag{15}$$

leads to computational problems in solving the Kohn-Sham equation. In this equation *Ze* is the nuclear charge and *r* is the distance of the electron from the nucleus. To overcome these problems the nuclear potentials are replaced by pseudo-potentials. These pseudo-potentials allow the Kohn-Sham wave functions to be expanded into a sum of plane waves $\phi_{i,G}$ .This is in effect an orthogonal plane wave basis, and leads to the expression

$$\psi_i(\boldsymbol{r}) = \sum_{\boldsymbol{G}} C_{i,\boldsymbol{G}} \phi_{i,\boldsymbol{G}} \tag{16}$$

In DFT it is only the interaction of the valence electrons that is considered (frozen core approximation) just like in chemical reactions. This is because core electrons screen the nucleus, so that the valence electrons experience only an effective pseudo-potential, which is much smoother than the bare nuclear Coulomb potential and as a result the wave

functions corresponding to the pseudo potentials have no nodes, as illustrated in Fig. 2.2.1,

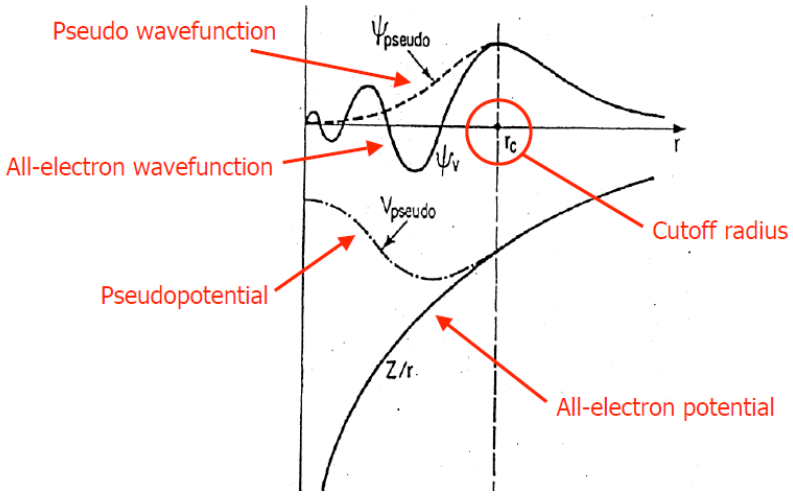

Figure 2.2.1: Illustration of a pseudo-potential [52].

In the figure,

$\psi_V = \psi_{ae}$ is the all-electron wave function, under bare nuclear potential;

ψ_{pseudo} is the pseudo wave function;

V_{pseudo} is the pseudo potential which gives rise to the wave function ψ_{pseudo};

r_c is the cut-off radius.

2.2.1 THE PROPERTIES OF PSEUDO-POTENTIAL WAVE FUNCTIONS

Pseudo-potentials are generated for many different applications and as such it is important to carefully look at their properties before making use of them. One important requirement for pseudo-potentials is that they must be *transferable*, meaning that we should be able to use the same pseudo-potential per element in different chemical environments. The property that is responsible for

transferability is that the pseudo-potentials should have the same scattering properties as the all-electron potentials. Quantum mechanically this is related to the logarithmic derivatives as expressed below.

$$\frac{d}{d\boldsymbol{r}}\ln(\psi_{ae}(\boldsymbol{r})) = \frac{d}{d\boldsymbol{r}}\ln\left(\psi_{pseudo}(\boldsymbol{r})\right) \tag{17}$$

A pseudo-potential is also considered to be ideal if its pseudo wave functions are identical to the all-electron wave functions outside the cut-off radius so that

$$\psi_{ae}(\boldsymbol{r}) = \psi_{pseudo}(\boldsymbol{r}). \tag{18}$$

Another important feature of good pseudo-potentials is that they should have eigenvalues that are independent of the quantum numbers, *l.* Hence

$$\boldsymbol{\varepsilon}_{\boldsymbol{l}}^{ae} = \boldsymbol{\varepsilon}_{\boldsymbol{l}}^{pseudo}. \tag{19}$$

Ideal pseudo-potentials should also possess the property of *norm-conservation*, which refers to the fact that the total charge of each wave function should be equal to the charge of the all-electron wave function within the sphere of the cut-off radius r_c. Thus

$$4\pi \int_0^{r_c} |\psi_{ae}(\boldsymbol{r})|^2 \boldsymbol{r}^2 d\boldsymbol{r} = 4\pi \int_0^{r_c} |\psi_{pseudo}(\boldsymbol{r})|^2 \boldsymbol{r} d\boldsymbol{r} \tag{20}$$

2.2.2 SOFT AND HARD PSEUDO-POTENTIALS

Fig. 2.2.2 helps to explain the concept of soft and hard pseudo-potentials which is determined by the position of the cut- off radius, r_c.

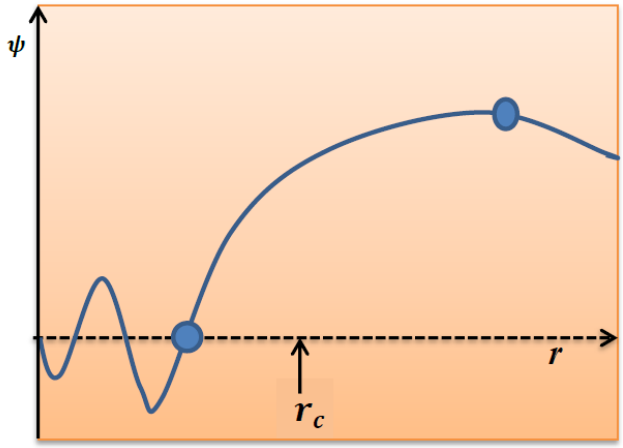

Figure 2.2.2: Positioning of the cut-off radius.

The value of the cut-off radius r_c is picked using the following criteria:

- It should be larger than r for the outer most node of the all-electron wave function;
- It should be between the outermost node of the all-electron wave function and the maximum wave function value beyond the outermost node.

If r_c is too small, a 'hard' pseudo-potential is obtained. Such a pseudo-potential requires the expansion of the Kohn-Sham wave functions into a large sum of plane waves in order to achieve convergence. However, if r_c is too large, the transferability is poor. There is therefore need to choose r_c such that the pseudo-potential is reasonably 'soft' (large r_c) so that the cut-off energy $E_{ecutwfc}$ for the plane wave basis in the DFT calculations is not too large.

In most DFT software, the three terms in $V_{eff}(\boldsymbol{r})$ are pre-calculated, added together and stored in pseudo potential files that are available to the user.

2.2.3 NAMING CONVENTION FOR PSEUDO-POTENTIALS

Performing LDA, GGA and DFT + Hubbard U (DFT+U) calculations in Quantum Espresso (QE) requires a good understanding of pseudo-potentials. The choice of the type of pseudo-potential to be applied in the input files for LDA, GGA and DFT+U is very important. The use of different types of pseudo-potentials for the different elements of a compound would result in wrong data generation. In this work a naming convention has been utilized for all the LDA, GGA and DFT+U calculations within QE. The input files given in Appendix D show how the pseudo-potential naming convention was applied to the input files.

All pseudo-potential (PP) files used in Quantum Espresso are named in the Unified Pseudo-potential Format (UPF). The naming convention for UPF PP files is:

element.description.UPF

The **description** is composed of fields separated by dashes. The following four description fields are explained:

Field 1: Used if the pseudo-potential is relativistic - otherwise this field is not included.

rel: full-relativistic

Field 2: One among the following should be given; this is not an optional field.

- pz: Perdew-Zunger, LDA exchange correlation.

- vwn: Vosko-Wilk-Nusair, LDA exchange correlation.
- pbe: Perdew-Burke-Ernzerhof, GGA exchange correlation.
- pw91: Perdew-Wang 91 gradient-corrected functional, GGA exchange correlation.
- blyp: Becke-Lee-Yang-Parr, GGA exchange correlation.
- tpss: Tao-Perdew-Staroverov-Scuseria, meta-GGA.
- coulomb: Coulomb bare –Ze/r potential.

Field 3: This field is optional; it would contain one of or a combination of the following:

- s: valence s state.
- p: valence p state.
- d: valence d state.
- f: valence f state.
- n: nonlinear core-correction.

Field 4: This final field is used to distinguish different versions of the same pseudo-potential or to identify the author(s). This field sometimes appears as two fields holding the PP version followed by the author identity:

- ae: All-Electron (no pseudization)
- mt: Martins-Troullier
- bhs: Bachelet-Hamann-Schlueter and derived
- vbc: Von Barth-Car (direct fit)
- van: Vanderbilt ultra-soft
- rrkj: Rappe Rabe Kaxiras Joannopoulos (norm-conserving)

- rrkjus: Rappe Rabe Kaxiras Joannopoulos (ultra-soft)
- kjpaw: Projector Augmented Wave (Kresse-Joubert paper)
- bpaw: Projector Augmented Wave (original Bloechl recipe)

The pseudo-potentials that are used in this work are of the forms, namely, **pz-mt_fhi.UPF** and **pbe-mt_fhi.UPF**,

- pz: Perdew-Zunger, LDA exchange correlation.
- pbe: Perdew-Burke-Ernzerhof, GGA exchange correlation.
- mt: Martins-Troullier.
- UPF: Unified Pseudo-potential Format.

2.2.4 DFT+U COMPUTATION

The strongly correlated nature of transitional metal compounds makes it very challenging to do predictive electronic structure calculations with reasonable accuracy for materials such as the chalcopyrites and chalcogenides. For some time now, the LDA and GGA energy exchange correlational functionals of the DFT have taken center stage for the computation of electronic structure calculations for crystalline solids. The term "strongly correlated" is usually applied to materials containing transition metals where the d- or f-electrons are localized and strongly correlated. The LDA and GGA methods fail to correctly predict the electronic structures of these systems because the potentials used with these methods are not orbital dependent potentials. To overcome the challenges associated with strongly correlated materials, new types of methods known as the DFT + Hubbard U (DFT+U) have been developed. These approaches introduce orbital dependent potentials to help take into account the issue of being strongly correlated [18].

The Coulomb interaction among electrons on a single transitional metal site is always included in the total energy functional of the DFT+U, more like the U-term in the Hubbard model. In the Hubbard model, the on-site repulsion is as a result of the Coulomb repulsion between electrons in the same atomic orbitals. The Hubbard model is the simplest model for interacting particles in a lattice, with only two terms in the Hamiltonian and it is given by

$$H_{Hub} = -T \sum_{\langle i,j\rangle,\sigma} \left(a_{i,\sigma}^{\dagger} a_{j,\sigma} + h.c\right) + U \sum_{i} n_i \uparrow n_j \downarrow \qquad (21)$$

where

$\langle i, j\rangle$ represents the nearest-neighbour atomic sites on the lattice

$a_{i,\sigma}^{\dagger} a_{j,\sigma} = n_{i\sigma}$ is the density of electrons of spin σ at sites i while *h.c* is the Hermitian conjugate.

$n_i \uparrow n_j \downarrow$ denote the electron densities for spin up and spin down respectively.

In the Hubbard Hamiltonian, the first component which is represented by the letter *T* represents the kinetic energy of electrons between atoms. The second term is represented by the letter *U* because it is representative of the potential energy arising from the charges on the electron.

Results obtained using these approaches are accurate than those obtained with LDA and GGA [19], [20], [21]**.** In strongly correlated materials, each electron has a complex influence on its neighbours due to a localized (as opposed to average) 'on-site' Coulomb interaction. Standard exchange-correlation functionals like LDA and GGA have the tendency of over-delocalizing electrons. The DFT+U method makes a correction to the

LDA or GGA energy functionals to give a better description of electronic correlation. One of the appealing features of DFT+U lies in the fact that it allows for the efficient calculation of energy derivatives [22]. The energy derivatives are the derivatives of the total energy of the materials computed in the form of forces, stresses and dynamical matrices.

An LDA+U functional, $E_{\mathrm{LDA+U}}$, was introduced to account for the 'on-site' Coulomb repulsive interaction by adding a Hubbard-like term to obtain

$$E_{LDA+U}[n] = E_{LDA}[n] + E_u\left[n_i^{\sigma} - E_{DC}[n_i^{\sigma}]\right] \tag{22}$$

where $\boldsymbol{n_{i\sigma}}$ is the density of electrons of spin σ at sites *i*.

This in short can be written as

$$E_{LDA+U} = E_{LDA} + E_{Hub} - E_{DC}. \tag{23}$$

The Hubbard parameter U is added explicitly [23], and hence the energy contribution of these orbitals which are included in the LDA/GGA functional must be eliminated so that their contributions are not double counted. That is the reason why the last term E_{DC} is subtracted.

The parameter *U* is evaluated as a potential corresponding to the Hubbard correction interaction E_{Hub}. The LDA+U potential is

$$V_{LDA+U}(\boldsymbol{r}) = V_{LDA} + U\left(\frac{1}{2} - n_i\right)P_i. \tag{24}$$

where $\boldsymbol{P_i}$ is projection operator on the localized orbital.

This expression reveals that in cases when the state i is at the beginning less than half empty, the Hubbard potential has a repulsive effect on electrons. Also, in the event that it is more than half occupied the potential has an attractive effect and localizes electrons.

2.3 PLANE-WAVE CUTOFFS AND K-POINT SAMPLING

Whenever dealing with first-principles plane-wave pseudo-potential calculations, two things are very important, namely, energy *cut-offs* and ***k**-points*. The energy cut-off is the cut-off for the wave function expansion while the **k**-points measure how well the discrete grid has approximated the continuous integral over the Brillouin zone. One point worth noting is that the higher the cut-offs, either the energy *cut-offs* or the ***k**-points*, the higher the accuracy. The only challenge is that the higher *cut-offs* demand more computational time. Thus, one needs to strike a balance between accuracy and computational time.

2.3.1 CONVERGENCE AND PLANE-WAVE BASIS

This work involves infinite systems using periodic boundary conditions. To deal with these systems one has to make use of the Bloch theorem. The Bloch theorem is

$$\psi_{nk}(\boldsymbol{r}) = exp(i\boldsymbol{k}.\boldsymbol{r})\mu_{nk}(\boldsymbol{r}) \tag{25}$$

where

$$\mu_{n\boldsymbol{k}}(\boldsymbol{r}) = \sum_{G} C_G exp(i\boldsymbol{G}.\boldsymbol{r}). \tag{26}$$

In Equation 25, $\psi_{n\boldsymbol{k}}$ is the electronic wave function in the lattice, $\boldsymbol{G}$ in equation 26 sums over all reciprocal lattice vectors though in practice it must be truncated at some point.

C_G are coefficients in the expansion. In QE, the basis functions are the plane waves. Plane-waves with a periodicity compatible with the boundary conditions of the direct lattice are selected by limiting the plane-wave expansion to the discrete set of $\boldsymbol{G}$ vectors. The $\boldsymbol{G}$ vectors are integer multiples of the three primitive lattice vectors. To be complete, the plane-wave basis has to be taken in the limit of an infinite number of $\boldsymbol{G}$ vectors. In practice, however, the plane waves have to be truncated at some point called the plane-wave cut-off [53]. It is important to bear in mind that the cut-off energy is given in Rydberg or eV corresponding to the kinetic energy of the highest included value of $\boldsymbol{k} + \boldsymbol{G}$. It is also important to remember that the electronic states in the Brillouin zone are classified by the $\boldsymbol{k}$-*points* in the Brillouin zone. The number of $\boldsymbol{k}$-points is proportional to the number of repeated unit cells *N*.

2.3.2 CONVERGENCE AND K-POINT SAMPLING

The Bloch theorem demands that for an infinite periodic system, a Schrödinger-like Kohn-Sham equation must be solved at all points in the Brillouin zone. To achieve this task involves self-consistent interactive diagonalization of an $M \times M$ matrix, where M is the number of basis functions. Integration is over the first Brillouin zone where the bands are occupied. We need to have band energies at every possible reciprocal lattice point in the Brillouin zone. It must be emphasized that to do a practical calculation, the integral over the Brillouin zone is replaced by a finite sum over discrete $\boldsymbol{k}$-*points*, which is designed to reproduce the integral to a very good approximation. Care must however be taken so that one has enough $\boldsymbol{k}$-*points* to allow convergence to the total energy of the system. To discretely sample the Brillouin zone with a set number of $\boldsymbol{k}$ values, one can choose to use a "special-points" scheme. The "special-points" scheme is very useful

when sampling the Brillouin zone because they provide an efficient means of integrating periodic functions.

2.4 STRUCTURAL PROPERTIES

2.4.1 THE ZINC BLENDE STRUCTURE

Some of the most important semiconductors such as silicon (Si) and germanium (Ge) have a crystal structure similar to the diamond lattice crystal structure. In the diamond lattice, each atom is at the center of a tetrahedron having four neighbouring atoms at each corner (Fig. 2.4.1). The lattice looks like a pyramid with a triangular base and three triangular faces connected to a common point.

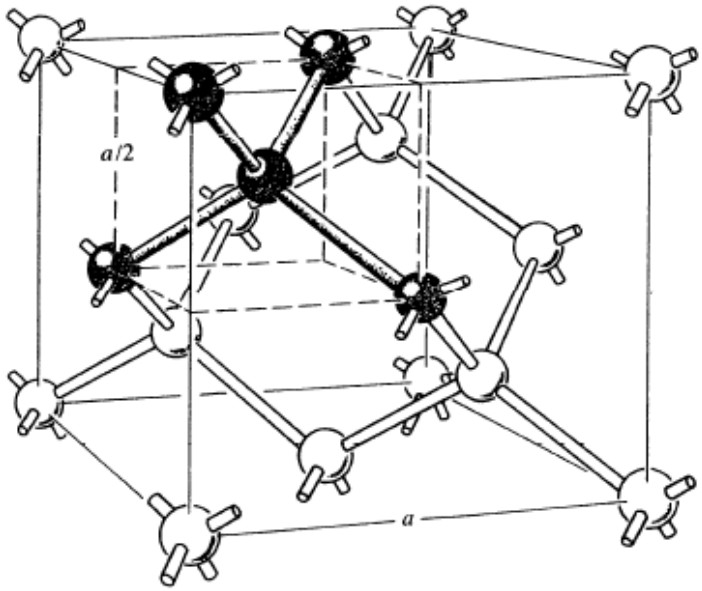

Figure 2.4.1: A diamond lattice unit cell with four nearest neighbour atoms forming a tetrahedron [24].

The diamond lattice is a face-centered cubic (FCC) with one more atom placed at $\left(\frac{a}{4},\frac{b}{4},\frac{c}{4}\right)$ from every atom within the structure with a = b = c. It can be seen that the

diamond structure is composed of two interpenetrating FCC sub-lattices. In the Bravais lattice of the diamond structure, the primitive basis has two identical atoms located at (0,0,0) and $\left(\frac{1}{4},\frac{1}{4},\frac{1}{4}\right)$ connected to each lattice point of the FCC. The basis of the diamond structure is made up of two atoms, implying that the conventional unit cube of the diamond structure has eight atoms unlike the conventional FCC unit cell which has four atoms. Another FCC structure of interest is the zinc-blende structure. It is unique in that the two sub-lattices have different atomic types as in the gallium arsenide (GaAs) structure which has two interpenetrating FCC structures of Ga and As as shown in Fig. 2.4.2.

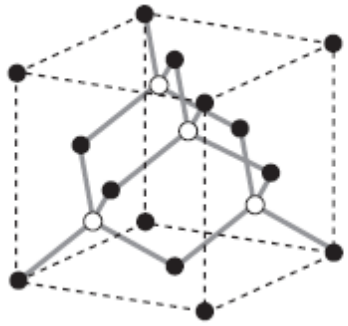

Figure 2.4.2: The zinc-blende crystal structure [25].

The open circles and the black circles represent interpenetrating sub-lattices of two different lattice types. Another feature of this type of structure is that it has no center of symmetry. Here the basis of the structure is the tetrahedral bonds like Ga-As or Ge-Ge. It is apparent that inversion symmetry does not exist on these tetrahedral bonds (Fig. 2.4.3).

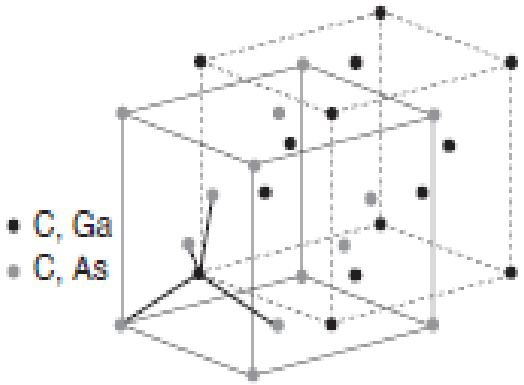

Figure 2.4.3: Tetrahedral bonds of zinc-blende structure [25].

If the carbon (C) atoms in diamond are alternately replaced by a Zn and S atom a zinc-blende (ZnS) structure is obtained as shown in Fig. 2.4.4 The ZnS structure is what gave the name, 'zinc-blende' to all such structures.

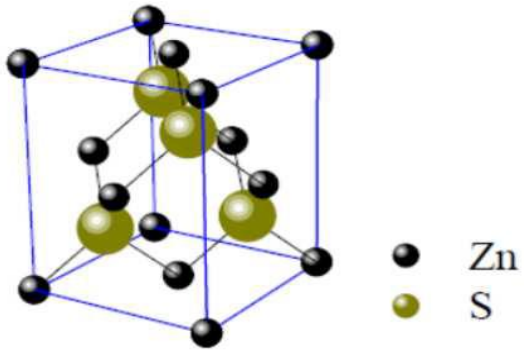

Figure 2.4.4: Carbon atoms replaced by Zn and S atoms in the diamond structure [3].

The atomic positions in each cubic cell of the zinc-blende structure are projected on a cube face, giving a top view. The numbers in the circles represent the height above the base in units of a cube edge. On the FCC sub-lattice the points are 0 and $\frac{1}{2}$ while those at

$\frac{1}{4}$ and $\frac{3}{4}$ are positioned on a sub-lattice displaced along the body diagonal by $\frac{1}{4}$ of its actual length as shown in Fig. 2.4.5.

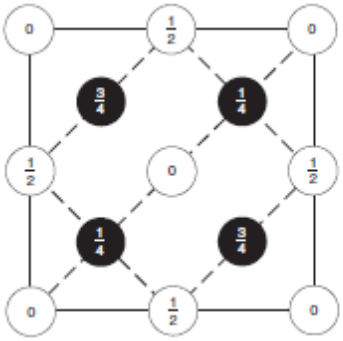

Figure 2.4.5: Top view of zinc-blende lattice structure [26].

From Fig. 2.4.5 above it can be seen that the atomic positions of the primitive cell for a general material with the zinc-blende structure and a chemical composition, AB are A $(0,0,0)$ and B $\left(\frac{1}{2},\frac{1}{4},\frac{3}{4}\right)$ just like in the diamond lattice structure.

2.4.2 CRYSTAL STRUCTURE OF CHALCOPYRITE

The chalcopyrite compounds belonging to the $I-III-VI_2$ and $II-IV-V_2$ groupings are ternary materials analogous to zinc-blende (a binary material) of the type II-VI and III-V respectively [26], [27], [28]**.** These chalcopyrite structures reveal some striking structural anomalies [29] as compared to their binary analogous compounds. These structural anomalies result in anion displacement as explained later in this section.

In order to give an overview of the physical structures of the chalcopyrites studied, we refer to the chemical groups in Roman numerals as I, II, III, IV, V and VI. These correspond to the elements in the periodic table column numbers 11, 12, 13, 14, 15 and

16 respectively. III-V semiconductors such as GaAs and InP have the zinc-blende crystal structure possessed by ZnS and several other II-VI compounds. The zinc-blende structure consists of two inter-penetrating face centered cubic sublattices. One is occupied by the cations (from Group III or II) and the other by anions (from Group VI or V). In a ternary chalcopyrite, the anion sublattice remains but the cation sublattice is filled by two types of cations, one of a high valence and the other of a lower valence, which are arranged in an ordered manner. Since the cation sites are equally shared by two atomic types, it means that there are twice as many anion atoms as any single cation atom, resulting in the chemical compositions, $I - III - V\ I_2$ and $II - IV - V_2$. The valence electronic configurations of all the elements that constitute the materials studied in this work are given below.

Group I → Cu ($11 \rightarrow 3d^{10}\,4s$) and Ag ($11 \rightarrow 4d^{10}\,5s$)
Group II → Zn ($12 \rightarrow 3d^{10}\,4s^2$)
— Higher valence cations

Group III → Ga ($3 \rightarrow 4s^2 4p$) and In ($3 \rightarrow 5s^2 5p$)
Group IV → Si ($4 \rightarrow 3s^2 3p^2$) and Sn ($4 \rightarrow 5s^2 5p^2$)
— Lower valence cations

Group V → As ($5 \rightarrow 4s^2 4p^3$)
Group VI → S ($6 \rightarrow 3s^2 3p^4$), Se ($6 \rightarrow 4s^2 4p^4$) and Te ($6 \rightarrow 5s^2 5p^4$)
— Anions

The transition metals Cu, Ag and Zn provide the higher valence cations, the first number in the parentheses giving the valence.

The chalcopyrites that were studied in this work are:

$I - III - VI_2$: $AgGaSe_2$, $AgGaS_2$, $AgGaTe_2$, $CuGaS_2$, $CuInS_2$, $CuInSe_2$.

$II - IV - V_2$: $ZnSiAs_2$, $ZnSnAs_2$.

The covalent bonding mechanisms in these crystals are facilitated by hybridization of the valence electronic states (outermost orbitals) which mixes them to form new orbitals like sp^3 hybrid orbitals which form the bonds.

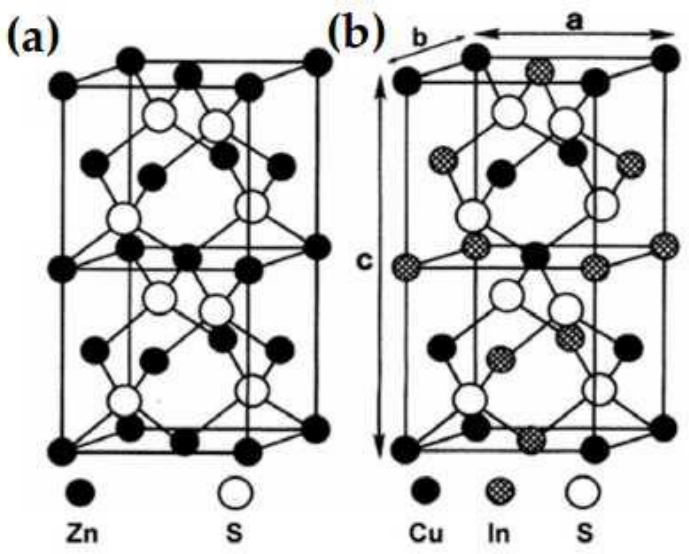

Figure 2.4.6: Structure of (a) zinc-blende (ZnS) (double cells) (b) chalcopyrite ($CuInS_2$) (single cell) [29].

In each tetragonal unit cell of a chalcopyrite semiconductor we find that there are two zinc-blende unit cells. This implies that there are four group I/II atoms, four group III/IV atoms and eight group V/VI atoms in each unit cell.

The chalcopyrite structure of $CuInS_2$ can be derived from the zinc-blende structure by replacing half of the cations (Zn) by Cu and the other half by In atoms but leaving the S atoms in the same positions. One important point worth noting is that in the chalcopyrite structure, there are two different cations with different physical and chemical properties and one anion whereas in zinc-blende there is one cation and one anion. In this type of structure, the *c* axis is doubled (doubling occurs in the *z*-direction) so that *c=2a*. The A and B cations lie on the corners of each face of the unit cell and the anion and *C* lies inside the unit cell. This structural arrangement results in the anion *C* having an

equilibrium position closer to one pair of cations than the other. This is known as anion displacement (μ) and eventually leads to unequal bond lengths, which is known as bond alternation. This shows that anion displacement measures the extent of bond alternation in chalcopyrites. Another result of having two different types of cations and anions is referred to as tetrahedral distortion (η). The crystal lattice parameter $\eta = c/2a$ is not equal to 1.0, or putting it another way, the ratio of c/a is no longer equal to 2.0. This is illustrated in Fig. 2.4.7 where $\mathcal{E}$ represents the tetragonal distortion of the unit cell along the crystal *c* axis [26].

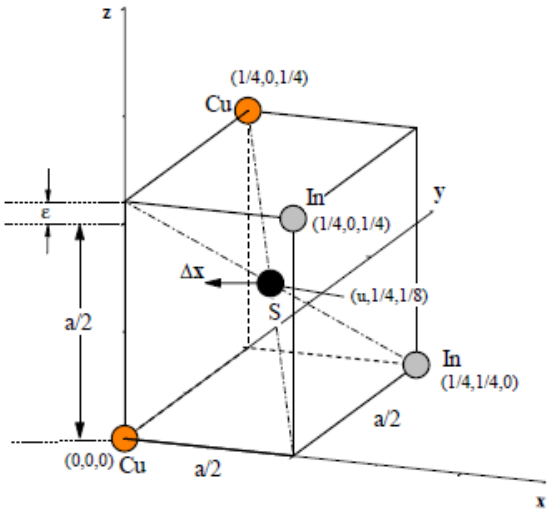

Figure 2.4.7: Tetragonal distortion in $CuInS_2$ [3].

As has been mentioned, anion displacement is the main cause of bond alternation, which means that the bond length R_{AB} is not equal to $R_{BC,}$ ($R_{AB} \neq R_{BC}$). This result is what is referred to as the non-ideal case because $\mu \neq 0.25$ and $\eta \neq 1$. The quantity

$$\mu - \frac{1}{4} = \frac{(R_{AC}^2 - R_{BC}^2)}{a^2} \tag{27}$$

measures the degree to which the bond has been altered in a system. The two near-neighbour distances A-C and B-C are

$$R_{AC} = a\left[\mu^2 + \frac{1+\eta^2}{16}\right]^{1/2}, \tag{28}$$

and

$$R_{BC} = a\left[\left(\mu - \frac{1}{2}\right)^2 + \frac{\left(1+\eta^2\right)}{16}\right]^{1/2} \text{ [3].} \tag{29}$$

2.4.3 DEFECT/DOPED CHALCOPYRITES

A defect chalcopyrite is one in which one type of cation is half the other type of cation and the other half is a vacancy. This is in contrast with the pure chalcopyrite. Compounds of the chalcopyrite having such an empty space are said to fall in the category of ***vacancy defect systems***. Suzuki *et al.* [30] also have a similar type of definition for defect chalcopyrites. When the pure and defect chalcopyrites are examined, it is found that the defect chalcopyrites, just like the pure ones have two types of cations. However, the defect type has seven atoms per unit cell of cations while the pure chalcopyrite has eight.

When the vacancy is substituted by another type of atom from the same group of the periodic table, the type formed is referred to as a doped chalcopyrite. This replacement causes the doped chalcopyrite to be occupied by three types of cations instead of two as in the pure type. The ratio of atoms in a defect chalcopyrite is much clearer when the formula of the chalcopyrite (ABC_2) is doubled. The formula of the chalcopyrite when doubled takes the form of $A_2B_2C_4$ but when a vacancy is created the formula of the defect chalcopyrite takes the form of AB_2C_4. The doped chalcopyrite can be evaluated in a

similar manner because if one of the first types of cation is replaced, the new form of the formula can be written as $A_xB_2C_4$. The defect and the doped chalcopyrites can be considered as variants of the pure chalcopyrite of the form ABC_2. In the ABC_2 type of chalcopyrites, the vacancies/doping atoms are occupied in such a way that the crystal periodicity is not lost, so that there is conservation of periodicity. Due to this phenomenon of crystal periodicity in the defect/doped chalcopyrites, these materials are referred to as ***ordered-defect*** compounds [30]. As has already been mentioned, a unit cell of a pure chalcopyrite comprises four A atoms, four B atoms and eight C atoms, whereas the ordered-defect compound unit cell has two A atoms, two vacancy/doped atoms and eight C atoms. Figs. 2.4.8 (a and b) below depict these types of compounds as produced with the help of the computer simulation package Xcrysden [31].

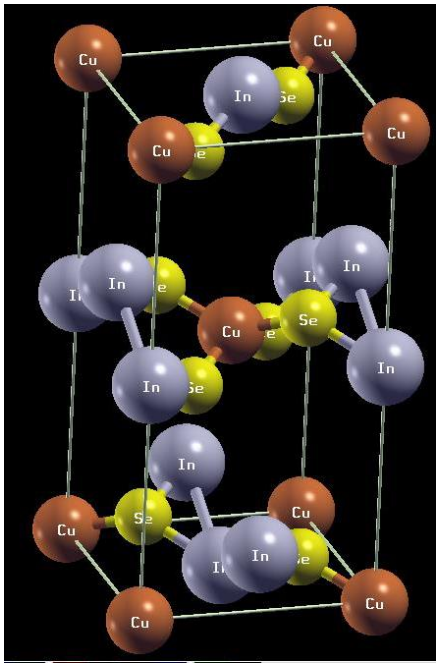

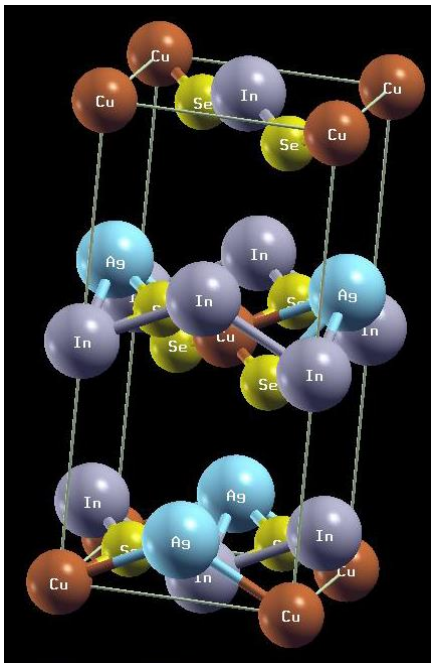

Figure 2.4.8: (a) Defect-$CuInSe_2$. **(b) Ag-doped-$CuInSe_2$.**

In the ordered-defect chalcopyrites the anion displacement does not only occur in the *x*-direction but in all the three coordinate directions. For an ideal case of a unit cell, the parameters η, u_x, u_y, u_z are given as 1, 0.25, 0.25 and 0.125 respectively [26]. Here η is the crystal lattice parameter earlier given as $c/2a$ and 'u_x', 'u_y' and 'u_z' are anion displacement parameters along the three axes. For defect/doped chalcopyrites, the cation-anion bond lengths are not of equal length.

The introduction of vacancy/doping which produces the defect/doped chalcopyrites causes anion displacement to occur in all the three coordinate directions implying that the position of anion VI of (I-III-VI_2) deviates from the ideal position of 0.25 in all the three directions. From this it can be deduced that there are three internal parameters in x, y, z [32] which take the atomic positions of the defect chalcopyrites as follows:

II: (0, 0, 0),

III: (0, 0, 0.5), (0, 0.5, 0.25),

VI: (x, y, z), (-x,-y, z), (y, -x, z), (-y, x, -z).

Mackinnon [33] gives atomic positions for the defect type as:

Vacancy: (0, 0, 0),

I: (0, 0.5, 0.25),

III: (0, 0, 0.5), (0.5, 0, 0.25),

VI: (x, y, z), (-x, -y, z), (-y, x, -z), (y, -x, -z).

In this work we adopted the use of the pure chalcopyrite atomic positions and then removed half of one type of cation in the chalcopyrite and then used the **pw.x** program within Quantum Espresso (QE) with a 'relax' command to acquire equilibrium. QE runs the program to calculate 'total energy' and 'total force' needed to rearrange the atoms in their new positions where the atoms acquire equilibrium. In this case the new positions acquired by the defect $CuInSe_2$ are:

Vacancy: (0.50, 0.00, 0.25),

I: (0.00, 0.00, -0.04),

III: (0.50, 0.50, -0.04), (0.00, 0.50, 0.48),

VI: (x, y, z), (-x, - y, z), (-y, x, -Z), (y, - x, - z).

2.4.4 BULK MODULUS

The bulk modulus is one of the elastic properties of materials. The bulk modulus determines how much a material will compress under a given amount of external pressure. It is defined as the ratio of the change in pressure to the fractional volume compression.

One way to compute the bulk modulus (B) of a material is by using Cohen's empirical formula [34]

$$B = \frac{(1971 - 220\lambda)}{d^{3.5}} \tag{30}$$

Where λ is the iconicity factor and d is the bond length.

This expression has been found to be appropriate for zinc blende solids [29]. In Cohen's the ionicity factor is given as 0, 1 or 2 for group IV, III-V and II-VI semiconductors respectively. The variation of λ is attributed to the difference iconicity of the materials. The central concept behind the introduction of λ in Cohen's empirical formula is that there is an inherent quantitative difference between ionic crystals and covalent crystals. The two extremes of ionic and covalent nature are straightforward but for some materials like Group IV, III-V and II-VI semiconductors; there is a degree of both ionicity and covalency. Ionicity is the fractional extent to which a material is ionic. Surabala [29] used a modified form of Equation 30 for *B.*

$$B = \frac{1971 - 220\lambda}{4} \sum_{i=1,2,3,4} \frac{1}{d_i^{3.5}} \ . \tag{31}$$

This type of expression takes into account the fact that in chalcopyrites the bond lengths are not equal due to the two different types of cations. The *B* is taken as an average bulk modulus considering the different tetrahedral bonds. It is given in GPa and the nearest-neighbour distances d_i is given in Å. λ is expected to be 1 and 2 for II-IV-V_2 and I-III-VI_2compounds respectively. This is because, as has already been mentioned, the chalcopyrites of II-IV-V_2 and I-III-VI_2 types are ternary analogues of Groups III-V and II-VI binary compounds respectively.

It can be shown for the zinc-blende and chalcopyrite structure that the average nearest neighbour distance is given by

$$d = \frac{\sqrt{3}}{4} a \tag{32}$$

where *a* is the lattice constant. This will be used in this work to determine the bulk modulus using Cohen's formula.

2.5 ELECTRONIC BAND STRUCTURE

The FCC structure is the basis of the materials being studied in this work. The conventional unit cell of the FCC structure is a cube that has lattice vectors:

$\boldsymbol{a}_1 = (1,0,0),$

$\boldsymbol{a}_2 = (0,1,0),$

$\boldsymbol{a}_3 = (0,0,1).$

It is four times bigger than the primitive unit cell and has four atoms in it whose position vectors are

$\boldsymbol{r}_1 = (0,0,0),$

$\boldsymbol{r}_2 = (1/2\,, 1/2\,, 0),$

$\boldsymbol{r}_3 = (0, 1/2\,, 1/2),$

$\boldsymbol{r}_4 = (1/2\,, 0, 1/2).$

Fig. 2.5.1 gives the FCC primitive unit cell.

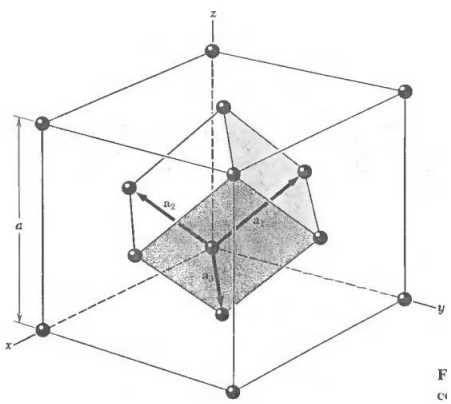

Figure 2.5.1: Primitive unit cell of FCC.

From Fig. 2.5.1 one can see that inside the conventional cell the construction of the primitive unit cell is dictated by the primitive translation unit vectors $\boldsymbol{a_1}, \boldsymbol{a_2}, \text{and } \boldsymbol{a_3}$. These unit vectors are run from one corner position to the nearest three face center positions. It can be seen that the three translation unit vectors are given by

$$\boldsymbol{a_1} = \frac{\mathrm{a}}{2}(\boldsymbol{j} + \boldsymbol{k}), \tag{33}$$

$$\boldsymbol{a_2} = \frac{a}{2}(\boldsymbol{i} + \boldsymbol{k}), \tag{34}$$

$$\boldsymbol{a_3} = \frac{a}{2}(\boldsymbol{i} + \boldsymbol{j}). \tag{35}$$

These can also be written as:

$$\boldsymbol{a} = \frac{a}{2}(\boldsymbol{j} + \boldsymbol{k}), \tag{36}$$

$$\boldsymbol{b} = \frac{a}{2}(\boldsymbol{i} + \boldsymbol{k}), \tag{37}$$

$$\boldsymbol{c} = \frac{a}{2}(\boldsymbol{i} + \boldsymbol{j}). \tag{38}$$

The volume of the FCC primitive unit cell is

$$\boldsymbol{V_c} = \boldsymbol{a} \bullet (\boldsymbol{a_2} \times \boldsymbol{a_3}) = \frac{\boldsymbol{1}}{\boldsymbol{4}}\boldsymbol{a^3} \tag{39}$$

The reciprocal lattice unit vectors are given by

$$\boldsymbol{A} = 2\pi \frac{\boldsymbol{b}\times\boldsymbol{c}}{\boldsymbol{b}\bullet(\boldsymbol{b}\times\boldsymbol{c})}\,, \tag{40}$$

$$\boldsymbol{B} = 2\pi \frac{\boldsymbol{c}+\boldsymbol{a}}{\boldsymbol{b}\bullet(\boldsymbol{c}\times\boldsymbol{a})}\,, \tag{41}$$

$$\boldsymbol{C} = 2\pi \frac{\boldsymbol{a}\times\boldsymbol{c}}{\boldsymbol{c}\bullet(\boldsymbol{a}\times\boldsymbol{c})}\,, \tag{42}$$

From Equations 40, 41 and 42 the primitive translation vectors of the reciprocal lattice of the FCC crystal structure are found to be

$$\boldsymbol{A} = \frac{2\pi}{a}(-\boldsymbol{i}+\boldsymbol{j}+\boldsymbol{k}), \tag{43}$$

$$\boldsymbol{B} = \frac{2\pi}{a}(\boldsymbol{i}-\boldsymbol{j}+\boldsymbol{k}), \tag{44}$$

$$\boldsymbol{C} = \frac{2\pi}{a}(\boldsymbol{i}+\boldsymbol{j}-\boldsymbol{k}). \tag{45}$$

The reciprocal lattice of the FCC structure is a body-centered, BCC, crystal structure and the volume V_G of the primitive unit cell of the reciprocal lattice is:

$$V_G = |\boldsymbol{A}\bullet\boldsymbol{B}\times\boldsymbol{C}| = \frac{(2\pi)^3}{V_C} = 4\left(\frac{2\pi}{a}\right)^3 \tag{46}$$

Fig. 2.5.2 below shows the construction of the first Brillouin zone in a 2-D reciprocal lattice.

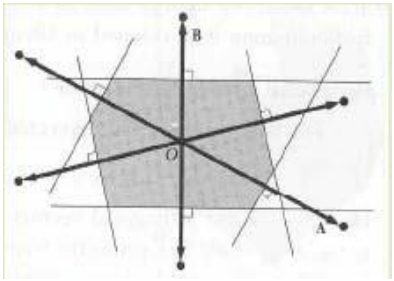

Figure 2.5.2: Construction of first Brillouin zone in a two-dimensional reciprocal lattice.

To obtain the construction of Fig. 2.5.2 above a number of vectors are drawn from a reciprocal lattice point to nearby points in the lattice. Perpendicular lines to these vectors are constructed at their midpoints. The smallest enclosed area is the first Brillouin zone. To construct the first Brillouin zone in 3-D we follow a similar process but we now talk about planes and the smallest volume enclosed and not the area. Fig. 2.5.3 shows two adjacent first Brillouin zones of the FCC structure in 3-D.

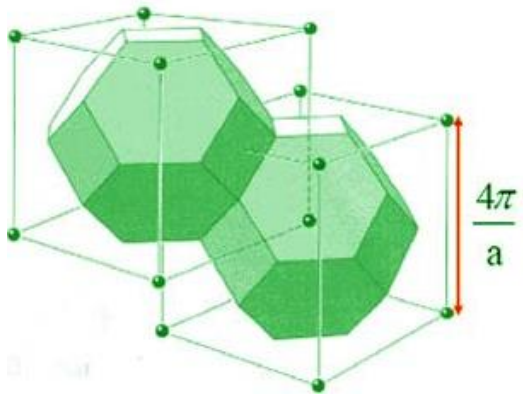

Figure 2.5.3: Two adjacent first Brillouin zones of the FCC structure in 3-D.

Fig. 2.5.3 helps one to see that the reciprocal lattice of the FCC structure is BCC. The reciprocal space can be defined as ***k***-space, where ***k*** represents a 3-D vector that is related to the wave number $2\pi/\lambda$ where λ is the wavelength. The manner in which the energies of all of the electronic states change with ***k*** is called the band structure. Since ***k*** is a 3-D vector, it is usual to plot these energies along special high symmetry directions. These directions are referred to as paths. In Fig. 2.5.4 below the first Brillouin zone for the FCC structure with various paths indicated is shown.

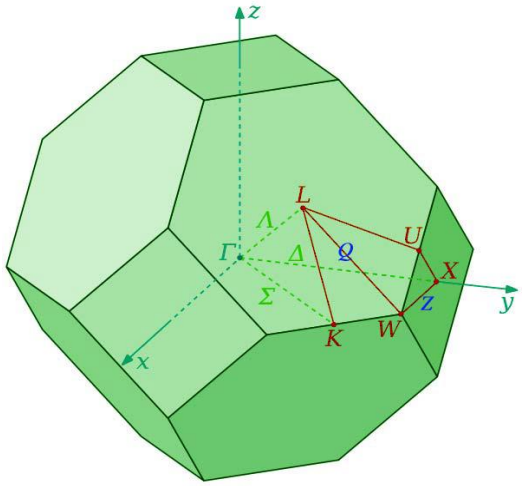

Figure 2.5.4: First Brillouin zone of the FCC lattice showing labels for high symmetry lines and points.

Some of the critical points in the first Brillouin zone are defined as:

1. *Γ:* center of the Brillouin zone
2. *K:* middle of an edge joining two hexagonal faces
3. ***L:*** center of hexagonal face
4. *U:* middle of an edge joining a hexagonal and a square face
5. *W:* corner point
6. *X:* center of a square face

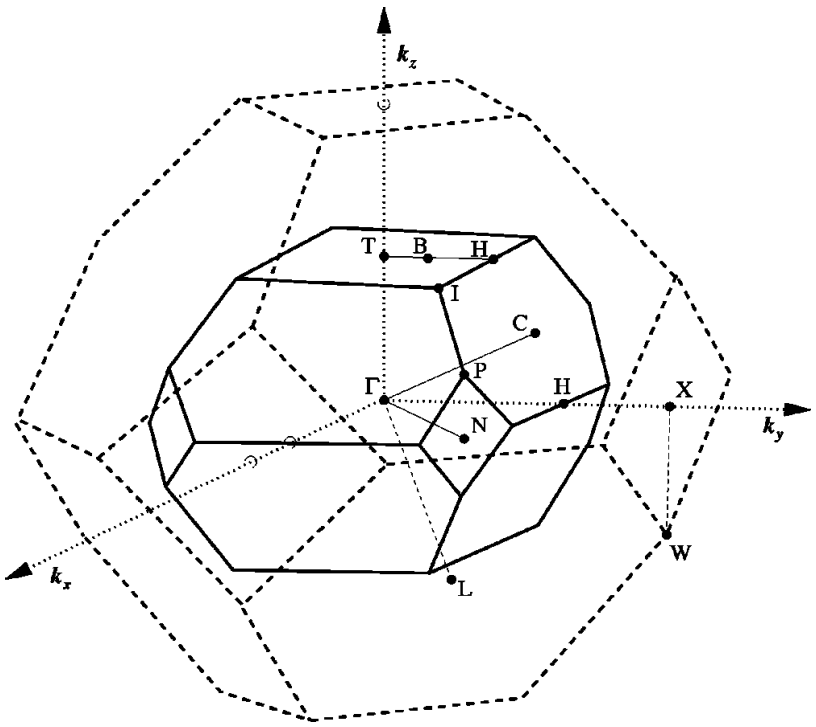

Figure 2.5.5: First Brillouin zone for the chalcopyrite structure (solid line) inside that of the zinc blende structure (dotted line) [31].

The Band Theory models the way electrons behave in solids and many physical phenomena of solids such as optical absorption can be explained using the theory. In this work the chalcopyrite band structure calculations were done in the zinc blende Brillouin zone because the chalcopyrite structure is a derivative of the zinc blende structure. Thus, the ***k***-space path that is used in the first Brillouin zone of the zinc blende crystal structure is $\Gamma \to L \to \Gamma \to X \to W \to K \to \Gamma$.

2.5.1 EMPIRICAL ELECTRONIC BAND STRUCTURE SHIFT

The chalcopyrite compounds of chemical formula II-IV-V_2 and I-III-VI_2 can be thought of as being derived from a parent binary compound with formula III-V and II-VI respectively, by replacing the group-III element by alternating a group-II and group-IV element or the group-II element by a group-I and group-III elements. It is well known that the Local Density Approximation often underestimates the band gap in strongly

correlated systems. Jiang et al. [32] estimated empirical shift corrections to the LDA derived chalcopyrite band gaps based on the similarities of the band structures with the parent and grandparent compounds.

The reason for the band gap underestimation by the LDA correlation functional for strongly correlated systems is that the Kohn-Sham one-particle Equation 12 does not provide quasiparticle excitation energies. The equation for quasiparticle energies in the so-called GW method [20-23] differs from the Kohn-Sham equation by the fact that the local exchange-correlation potential is replaced by a nonlocal energy operator. Jiang et al. [32] adjusted the LDA band gaps so as to reproduce the GW results of Zakharov et al. [26] rather than experimental results because they wished to adjust not only the minimum gaps, as given by available experimental results, but both gaps at Γ and X. They found that fairly good agreement with GW results could be obtained by applying either of two universal empirical shifts of either 0.14 Ry (1.905 eV) or 0.21Ry (2.858 eV). These results were found to hold fairly well for both chalcopyrites and their parent binary zinc blende compounds. We will therefore use this result for both chalcopyrites and binary chalcogenides.

The empirical shift methods of Jiang *et al* [32] can also be applied to correct the GGA results because the difference between the LDA and GGA exchange-correlation energy lies in the enhancement factor $F_{XC}[n(\boldsymbol{r})], \nabla n(\boldsymbol{r})]$, which changes the LDA energy density to the GGA energy density. The enhancement factor does not alter the effect of the Kohn-Sham one-particle equation 12 which fails to provide quasiparticle excitation energies.

CHAPTER 3 COMPUTATIONAL DETAILS

3.1 DFT IN QUANTUM ESPRESSO

3.1.1 SELF-CONSISTENT FIELD CYCLE

The Kohn-Sham equations provide us with a practical approach to determining the ground state energy and density of particles in a system [35]. These calculations basically employ the Schrödinger equation to perform self-consistent calculations.

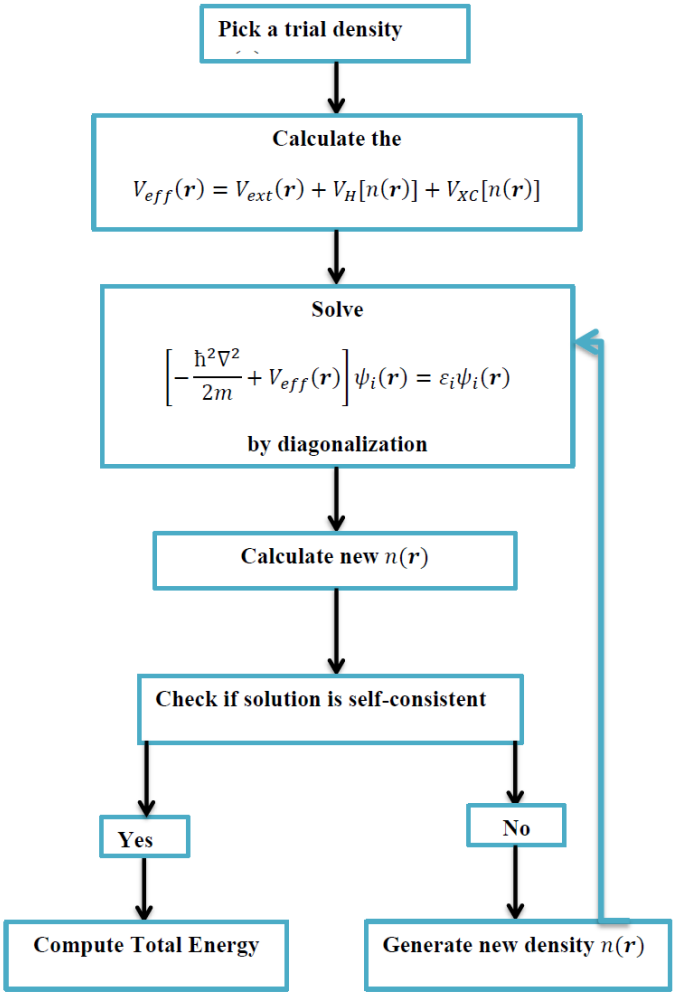

Figure 3.1.1: Self-consistent field (SCF) flow chart.

Fig. 3.1.1 is a flow chat which illustrates the process of solving the Kohn-Sham equations for the electronic charge density. The process starts with an initial guess of the electronic

charge density. The charge density is used to determine the effective potential; V_{eff}, which is later used to determine the ground state solution of the system in the Kohn-Sham equations. To get the new electron density, the self-consistent field (SCF) cycle uses the solution of the Kohn-Sham equations. When the electron charge density is calculated the system checks for convergence; if convergence is achieved, the system goes on to evaluate observables such as energy. If convergence is not achieved, the system starts all-over again using the last calculated value of the electron charge density as the initial value. This goes on until convergence is attained. In Quantum Espresso, the system terminates after a hundred trials are made without achieving convergence.

The SCF cycle has been successfully implemented in the Plane Wave Self-Consistence Field (PWSCF) code of the Quantum Espresso computer simulation package. In this work the SCF cycle has been used in Quantum Espresso to determine the band gaps of some ternary chalcopyrites and two binary chalcogenides ($AgGaS_2$, $AgGaSe_2$, $AgGaTe_2$, $CuGaS_2$, $CuInS_2$, $CuInSe_2$, $ZnSiAs_2$, $ZnSnAs_2$, PdS and PdSe).

3.1.2 DFT METHODS IN THE STUDY OF CHALCOPYRITES AND PLATINUM GROUP METAL CHALCOGENIDES

Electronic and ionic calculations are performed using the PWSCF code as implemented in Quantum Espresso after running an SCF cycle by executing a program called ***pw.x*** [36]. To execute ***pw.x*** one needs to write input files in a text editor which give out commands for the system to carry out the determination of convergence.

To perform band gap calculations and the plotting of band structures, Quantum Espresso has to execute three programs, namely***, pw.x, bands.x and plotband.x*** [36]. The structure

of the ***pw.x*** input files is made up of NAMELISTS and INPUT_CARDS. In the NAMELISTS there are three mandatory input files and these are:

- &CONTROL which is input variables that control the type of calculations performed and the amount of input/out.
- &SYSTEM, input variables which specify the system
- &ELECTRONS, these are input variables that control the algorithms used to reach a self-consistent solution of the Kohn-Sham equations.

The INPUT_CARDS also work with the three mandatory files below

- ATOMIC_SPECIES, which specifies the name, mass and pseudopotentials used for each species in the system.
- ATOMIC_POSITIONS, specify coordinates of each atom in the unit cell.
- ***K***-POINTS which provide coordinates and weights of the ***k***-points used for the Brillouin zones [51].

Sample ***pw.x*** input files for the LDA+U are presented in APPENDIX D. A summary of the procedure in the determination of band structures and density of states (DOS) in Quantum Espresso is presented in the block diagram in Fig. 3.1.2.

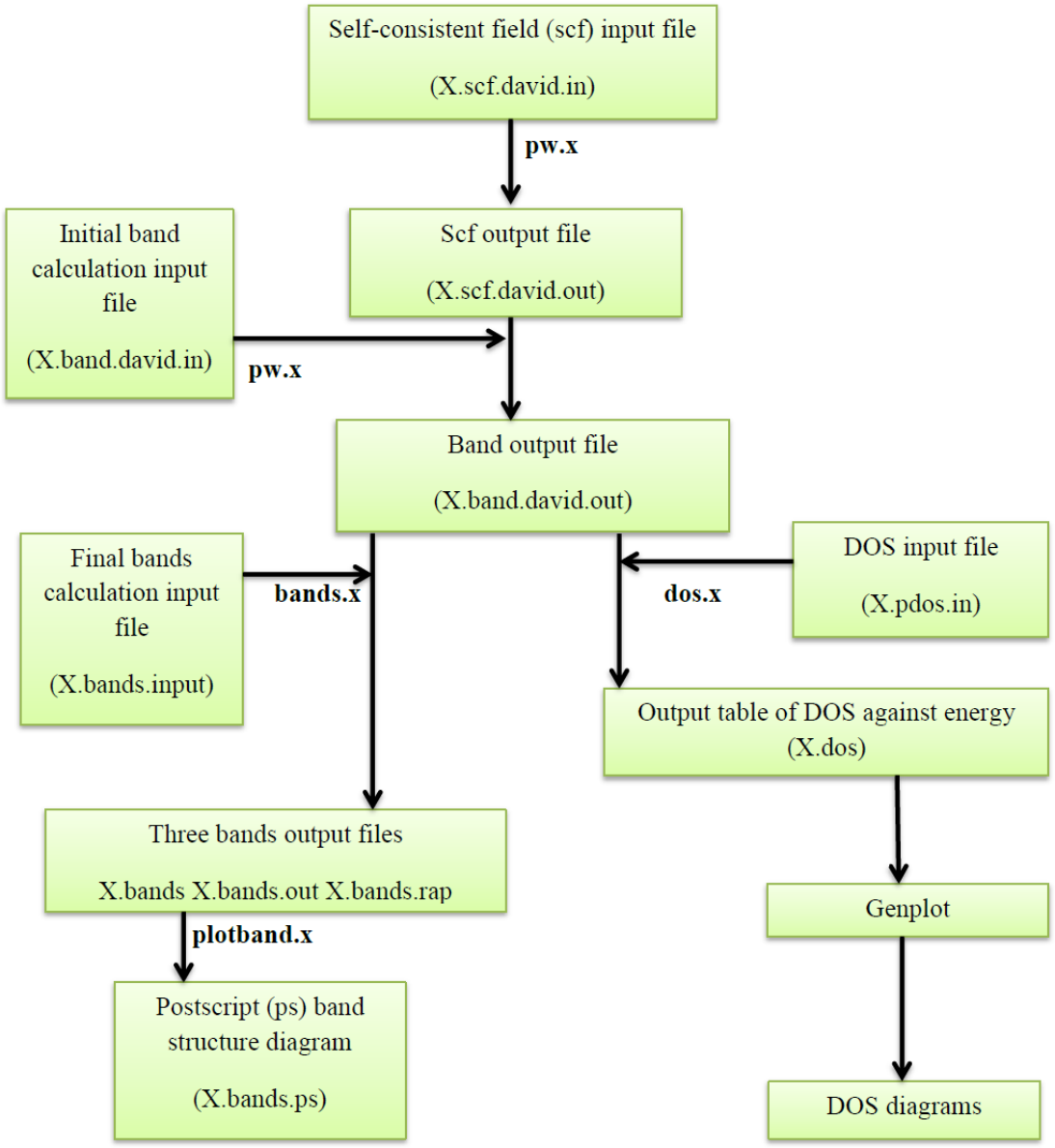

Figure 3.1.2: Block diagram for determination of band structure and density of states in quantum espresso.

The crystal structures of the materials under investigations were generated by use of PWSCF codes (input files) as implemented in the computer visualization package Xcrysden [36]. To produce the crystal structure diagrams, knowledge of the atomic positions of the materials being investigated is very important because the data has to be

used to run a self-consistent file (scf) input file. This information can be acquired from science data books [33]. In this work an adjustment was made for the doped chalcopyrites by replacing one cation atom with a dopant. This can be checked in Appendix D in the programmes labelled *band.david.in and scf.david.in* under ATOMI_POSITIONS. Xcrysden helps to check if the crystal structure is consistent with the expected structure. Thus to produce the crystal structure of materials, one has to prepare an SCF input file and run the SCF input file using Xcrysden. This procedure is outlined in the block diagram in Fig. 3.1.3

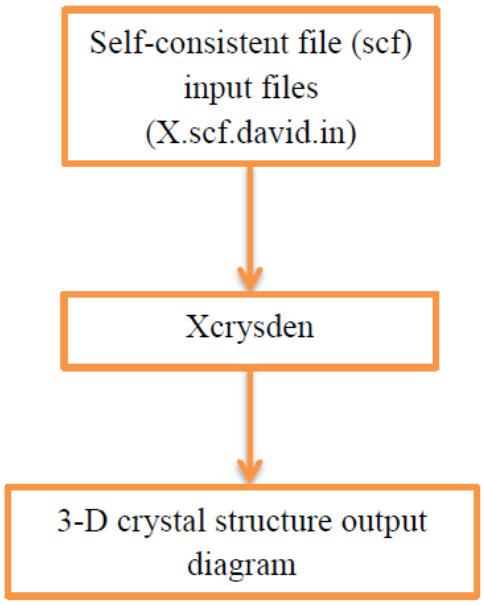

Figure 3.1.3: Xcrysden flow chart for producing crystal structures of materials.

CHAPTER 4 RESULTS AND ANALYSIS

4.1 STRUCTURAL PROPERTIES

4.1.1 LATTICE PARAMETER

By going through the process of total energy minimization per unit cell for the material under investigation whose crystal structure is known, the equilibrium lattice parameters can be evaluated. An SCF program in Quantum Espresso is used to determine the lattice parameter for which the energy is a minimum. In this work the process was only done for silicon to demonstrate how the lattice parameters are obtained using the principle of energy minimization. The lattice parameters used in this work for the chalcopyrites were obtained from available experimental data [28, 33, and 50]. To get a particular value, a series of values are plotted and at each point the energy is noted. A graph of energy versus lattice parameter is plotted. The graph which was obtained is shown in Fig. 4.1.1.

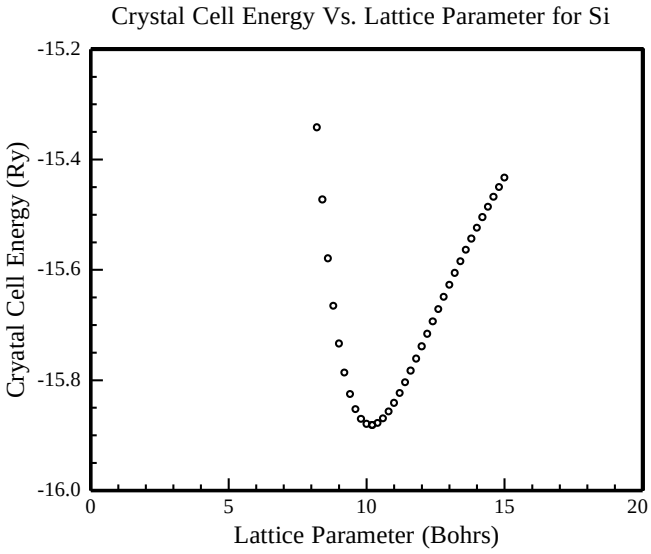

Figure 4.1.1: Lattice parameter, *a*, for silicon.

The equilibrium value of the lattice parameter *a* obtained at the point of minimum energy is about 10.2 Å. The experimental result often used in literature is 10.21Å [58]; the lattice

parameter value that is determined in this work matches the experimental value. It can therefore be said that the equilibrium lattice parameters for various crystal structures can be evaluated using this method of energy minimization.

4.1.2 PLANE WAVE CUT-OFF ENERGY

This work primarily involves electrons in a periodic lattice and Bloch's theorem is applicable to the electronic wave functions. Quantum Espresso makes use of wave functions that are a sum of plane waves of increasing energies in a periodic pseudo-potential. In practice the plane waves have to be truncated at the point where the lattice unit cell energy remains constant even as the plane-wave energy increases. The point at which this begins to occur is known as the plane-wave cut-off energy.

By means of the SCF program, the equilibrium lattice parameter *a* obtained from Fig. 4.1.1 was used to find the total lattice unit cell energy for various plane wave cutoff energies which were varied in intervals of 5.0 Ry beginning at 5.0 Ry up to 50.0 Ry. The results are plotted in Fig. 4.1.2.

The cut-off energy obtained from the above graph is 45.0 Ry. Most of the literature uses 15.0 Ry [56] but in view of our result from Fig. 4.1.2 we chose to use the value 45.0 Ry. Generally, the greater the value of the plane wave cut-off energy, the more accurate the results obtained for the lattice cell energy, because the calculation includes more terms in the summation of the plane waves. This helps to achieve smoother energy surfaces when calculating the band gap of materials. This however means that more computational time is required.

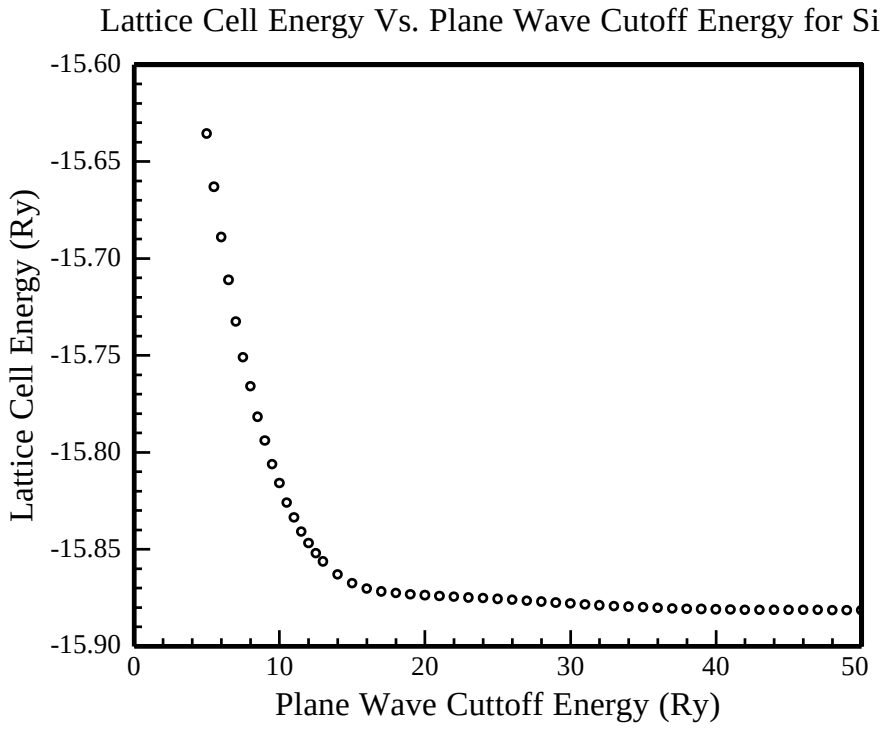

Figure 4.1.2: Total cell energy Cut-off energy for silicon.

4.1.3 BULK MODULUS

I. Chalcopyrites

Crystal structure diagrams were constructed for all the eight chalcopyrites using the Xcrysden software package. The results are presented in Appendix A.

Results obtained for the bulk modulus of the chalcopyrites investigated using Cohen's formula for both $\lambda = 1$ and $\lambda = 2$ are shown in Table 4.1.1. Experimental values were not available for three of the materials, as seen in the table.

Table 4.1.1: Results obtained for the bulk modulus of the chalcopyrites investigated, using Cohen's formula for both $\lambda = 1$ and $\lambda = 2$. Experimental values were not available for three of the materials as seen in the table.

Compound	Type of compound	a (Å)	Average interatomic distance, d (Å)	Bulk modulus, B using $\lambda = 1$ (GPa)	Bulk modulus, B using $\lambda = 2$ (GPa)	Experimental bulk modulus, B (GPa)
$AgGaS_2$	I-III-VI_2	5.74	2.486	72.3	63.2	77.6[37]
$AgGaSe_2$	I-III-VI_2	5.97	2.585	63.1	55.1	54.8[37]
$AgGaTe_2$	I-III-VI_2	6.28	2.719	52.8	46.2	38.9[38]
$CuGaS_2$	I-III-VI_2	5.347	2.315	92.8	81.1	-
$CuInS_2$	I-III-VI_2	5.523	2.392	82.7	72.3	75[39]
$CuInSe_2$	I-III-VI_2	5.781	2.503	70.6	61.7	72[39]
$ZnSiAs_2$	II-IV-V_2	5.606	2.428	78.5	68.7	-
$ZnSnAs_2$	II-IV-V_2	5.852	2.534	67.6	59.1	-

It was mentioned in Section 2.4.4 that λ is expected to have the values of 1 and 2 for Groups I-III-VI_2 and II-IV-V_2 respectively. However a comparison of our results with experimental results shows that there are a few exceptions to this rule. Table 4.1.2 picks the value of B for either $\lambda = 1$ and $\lambda = 2$ depending on which λ gives a corresponding value of B which is closest to the experimental value and shows the errors calculated. A blank is left in cases where no experimental value is available.

Table 4.1.2: Error calculations, where experimental values were available, for the results obtained of the bulk modulus for the chalcopyrites investigated.

Compound	*a* (Å)	Average interatomic distance, *d* (Å)	Bulk modulus, *B* by the Cohen's formula (GPa)	Error in the Cohen method (GPa)	Percentage error in the Cohen method	Experimental results of the bulk modulus, *B* (GPa)
$AgGaS_2$	5.74	2.486	72.3	5.3	6.8	77.6[37]
$AgGaSe_2$	5.97	2.585	55.1	0.3	0.6	54.8[37]
$AgGaTe_2$	6.28	2.719	46.2	7.3	18.8	38.9[38]
$CuGaS_2$	5.347	2.315	-	-	-	-
$CuInS_2$	5.523	2.392	72.3	2.7	3.6	75[39]
$CuInSe_2$	5.781	2.503	70.6	1.4	1.9	72[39]
$ZnSiAs_2$	5.606	2.428	-	-	-	-
$ZnSnAs_2$	5.852	2.534	-	-	-	-

Using data given in Table 4.1.2 the average error in our results for the bulk modulus for chalcopyrites is found to be 6.3 %. This result shows that the computed bulk modulus values are within the range of experimentally determined values and as such this technique can be extended to other chalcopyrite materials with undetermined bulk modulus values.

Table 4.1.3: Results obtained for the bulk modulus of the chalcopyrites investigated using Cohen's formula. This table picks the value of λ which gives a corresponding value of *B* closest to the experimental value. A blank is left in cases where no experimental value is available.

Compound	Type of compound	Average interatomic distance, *d* (Å)	Theoretical bulk modulus, *B* (GPa)	Experimental bulk modulus B (GPa)	Value of λ used
$AgGaS_2$	I-III-VI_2	2.486	72.3	77.6[37]	1
$AgGaSe_2$	I-III-VI_2	2.585	55.1	54.8[37]	2
$AgGaTe_2$	I-III-VI_2	2.719	46.2	38.9[38]	2
$CuGaS_2$	I-III-VI_2	2.315	-	-	-
$CuInS_2$	I-III-VI_2	2.392	72.3	75[39]	2
$CuInSe_2$	I-III-VI_2	2.503	70.6	72[39]	1
$ZnSiAs_2$	II-IV-V_2	2.428	-	-	-
$ZnSnAs_2$	II-IV-V_2	2.534	-	-	-

Table 4.1.3 is derived from Table 4.1.2. This picks the value of λ which gives a corresponding value of *B* which is closest to the experimental value. A blank is left in cases where no experimental value is available. We see that the bulk modulus values of the chalcopyrites of the type I-III-VI_2 are better determined using λ=2 rather than λ=1. Our theoretical predictions for the bulk modulus values of the three chalcopyrite materials where no experimental results were available are given in Table 4.1.4

Table 4.1.4: Theoretical predictions for the bulk modulus values of chalcopyrite material where no experimental results are available.

Compound	Type of compound	*a* (Å)	Average interatomic distance, *d* (Å)	Predicted values of the bulk modulus in GPa
$CuGaS_2$	I-III-VI_2	5.347	2.315	Close to or within the range: 81.1 to 92.8
$ZnSiAs_2$	II-IV-V_2	5.606	2.428	Close to or within the range: 68.7 to 78.5
$ZnSnAs_2$	II-IV-V_2	5.852	2.534	Close to or within the range: 59.1 to 67.6

II. Chalcogenides

The two binary chalcogenides PdSe and PdS were investigated. The results obtained for the bulk modulus, using Cohen's formula (as explained in section 2.4.4) for both $\lambda = 1$ and $\lambda = 2$, are presented in Table 4.1.5. Experimental values were not available for both materials.

Table 4.1.5: Results obtained for the bulk modulus for the chalcogenides investigated, using Cohen's formula for both $\lambda = 1$ and $\lambda = 2$. Experimental values were not available.

Compound	*a* (Å)	Average interatomic distance, *d* (Å)	Bulk modulus, *B* using $\lambda = 1$ (GPa)	Bulk modulus, *B* using $\lambda = 2$ (GPa)
PdS	6.711[44]	2.906	41.9	36.6
PdSe	6.429[44]	2.784	48.6	42.5

4.2 ELECTRONIC PROPERTIES

4.2.1 ELECTRONIC BAND STRUCTURE

The eight ternary chalcopyrites and two binary chalcogenides which were investigated to determine their bulk modulus were also investigated to determine their electronic band structure. The band structure calculation method was first tested on silicon because the band structure of silicon has been well documented in the literature [40].

I. Silicon

To study the electronic band structure of silicon both the LDA and GGA were employed. The calculations were carried out with a plane wave cutoff energy of 45.0 Ry. The chalcopyrite structure is a derivative of the zinc-blende structure. The direction of the $\boldsymbol{k_z}$ axis of the first Brillouin zone of the chalcopyrite structure coincides with that for the first Brillouin zone of the zinc blende structure. The shapes of the two Brillouin zones are similar and their $\boldsymbol{k_x}$-$\boldsymbol{k_y}$ planes are co-planar with a rotational displacement as shown in Fig. 2.5.5. It is common to calculate the band structure of chalcopyrites in the zinc-blende Brillouin zone, which is the approach used in this work. The $\boldsymbol{k}$-space path that we used in the first Brillouin zone of the zinc blende crystal structures is $\Gamma \to L \to \Gamma \to X \to W \to K \to \Gamma$, as indicated in section 2.5. The electronic band structure diagrams for silicon as obtained using LDA and GGA exchange correlation functionals are shown in the Fig. 4.2.1 and Fig. 4.2.2 respectively. These two diagrams are electronic band structure diagrams which show that the valence band is very close to the conduction band. This implies that only a small amount of energy is needed to promote an electron from the valence band to the conduction band.

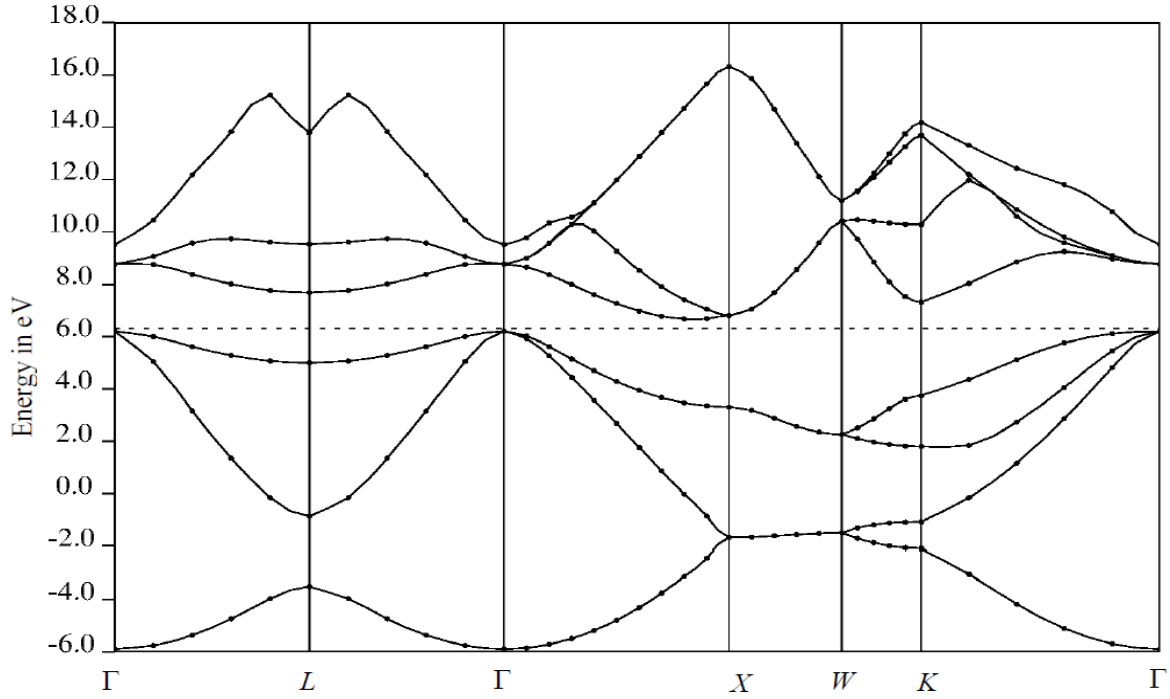

Figure 4.2.1: Band structure for silicon by LDA.

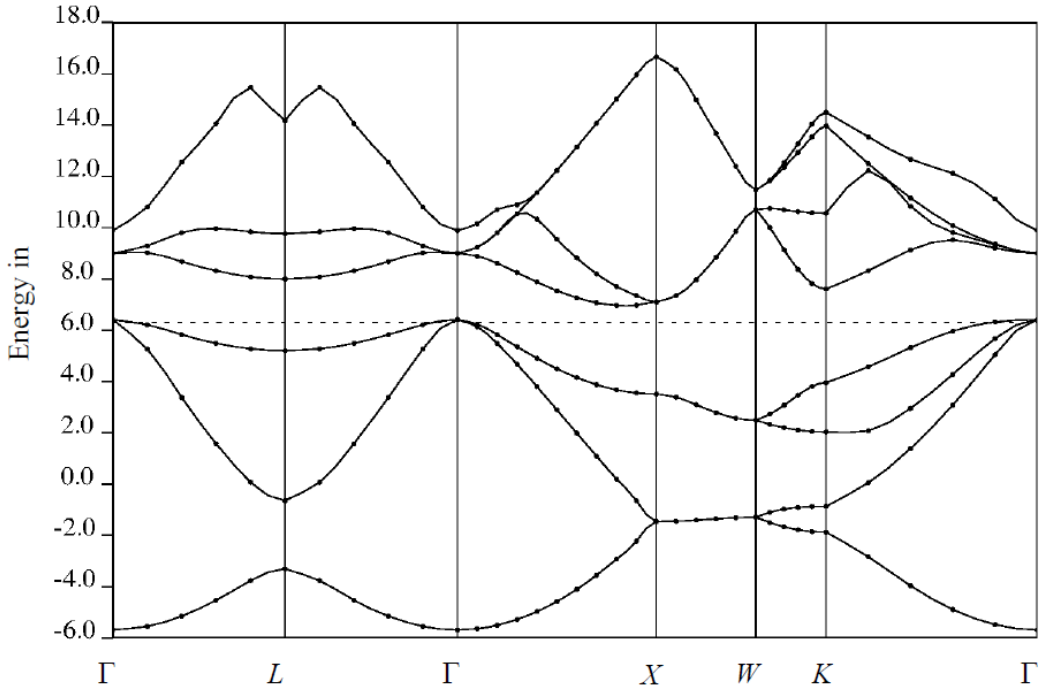

Figure 4.2.2: Si band structure diagram by GGA.

The electronic band structure diagrams in Figures 4.1.1 and 4.2.2 show that for silicon, the GGA functional performs better than the LDA. The LDA functional gives the value of E_g to be about 0.6 eV whereas the GGA functional gives the value of E_g to be about 0.9 eV. This shows that the GGA functional gives the band gap to be quite close to the experimental value of 1.1eV. This information is summarized in Table 4.2.1.

Table 4.2.1: Band structure results for silicon using LDA and GGA functionals.

Element	E_g (LDA) eV	E_g(GGA) eV	Experimental Value (eV)	Absolute error (eV)
Si	0.6	0.9	1.1[40]	0.2

Table 4.2.1 shows that the GGA functional method, with an error of 0.2 eV, is good enough for electronic band structure calculations for elemental semiconductors.

II. Chalcopyrites

The same type of electronic band structure calculations as those done for silicon were then carried out for the eight chalcopyrites, which are more strongly correlated materials. The calculations were carried out using LDA and GGA functionals but the results from these two exchange correlation functionals underestimated the values of the band gaps when compared to data obtained experimentally by other researchers. Due to the poor results obtained by using the LDA and GGA functionals, more investigations were carried out using the LDA+U and the empirical shift methods described in sections 2.2.4 and 2.5.1 respectively. These techniques present a new way of handling the poor results obtained with other techniques. We first present the results obtained for electronic band

structure for these chalcopyrites by looking at the band structure and density of states diagrams for each chalcopyrite being investigated. Since the band structures derived from the LDA and GGA functionals were very similar, we have not included the band structure diagrams obtained using the GGA functionals but the GGA results are summarized in Table 4.2.2. Only some representative LDA and LDA+U results of both band structure and density of states (DOS) diagrams are presented here. More of the band structure and density of states diagrams obtained are presented in Appendix B.

The first set of diagrams (Figs. 4.2.1, 4.2.5, 4.2.9) of each chalcopyrite material presented gives an electronic band diagram followed by the density of state diagram (Figs. 4.2.2, 4.2.6, 4.2.10) produced with the application of the LDA exchange correlation functional. The second set of diagrams (Figs. 4.2.3, 4.2.7, 4.2.11) gives the electronic energy band and density of state diagrams (Fig. 4.2.4, 4.2.8, 4.2.12) with the utilization of the LDA+U energy functional. The density of states diagram gives a representation of the number of electronic states per unit volume for electron energies. What must be kept in mind is that materials have infinitely many energy levels and band gaps in their band structure; however, the most relevant bands and band gaps - those important for photovoltaics, electronics and optoelectronics - are those with energies near the Fermi level. In our band structure plots, the Fermi level for almost all the materials investigated is set to zero. We note that with the application of LDA, most of the chalcopyrite materials give an almost zero energy band gap between the valence band and the conduction band. When LDA+U was applied, we noted that a relatively good energy band gap opens up between the valence band and the conduction band. The density of states reveals the distribution of electronic states by showing that with LDA+U, a gap opens up between the two bands.

This is due to the increase in the electron-electron repulsive forces that is brought about by the U term.

I. $AgGaS_2$

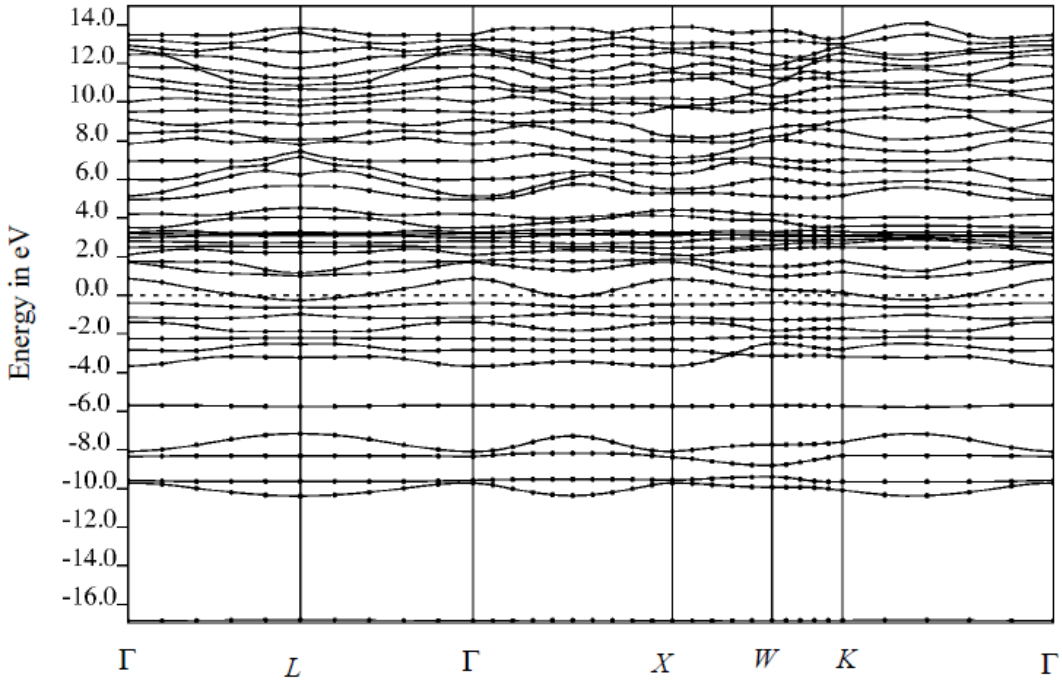

Figure 4.2.1: Band structure for $AgGaS_2$ by LDA. The origin of the energy axis lies slightly above the Fermi level.

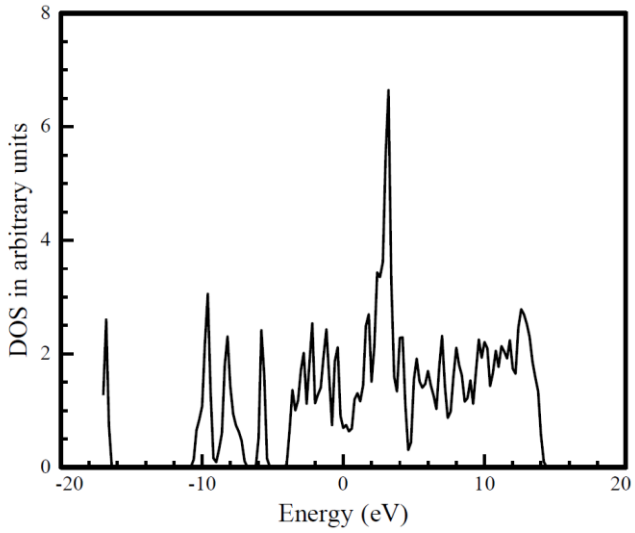

Figure 4.2.2: Density of states (DOS) diagram for $AgGaS_2$ by LDA.

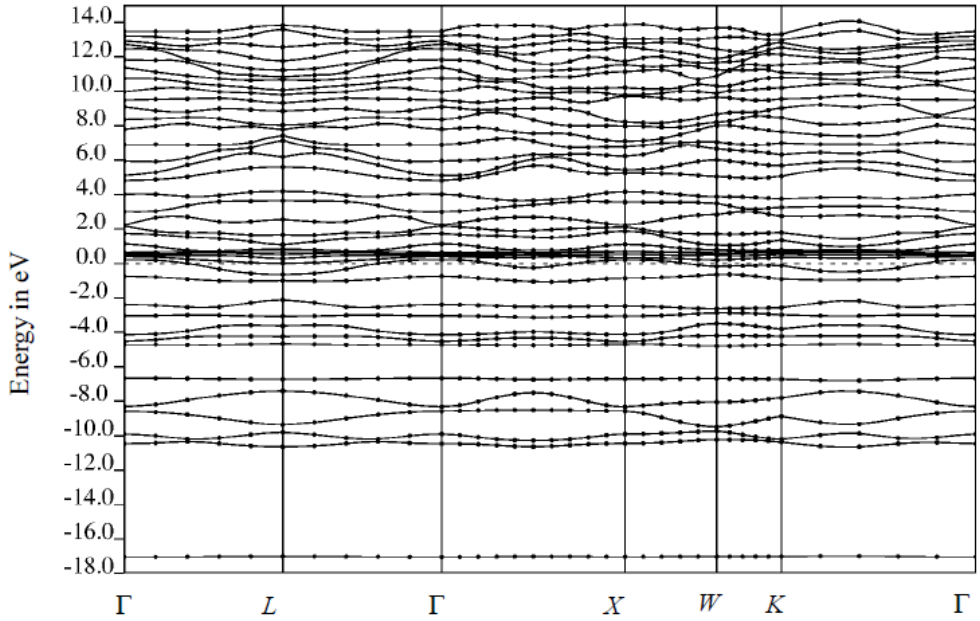

Figure 4.2.3 Band Structure of AgGaS2 by LDA+U. The origin of the energy axis lies slightly above the Fermi level.

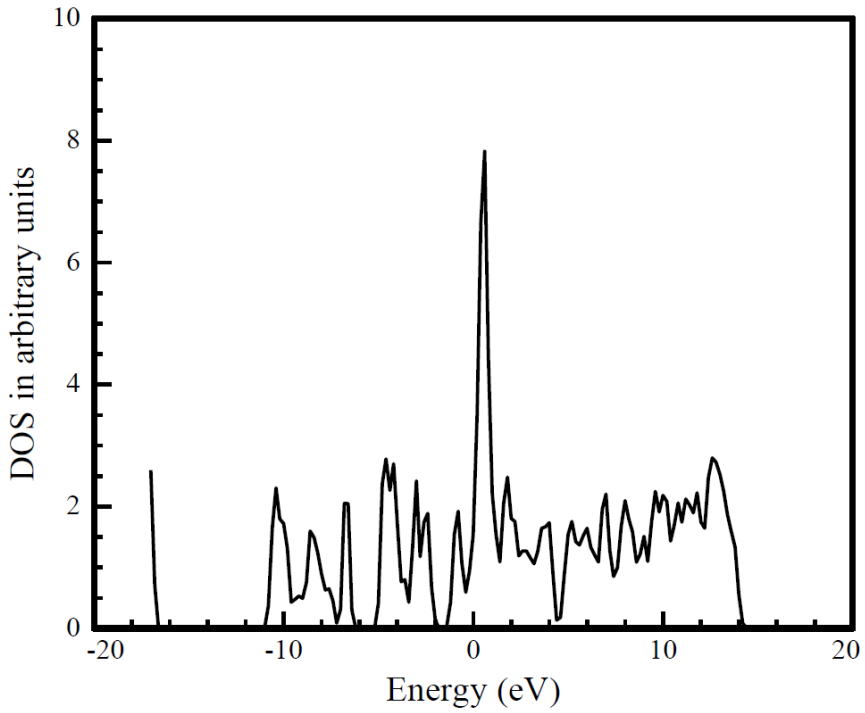

Figure 4.2.4 DOS diagram for AgGaS2 by LDA+U.

The results obtained using LDA and GGA functionals were similar and showed very small band gaps for the chalcopyrite $AgGaS_2$, as can be observed from the LDA electronic band structure and DOS diagrams in Fig. 4.2.1 and Fig. 4.2.2. There is almost no gap between the valence band and the conduction band. The value of E_g was effectively zero, indicating that the exchange-correlational functional predicted $AgGaS_2$ to be a conductor while experimental results indicate that this material is a semiconductor. Fig. 4.2.3 and Fig. 4.2.4 obtained by the application of the LDA+U show a significant improvement in the band gap value obtained. The LDA+U method gives an E_g value of 1.2 eV. It can be seen that an energy gap opens up between -1.0 and -2.0eV in the LDA+U method. This was achieved by using a Hubbard U value of 5.0.

I. $AgGaSe_2$

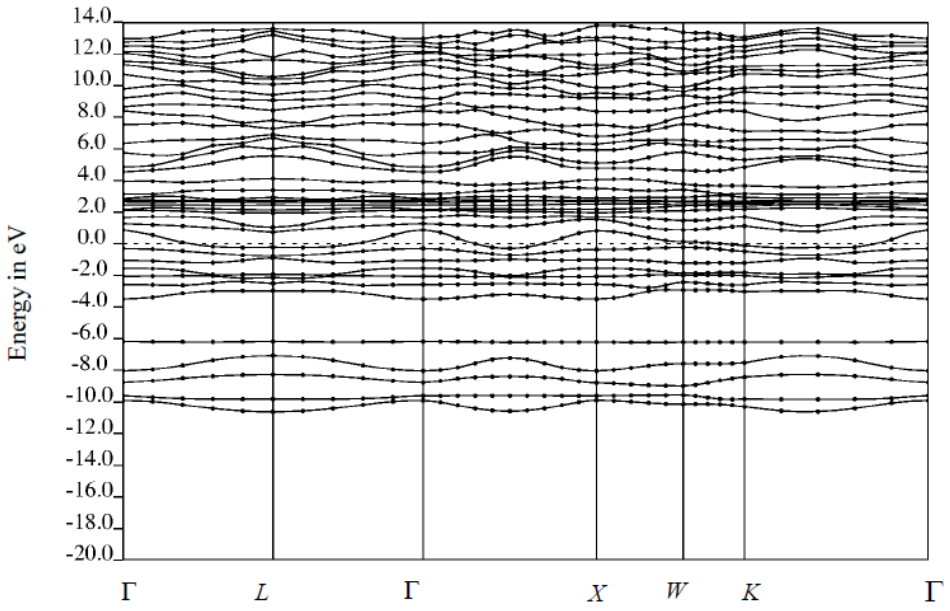

Figure 4.2.5: Band structure of $AgGaSe_2$ by LDA. The origin of the energy axis lies slightly above the Fermi level

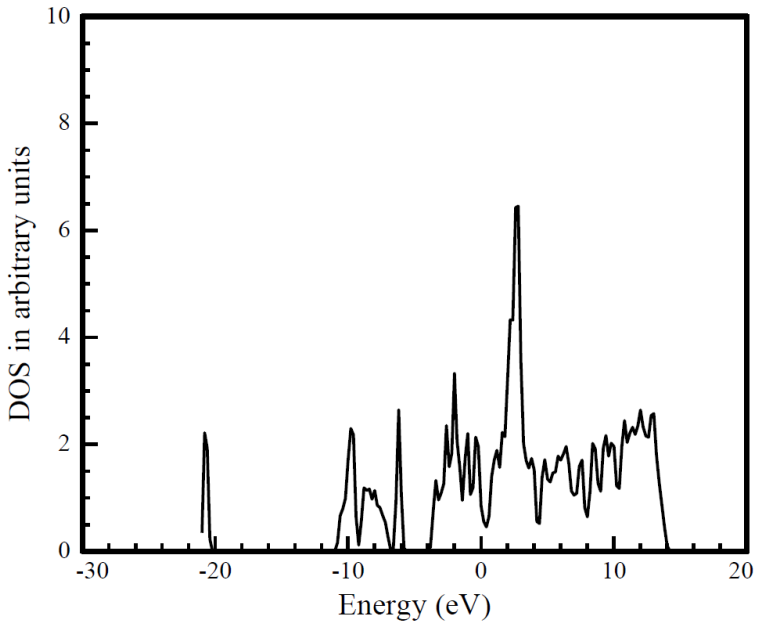

Figure 4.2.6: DOS diagram for $AgGaSe_2$ by LDA.

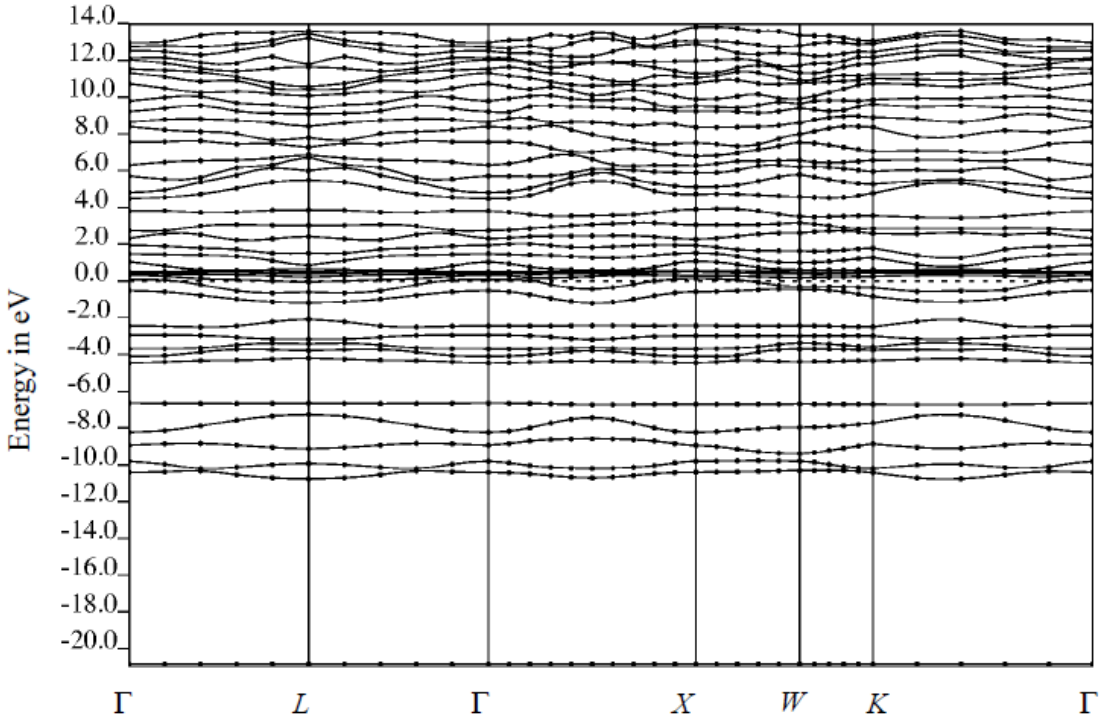

Figure 4.2.7: Band Structure of $AgGaSe_2$ by LDA+U. The origin of the energy axis lies slightly above the Fermi level.

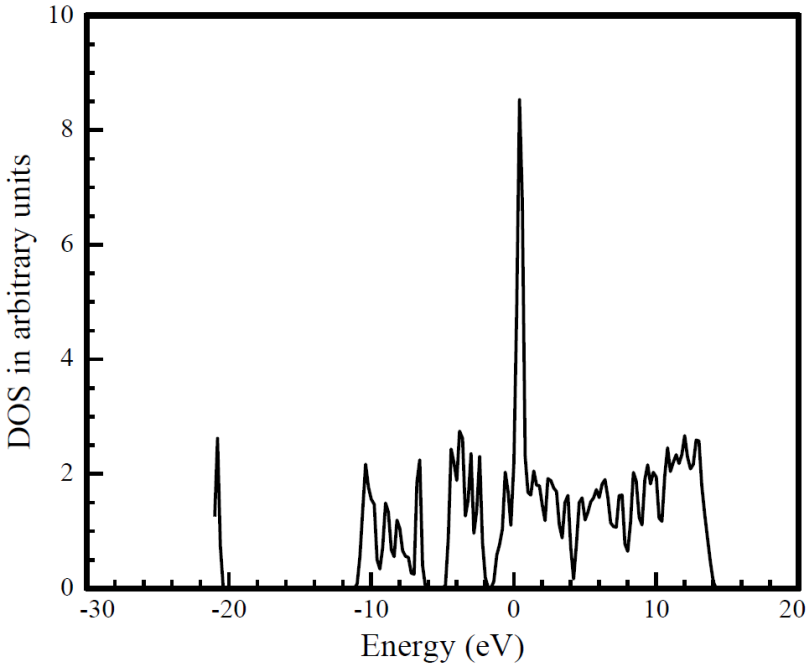

Figure 4.2.8: DOS diagram for $AgGaSe_{2\ by}$ LDA+U.

The LDA exchange correlational functional and the LDA+U method results for $AgGaSe_2$ are presented in the diagrams Fig. 4.2.5 to Fig. 4.2.8. The E_g values obtained by use of the LDA and GGA (diagram not included) exchange correlational functionals were close to zero. A small band gap opened up with an energy width of between -1.0 and -0.2eV when the LDA+U was applied. It was determined that the E_g value obtained was approximately 1.2 eV. This value is very close to the value obtained by other researchers using experimental investigations.

I. $AgGaTe_2$

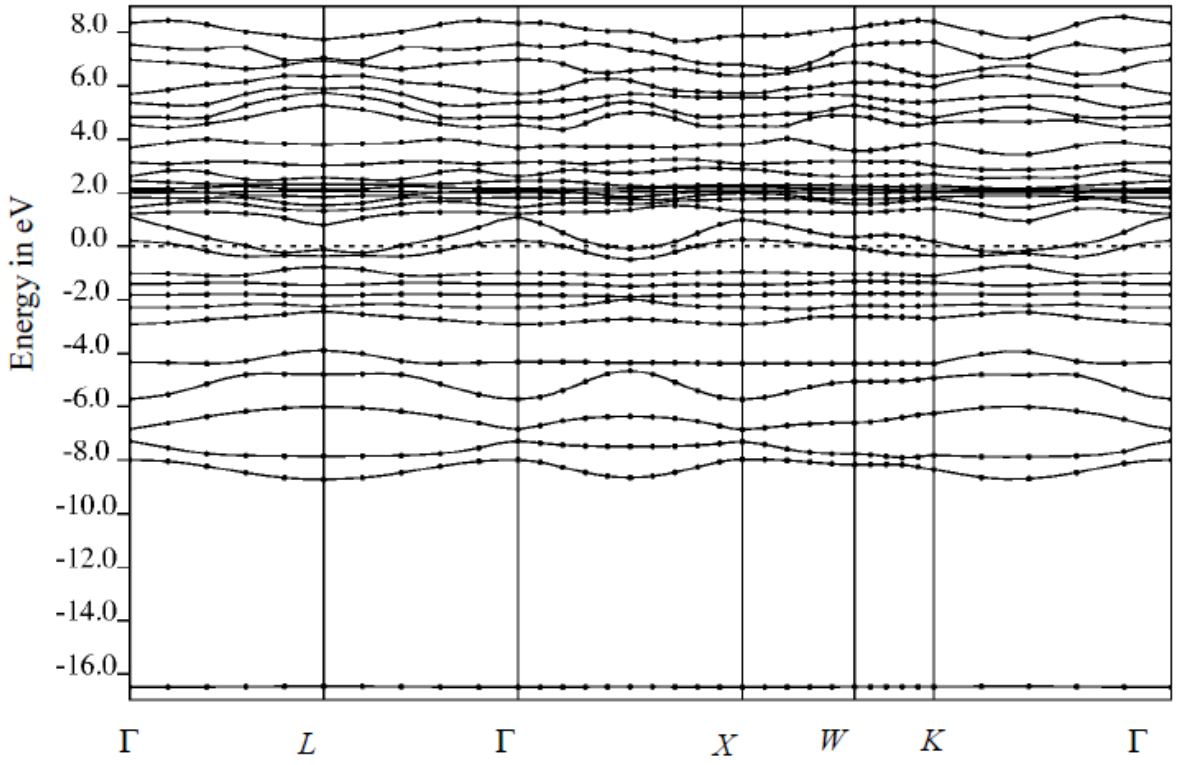

Figure 4.2.9: Band structure of $AgGaTe_2$ obtained by use of LDA. The origin of the energy axis lies slightly above the Fermi level.

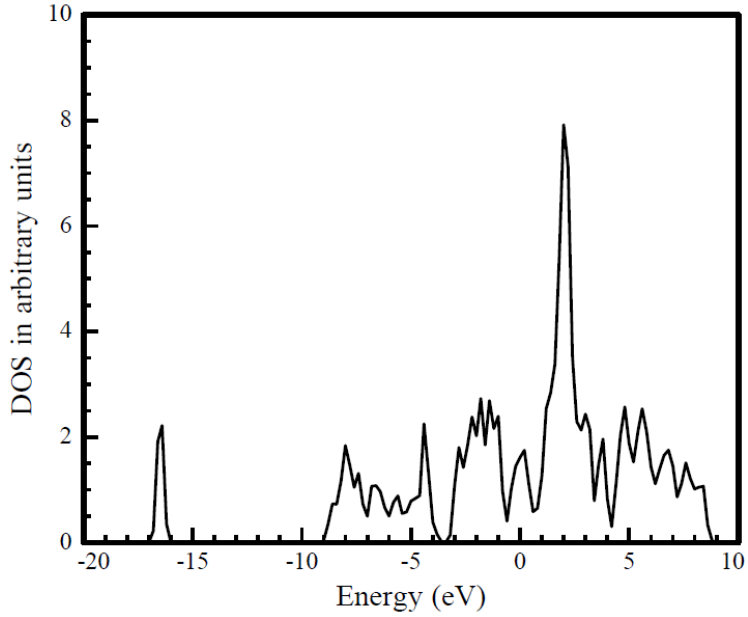

Figure 4.2.10: DOS diagram for $AgGaTe_2$ from LDA.

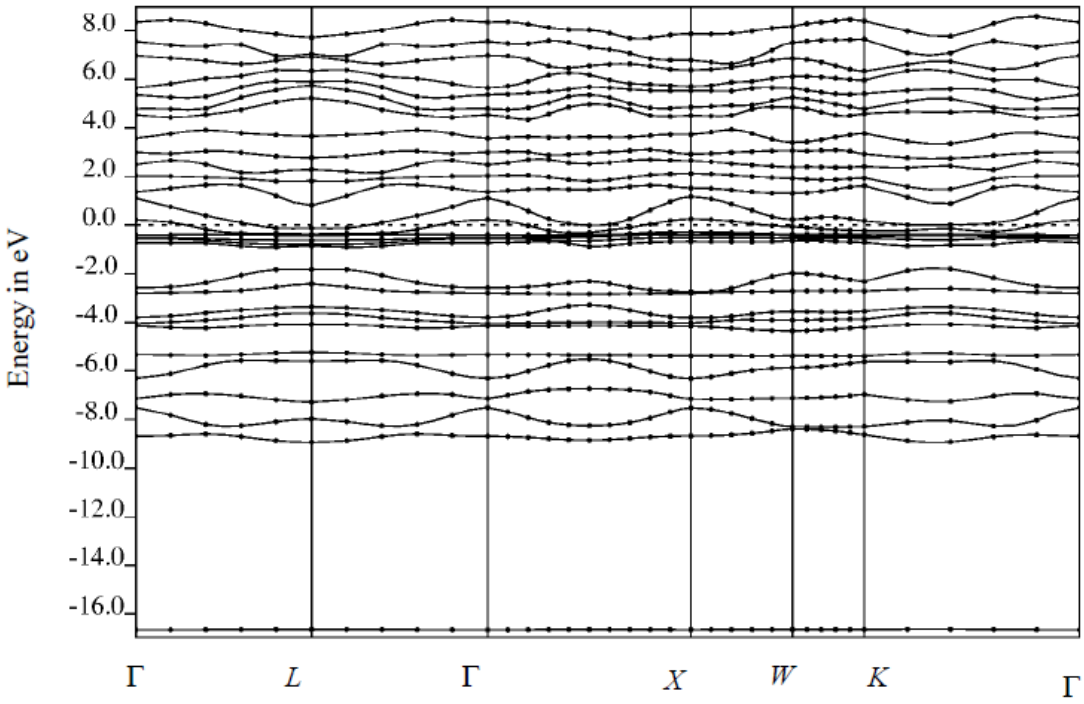

Figure 4.2.11: Band structure of $AgGaTe_2$ by use of LDA+U. The origin of the energy axis lies slightly above the Fermi level.

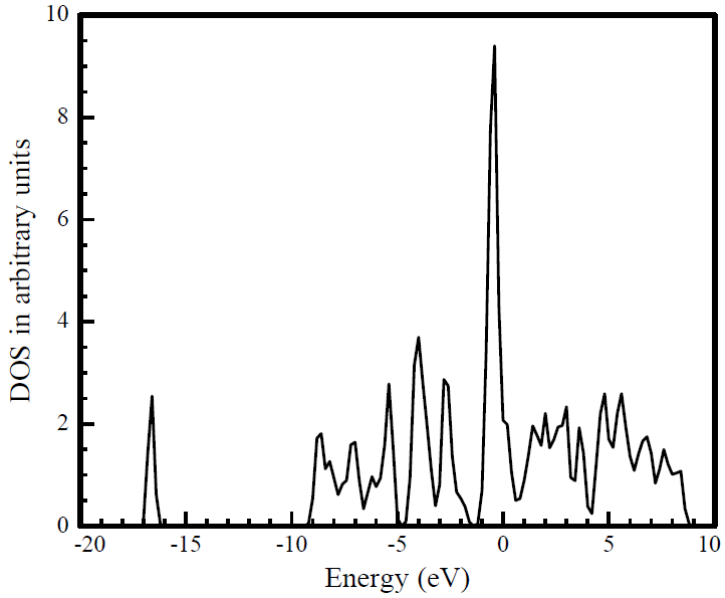

Figure 4.2.12: DOS diagram for $AgGaTe_2$ obtained by LDA+U.

Figures 4.2.9 and 4.2.10 show that the LDA functional gives an E_g value of 0.2 eV for $AgGaTe_2$. This extremely small gap is between 0.0 eV and -1.0 eV. When LDA+U was

employed the value of E_g improved to 1.2 eV as can be seen in Fig. 4.2.11 and Fig. 4.2.12.

Table 4.2.2 gives a compilation of the results from the LDA and GGA functional methods. Experimental values are included for comparison; two experimental values were not available.

Table 4.2.2: LDA and GGA electronic band gap results for chalcopyrites.

S/No	Compound	a(Å)	c/a(Å)	μ	E_g(LDA) (eV)	E_g(GGA) (eV)	Expt. E_g (eV)	% error
1.	$AgGaS_2$	5.74	1.78	0.309	0.00	0.00	2.70[41]	∞
2.	$AgGaSe_2$	5.97	1.82	0.301	0.00	0.10	1.85[42]	1750
3.	$AgGaTe_2$	6.28	1.895	0.277	0.15	0.25	1.3[43]	351
4.	$CuGaS_2$	5.347	1.953	0.262	0.00	0.00	1.67[44]	∞
5.	$CuInS_2$	5.523	2.014	0.46	0.15	0.10	1.5[45]	1400
6.	$CuInSe_2$	5.781	2.064	0.234	0.40	0.50	1.04[45]	108
7.	$ZnSiAs_2$	5.606	1.943	0.265	0.00	0.00	-	-
8.	$ZnSnAs_2$	5.852	2.00	0.250	0.00	0.00	-	-

As explained in section 2.5.1 the reason for the band gap underestimation by the LDA and GGA correlation functional for strongly correlated systems is that the Kohn-Sham one-particle equation (12) does not provide quasiparticle excitation energies. This phenomenon is the reason for the very poor results obtained for the energy band gaps as can be observed in Table 4.2.2. Another reason is that the GGA and LDA exchange-

correlation functionals have a tendency to over-delocalise the electrons. To remedy this extreme under estimation, the Hubbard-U-like term is added on to the d-orbital, which increases the electron-electron repulsive interaction as shown by the results obtained in Table 4.2.3.

Table 4.2.3: LDA+U and empirical shift electronic band gap results for chalcopyrites.

Compound	LDA E_g (eV)	LDA+U E_g (eV)	Error in LDA+U (eV)	LDA Empirically shifted E_g (eV)	Error in LDA Empirical shift (eV)	Experimental value (eV)	% error
$AgGaS_2$	0	1.2	1.5	1.9	0.8	2.70[41]	42
$AgGaSe_2$	0	1.2	0.7	1.9	0.1	1.85[42]	2.6
$AgGaTe_2$	0.15	1.2	0.1	2.1	0.8	1.3[43]	3.8
$CuGaS_2$	0.0	1.6	0.1	1.9	0.2	1.67[44]	12
$CuInS_2$	0.15	inconclusive	inconclusive	2.1	0.6	1.5[43]	29
$CuInSe_2$	0.4	inconclusive	inconclusive	2.3	1.3	1.04[45]	55
$ZnSiAs_2$	0.0	0.0	-	1.9	-	-	-
$ZnSnAs_2$	0.0	0.2	-	1.9	-	-	-

The results of the LDA+U method and Jiang's upward empirical shift of 0.14 Ry, described in section 2.5.1, are shown in Table 4.2.3. Errors with reference to experimental values are also included. Two results for the LDA+U method were inconclusive. The average error in LDA+U method was 0.6 eV while that in the empirical

shift was 0.63 eV. The calculated average error is 24.4%, which seems large. However, it should be noted that these materials are calculated to behave as semiconductors. This is in agreement with experimental findings that these materials are semiconducting. It is observed that the percentage error is not uniform even with the introduction of the Hubbard U term in the LDA formulation. This is due to the fact that the chalcopyrite materials do not have the same percentage of the d-bonding characteristic [55]. For example among the following chalcopyrite materials $CuGaS_2$, $CuInS_2$, $CuInSe_2$, and $CuAlS_2$, only $CuInS_2$ was found to possess the largest d-character bonding characteristics [55].

III. Chalcogenides

In contrast to the LDA and GGA functional results of the ternary chalcopyrites, the LDA exchange correlation functional tended to overestimate the band gap for the binary chalcogenides. This can be seen in Fig. 4.2.13 and Fig. 4.2.14. The results obtained show that PdS and PdSe have very large band gaps of about 5 eV. This magnitude of energy band gap is associated with insulators, whereas PdS and PdSe have been experimentally identified to be semi-conductors. This size of gap between the valence band and the conduction band is too big for electrons to acquire sufficient energy to be promoted from the valence band to the conduction band.

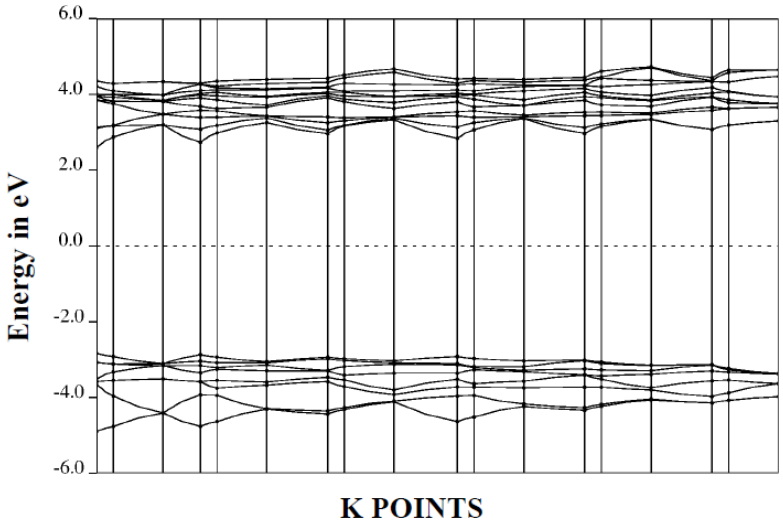

Figure 4.2.13: Band Structure of PdS. The origin of the energy axis lies slightly above the Fermi level.

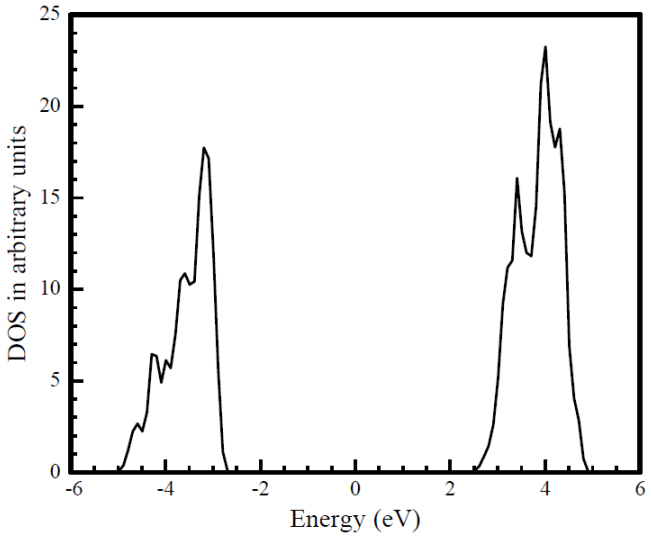

Figure 4.2.14: A density of states versus energy diagram for PdS.

In order to improve these results, Jiang's downward empirical shift of 0.21 Ry as described in section 2.5.1 was applied. The results are shown in Table 4.2.4.

Table 4.2.4: Electronic Band Gap for Chalcogenides.

Compound	LDA E_g (eV)	Empirically shifted E_g (eV)	Experimental value (eV)
PdS	5.8	2.9	2.0 - 3.0 [46]
PdSe	5.9	3.0	2.0 - 3.0 [46]

The LDA+U method was not employed in the study of the two binary chalcogenides.

4.3 IMPURITY PROPERTIES

4.3.1 CALCULATIONS OF THE ENERGY OF FORMATION, $E_{F,}$ OF IMPURITIES.

Impurity properties of the chalcopyrites were also investigated. Our methods were first tested on silicon, the most extensively studied semiconducting material.

I. Silicon

We determine the energy of formation of a single Si vacancy and an arsenic (As) donor impurity. Figs. 4.3.1 (a), (b) and (c) show conventional unit cells of pure Si, Si with a vacancy at the position (0.250, 0.250, 0.250) and Si with an As donor impurity at the position (0.250, 0.250, 0.250) respectively.

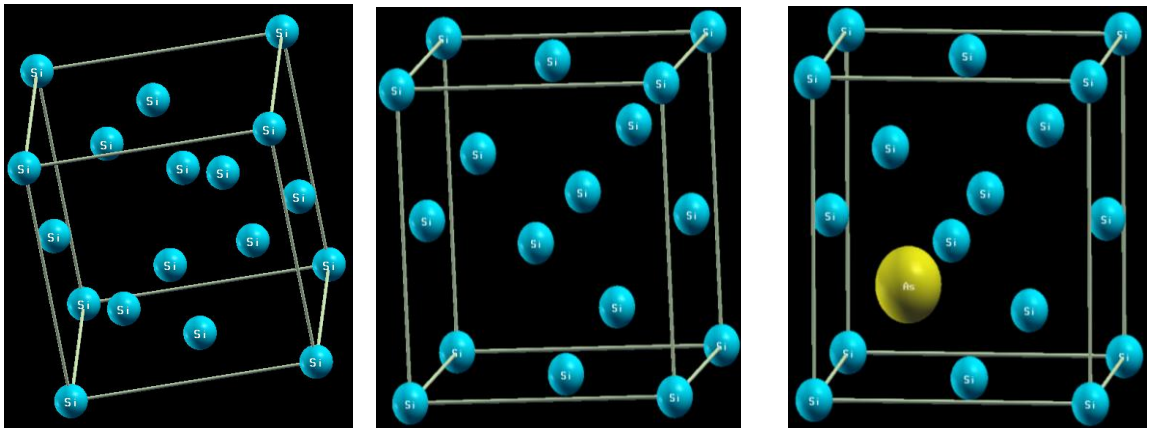

(a) **(b)** **(c)**

Figure 4.3.1: (a) Pure silicon (b) Silicon with a vacancy at (0.250, 0.250, 0.250) (c) Silicon with Arsenic (As) donor impurity at (0.250, 0.250, 0.250).

For a material with *n* vacancies, we used the following expression to determine the energy of formation E_f:

$$E_f = E_{tot}[N-n;n] - \frac{N-n}{N} E_{tot}[N;0] \quad (47)$$

For silicon and any material with *n* dopants, the following expression was used:

$$E_f = E_{tot}[N;n] - E_{tot}[N;0] \quad (48)$$

In the two expressions above, N is the total number of atoms per unit cell while E_{tot} is the total energy per unit cell as determined by the Quantum Espresso software. $E_{tot}[N;0]$ is the energy before creating a vacancy or vacancies; it is obtained after performing a self-consistent field (SCF) energy calculation on the material under investigation using the Quantum Espresso software package. The $E_{tot}[N\text{-}n;n]$ is the total energy obtained from the SCF output file of a defect material. This value is obtained after carrying out a relaxation operation on the unit cell structure, that is to say that the atomic positions were allowed to self-adjust according to the determined interatomic forces, until equilibrium of

the system was achieved. $E_{tot}[N;n]$ is the energy per unit cell of the doped material and was also obtained from an SCF calculation coupled with a relaxation operation. The results for silicon are shown in Table 4.3.1.

Table 4.3.1: Energy of Formation Results for Silicon.

Element	Our E_f results (eV)	Other E_f work (eV)	E_f error
Si with one vacancy per unit cell	3.33	3.17 [47]-3.6 [48]	5.05% - 7.5%
Si with one As donor per unit cell	4.77	-	-

The maximum error in our method when used for silicon was 7.5 %.

II. Chalcopyrites

Energy of formation of Cu vacancies and Ag impurities at four (0.500, 0.000, 0.250) positions in $CuInSe_2$ was calculated. Similar calculations were carried out for other chalcopyrites. The crystal structures of CuInSe2 and $CuInSe_2$ with vacancy defects and of $CuInSe_2$ with Ag dopant impurities, as generated using the Xcrysden software, are shown in Fig. 4.3.2. In this work $AgGaS_2$ and $CuGaS_2$ are doped with lithium (Li). $CuInS_2$ and $CuInSe_2$ are doped with Ag while $ZnSiAs_2$ and $ZnSnAs_2$ are doped with berylium (Be), while $AgGaSe_2$ is doped with Cu as shown in Table 4.3.3.

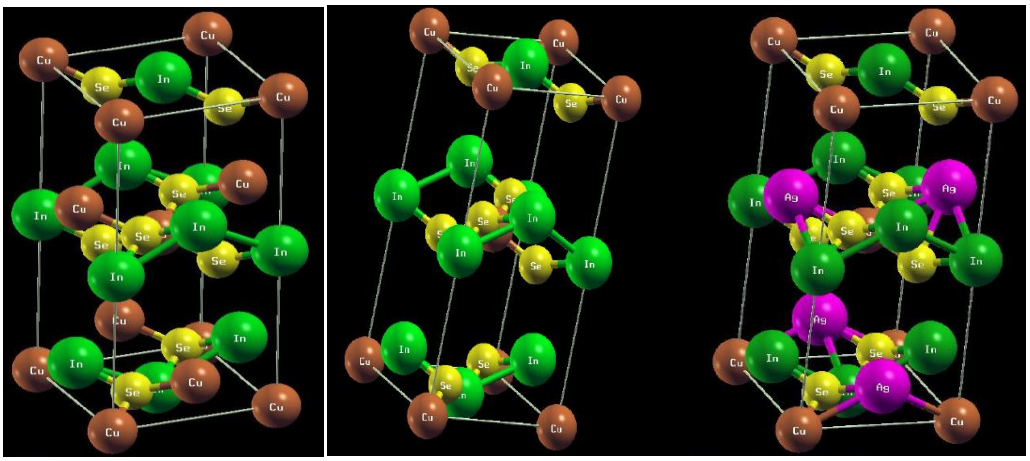

Figure 4.3.2: Pure, Defect and doped $CuInSe_2$.

Energy of formation results for vacancy defects are presented in Table 4.3.2.

Table 4.3.2 : Energy of Formation for vacancy Defect Chalcopyrites.

Chalcopyrite (4 vacancies)	Our E_f Results (eV)
$AgGaS_2$	-47.82 Ry
$AgGaSe_2$	-46.745Ry
$CuGaS_2$	-47.045Ry
$CuInS_2$	-75.435Ry
$CuInSe_2$	-72.88Ry
$ZnSiAs_2$	-35.34Ry
$ZnSnAs_2$	-59.284Ry

Energy of formation results for dopant defects are presented in Table 4.3.3.

Table 4.3.3 : Energy of Formation for Doped Chalcopyrites.

Chalcopyrite (Doped)	Dopant	Our E_f Results (eV)
$AgGaS_2$	Li	67.00Ry
$AgGaSe_2$	Cu	-23.649Ry
$CuGaS_2$	Li	87.01Ry
$CuInS_2$	Ag	14.28Ry
$CuInSe_2$	Ag	13.56Ry
$ZnSiAs_2$	Be	103.42Ry
$ZnSnAs_2$	Be	54.012Ry

Details of the energy of formation calculations are presented in Appendix C.

CHAPTER 5 DISCUSSION AND CONCLUSION

To compute the bulk modulus we have used the values we have determined of the average neighbour distance *d* in Cohen's formula. The value of λ is expected to be 1 and 2 for Groups I-III-$VI_2$and II-IV-V_2 respectively as was mentioned in Section 2.4.4. However a comparison of our results with experimental results shows that there are a few exceptions to this rule. In Table 4.1.3 we pick the value of λ which gives a corresponding value of *B* closest to the experimental value and leave a blank in cases where no experimental value is available. We notice from the results presented in Table 4.1.3 that $\lambda = 2$ gives better values of bulk modulus for a number of chalcopyrites of the type I-III-VI_2 than $\lambda = 1$.

It was found that the average error in our results of the bulk modulus for chalcopyrites was 6.3 %, which is acceptable for purposes of predicting the bulk modulus of other chalcopyrites for which no experimental values are available, as the other values we computed are within the range of experimentally determined values [37-39].

Our theoretical predictions for the bulk modulus values of the three chalcopyrite materials where no experimental results were available are given in Table 4.1.4. From Table 4.1.4 which gives our theoretical predictions of the bulk modulus for the these materials we notice $CuGaS_2$ is predicted as being the hardest of all the eight chalcopyrite materials investigated. It will be interesting to find out if this prediction holds when experimental results become available.

No experimental values of the bulk modulus are available for the two binary chalcogenides PdS and PdSe. We have predicted that the value of the bulk modulus of

PdS lies close to or within the range from 36.6 GPa to 41.9 GPa, while that for PdSe lies within or close to the range from 42.5 GPa and 48.6 GPa. It can be seen from our results that the chalcogenides are softer materials than the chalcopyrites.

Band structure calculations were carried out using LDA and GGA functionals but the results from these two exchange correlation functionals underestimated the values of the band gaps for chalcopyrites. The results presented in Table 4.2.2 give a very poor reflection regarding the effectiveness of the LDA and GGA functionals as implemented in Quantum Espresso for band gap calculations for chalcopyrites. Of the eight chalcopyrite materials investigated, only $AgGaTe_2$, $CuInS_2$ and $CuInSe_2$ were determined to be semiconductors, with very small band gaps. The others were determined to possess metallic conduction behaviour because their band gaps were effectively zero. We recall that a conductor is a material in which the valence and conduction band overlap giving an energy band gap of zero. This is in agreement with the fact that LDA and GGA greatly underestimate band gaps [1]. We, however, conclude that LDA and GGA functionals can be relied upon when investigating potential elemental semiconductor materials such as silicon as evidenced by the results presented in Table 4.2.1.

Due to the poor results obtained by using the LDA and GGA functionals, more investigations were carried out using the LDA+U and the empirical shift methods. The LDA+U and empirical shift methods both gave results that were much closer to the results obtained experimentally [41-45]; the two methods resulted in a similar average error of 0.6 eV as calculated from data presented in Table 4.2.3 in Sections 4.2.1. The conclusion drawn is that these two techniques did manage to show that the chalcopyrite materials are actually semiconductors with an average error in the range of 24.4%. With

this we conclude that LDA+U and empirical shift methods are good enough to employ when dealing with other chalcopyrite materials whose band gap may be unknown. Even with the introduction of the Hubbard U term in the LDA formulation, we noted that the error is quite varied. This is because these materials have different levels of the d-bonding character [55]. We conclude that the correction brought about by the Hubbard U term which increases the "on-site" repulsion between electrons at the same atomic orbitals cannot be uniform.

The results presented in Table 4.2.3 have revealed that the LDA+U method points to the fact that the chalcopyrites investigated in this study almost match the optimum value of the band gap needed for solar cell application of 1.5 eV [1] whereas Jiang's empirical shift methods show that these materials match this optimum value of band gap. Hence, we conclude that these materials are viable for application in photovoltaics.

Our band structure calculations suggest that most chalcopyrite semiconductors have a direct band gap. The ***k***-vector position in the first Brillouin zone, at the minimum of the band gap, was found to be either near the L reciprocal lattice point or in the region between K and the center of the first Brillouin zone Γ.

The binary chalcogenides PdS and PdSe are large band-gap semiconductors with experimentally determined band gaps in the range of 2.0 eV and 3.0 eV. The LDA exchange correlation functional tended to overestimate the band gap for these chalcogenides. Jiang's downward empirical shift of 0.21 Ry successfully corrected the LDA derived chalcogenide band gaps to agree with experimental results [46]. These results lead us to conclude that Jiang's downward empirical shift technique is very

effective for application when investigating energy band gaps of chalcogenides as these results lie within the range of values obtained by experimental techniques [46].

Impurity properties were also investigated. The maximum error in our method for determining the energy of formation of vacancy and dopant impurities, when tested on silicon, was 7.5 %. This is acceptable for most predictive applications as the value obtained is within the range of values determined in other works [47, 48]. Energy of formation values for Cu vacancies and Ag impurities at three (0.500, 0.000, 0.250) positions in $CuInSe_2$ were determined. Similar calculations were carried out for other chalcopyrites. Results obtained show that the energy of formation for vacancy defects in the chalcopyrites lies between -75.435 Ry and -35.34 Ry. This predicts that the vacancies would be formed through exothermal processes. The energy of formation for dopant impurities in the chalcopyrites investigated lies between 103.42 Ry and -23.649 Ry. All these results, except those for $AgGaSe_2$, predict endothermal processes. Our study of energy of formation and band structure is important in the field of band gap engineering. As experimental work on chalcopyrites progresses and more results become available, we will be able to see if the predictions made in this work will hold.

The bulk modulus results are important in determining the optimum materials to use under various pressure conditions. These could be used in for achieving semiconductor device stability in high stress equipment such as might be used in marine exploration.

A suggestion for future work arising from this project is a comprehensive study of ternary chalcogenides, like the one carried out on chalcopyrites in this work. A major constraint is the computational power available. In this work each LDA+U chalcopyrite band

structure calculation ran for more than 24 hours. It is therefore recommended that more computational power be obtained for use in future work.

APPENDIX A

CRYSTAL STRUCTURE

$AgGaS_2$

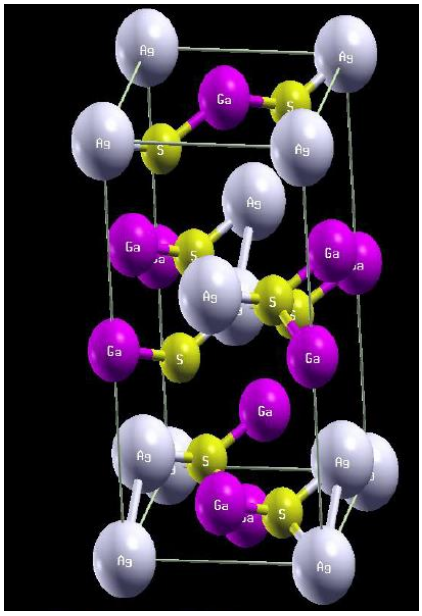

$AgGaSe_2$

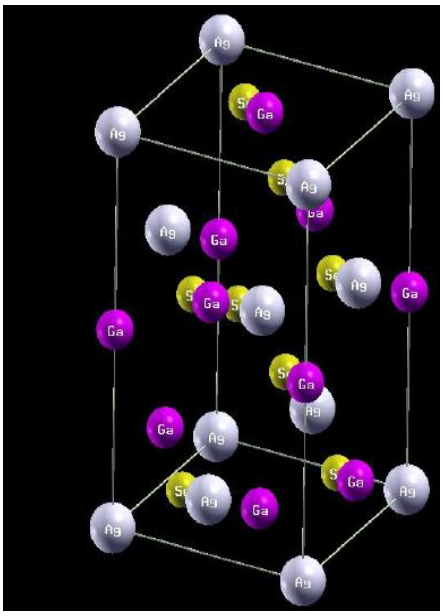

$AgGaTe_2$

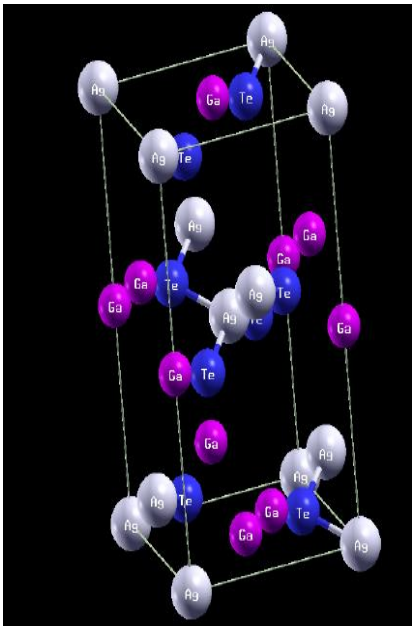

$CuGS_2$

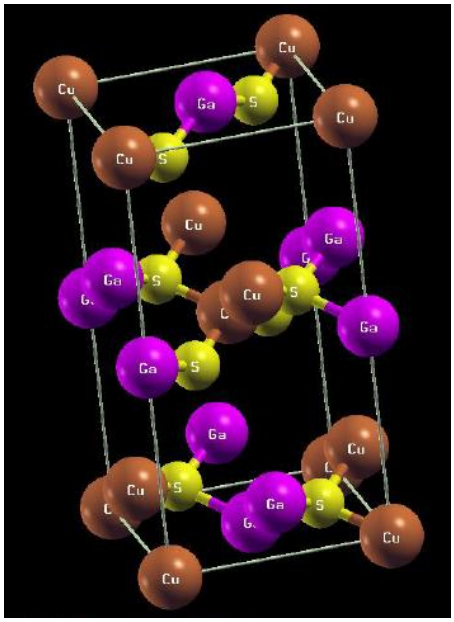

$CuInS_2$

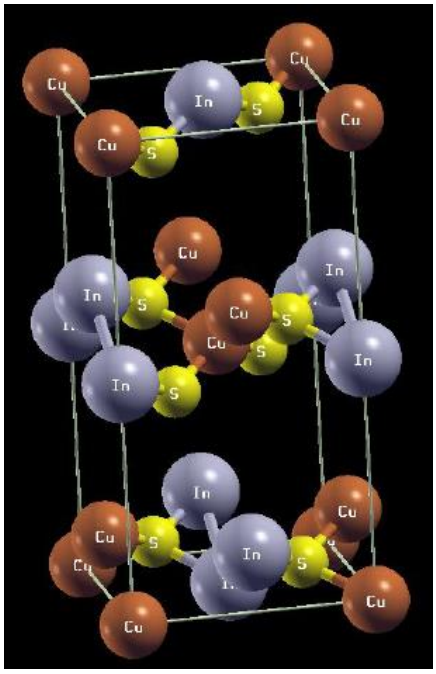

CuInSe

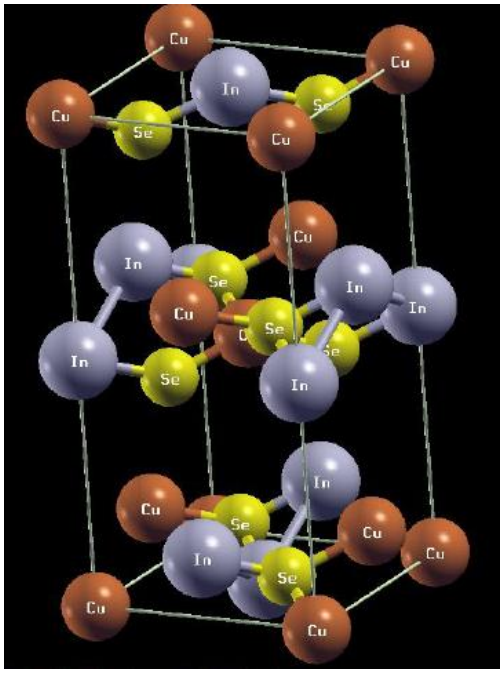

$ZnSiAs_2$

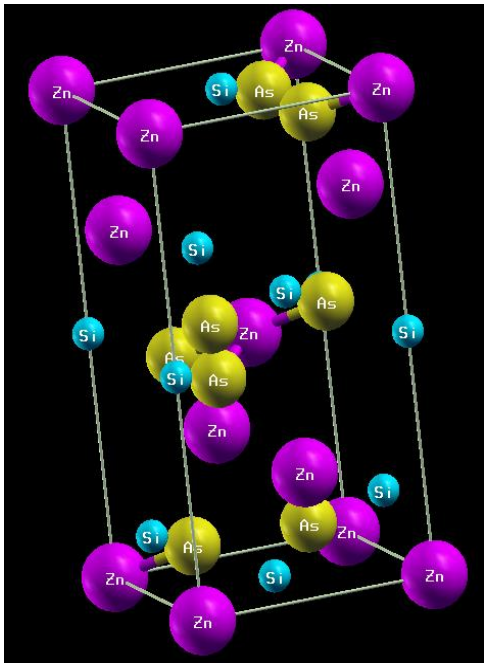

$ZnSnAs_2$

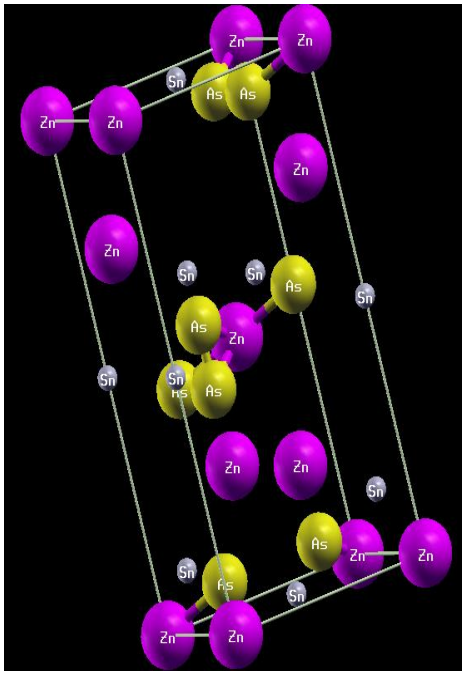

APPENDIX B

ELECTRONIC BAND GAP AND DENSITY OF STATES DIAGRAMS

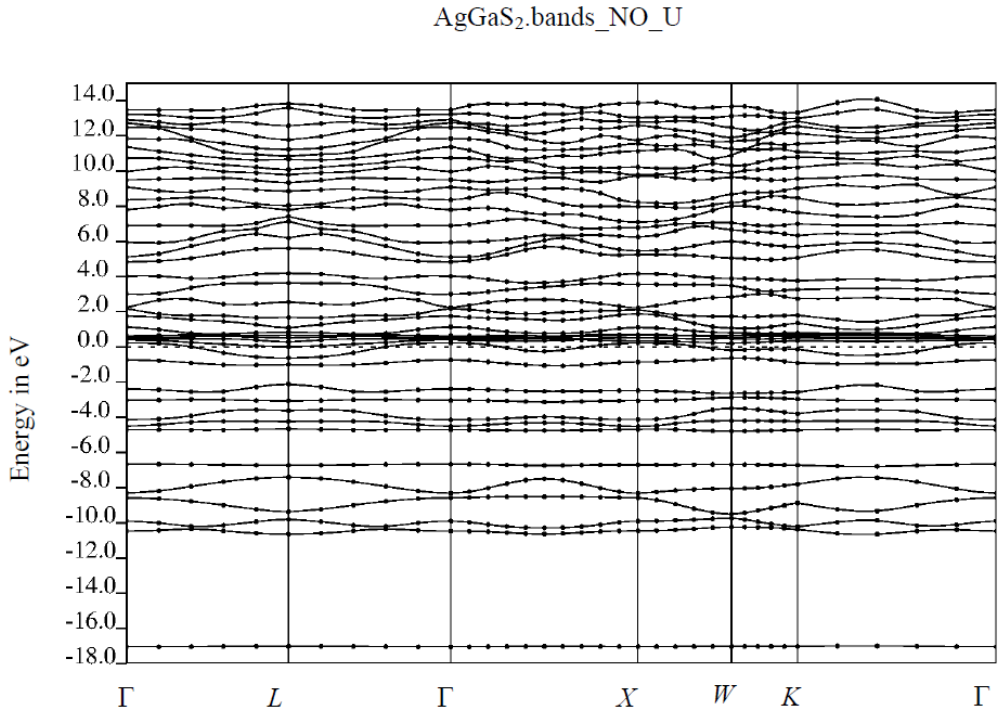

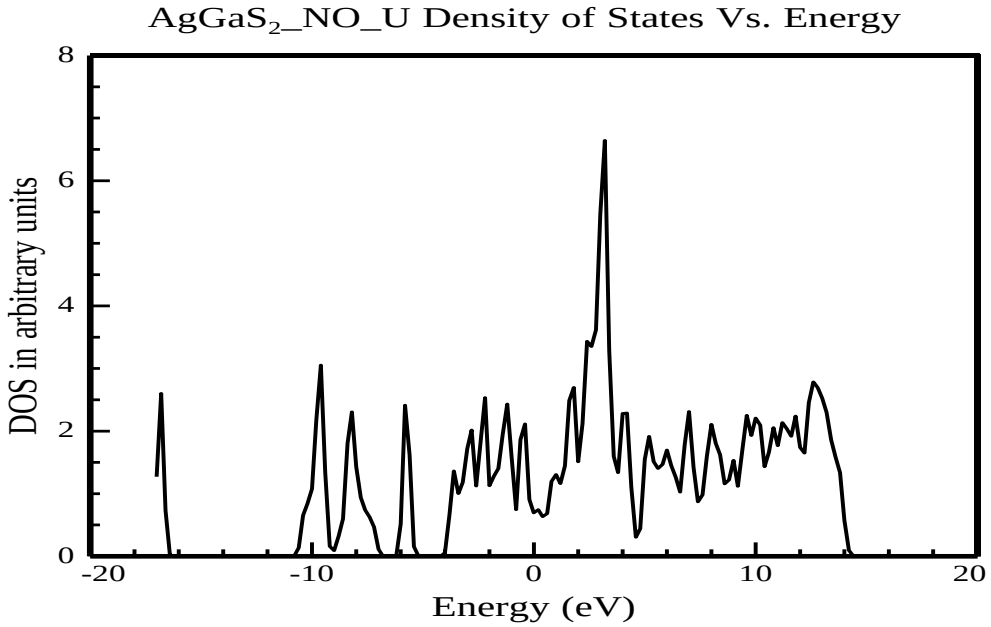

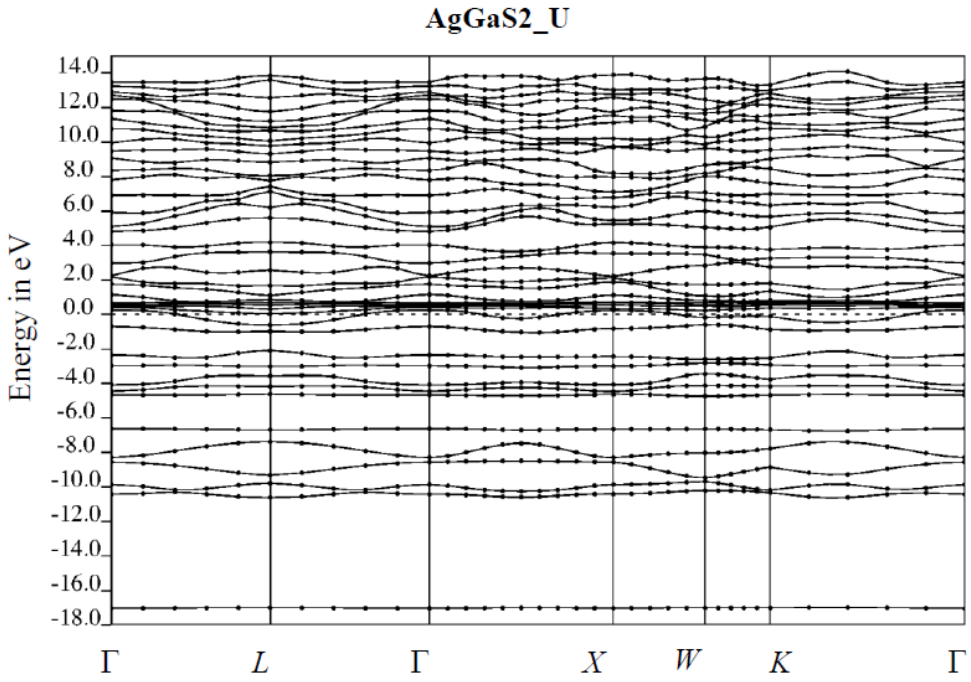
AgGaS2_U
Energy in eV
14.0
12.0
10.0
8.0
6.0
4.0
2.0
0.0
-2.0
-4.0
-6.0
-8.0
-10.0
-12.0
-14.0
-16.0
-18.0
Γ
L
Γ
X
W
K
Γ

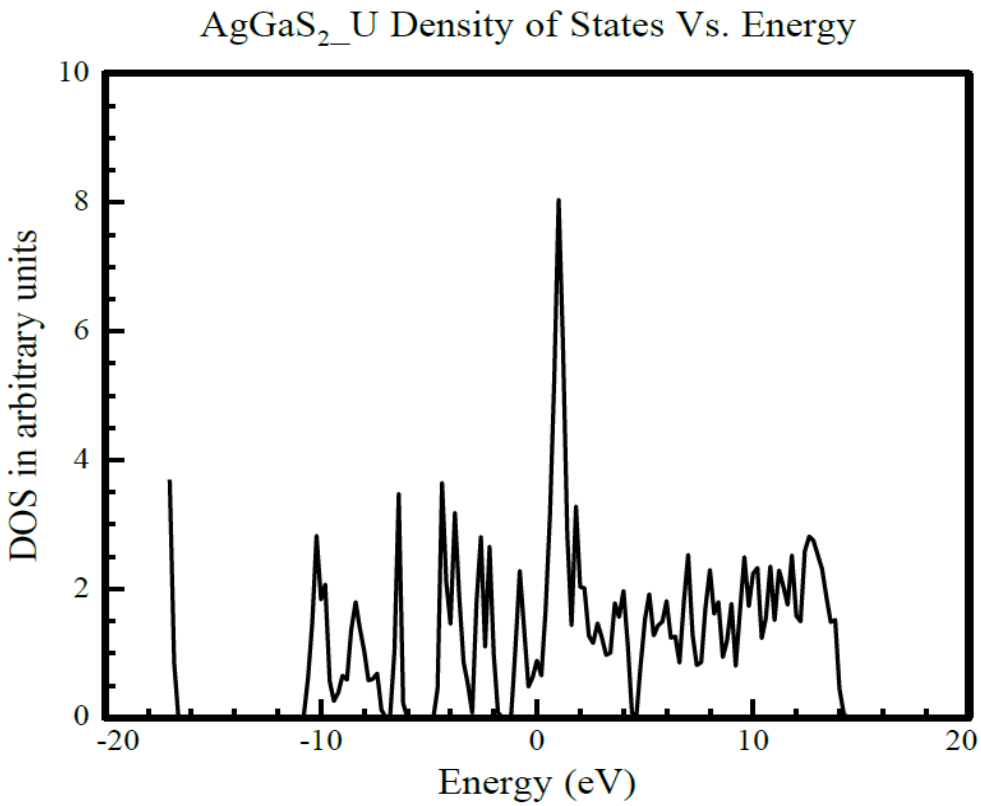
AgGaS2_U Density of States Vs. Energy
DOS in arbitrary units
10
8
6
4
2
0
-20
-10
0
10
20
Energy (eV)

AgGaSe$_2$.bands_NO_U

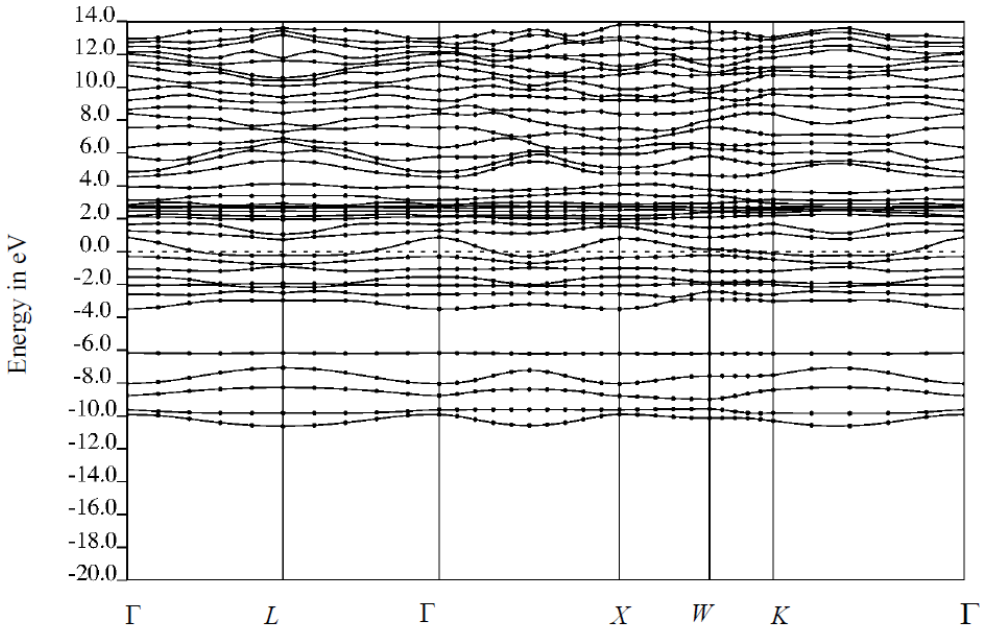

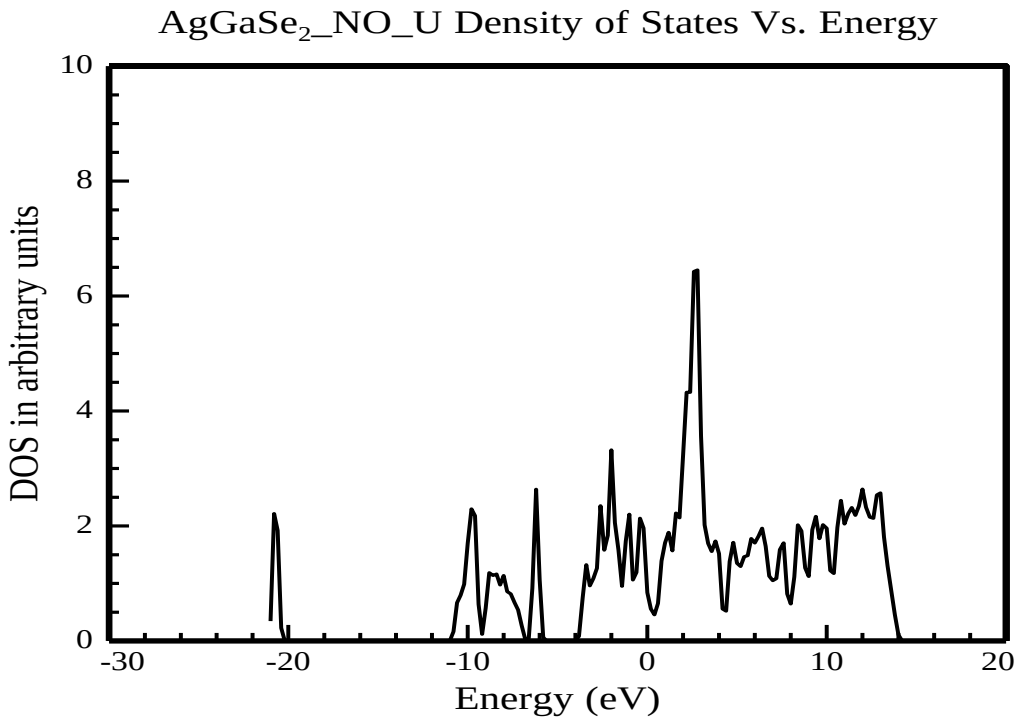

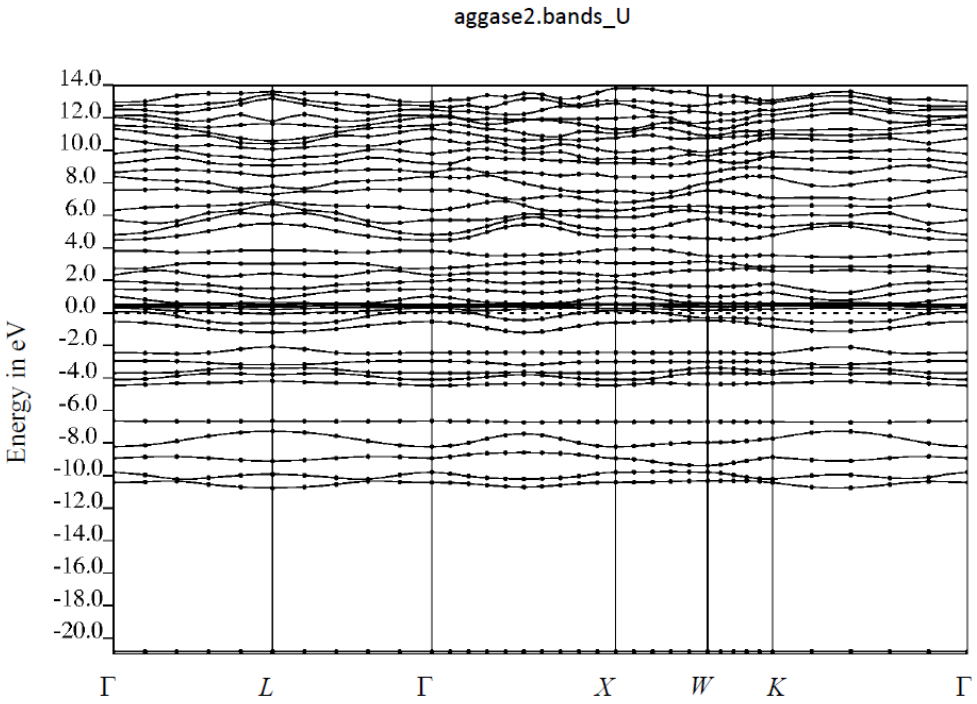
aggase2.bands_U
Energy in eV
14.0
12.0
10.0
8.0
6.0
4.0
2.0
0.0
-2.0
-4.0
-6.0
-8.0
-10.0
-12.0
-14.0
-16.0
-18.0
-20.0
Γ
L
Γ
X
W
K
Γ

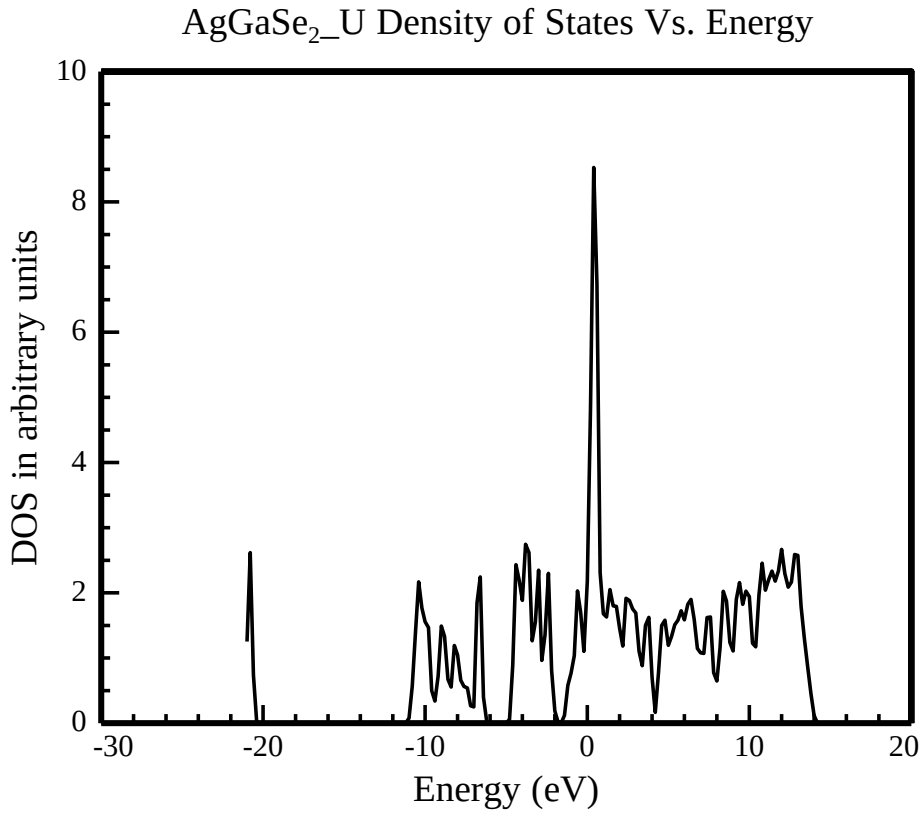
AgGaSe2_U Density of States Vs. Energy
DOS in arbitrary units
10
8
6
4
2
0
-30
-20
-10
0
10
20
Energy (eV)

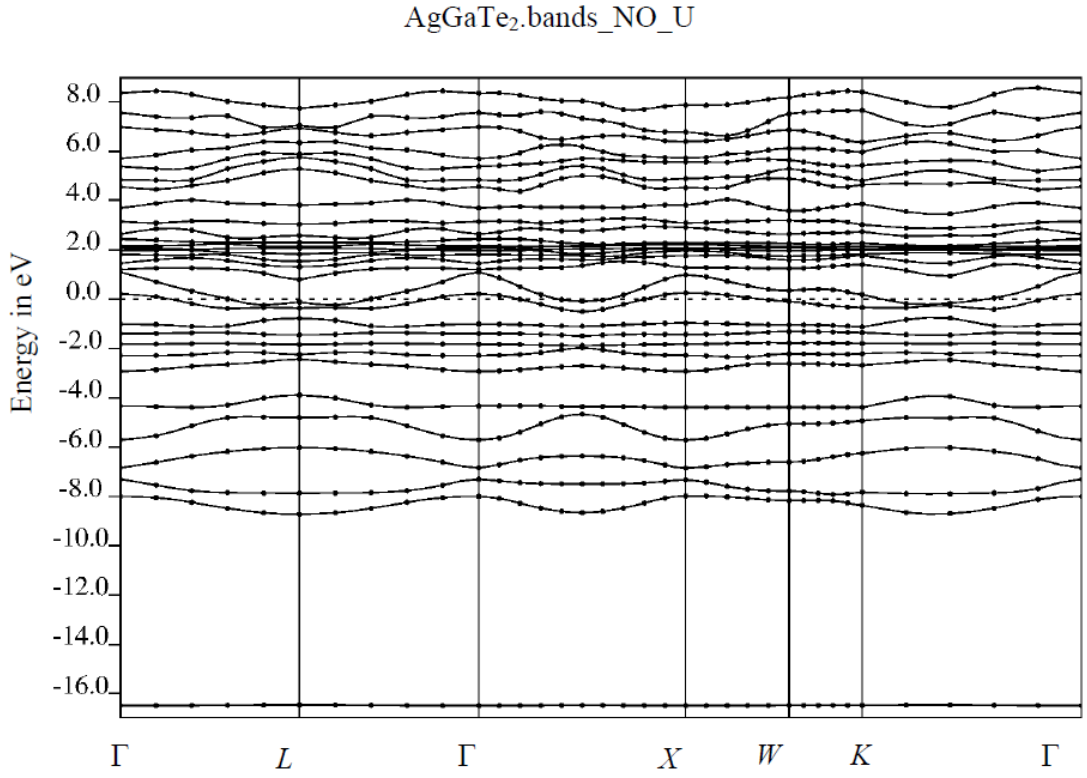
AgGaTe2.bands_NO_U
Energy in eV
8.0
6.0
4.0
2.0
0.0
-2.0
-4.0
-6.0
-8.0
-10.0
-12.0
-14.0
-16.0
Γ
L
Γ
X
W
K
Γ

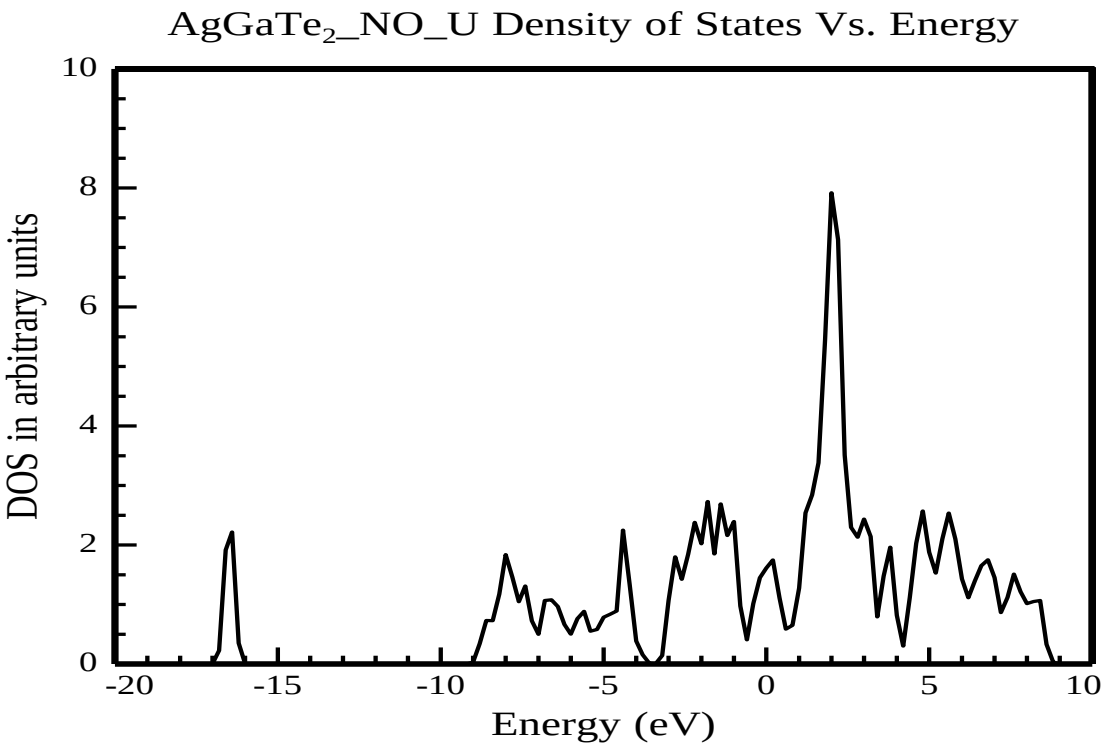
AgGaTe2_NO_U Density of States Vs. Energy
DOS in arbitrary units
0
2
4
6
8
10
-20
-15
-10
-5
0
5
10
Energy (eV)

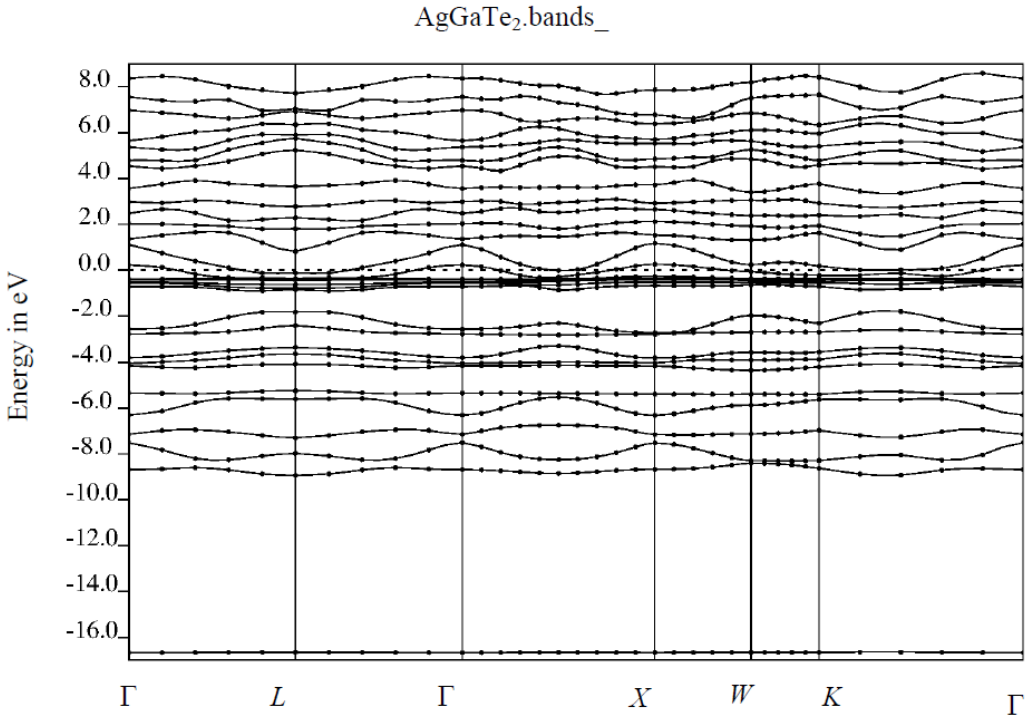
AgGaTe2.bands_
Energy in eV
8.0
6.0
4.0
2.0
0.0
-2.0
-4.0
-6.0
-8.0
-10.0
-12.0
-14.0
-16.0
Γ
L
Γ
X
W
K
Γ

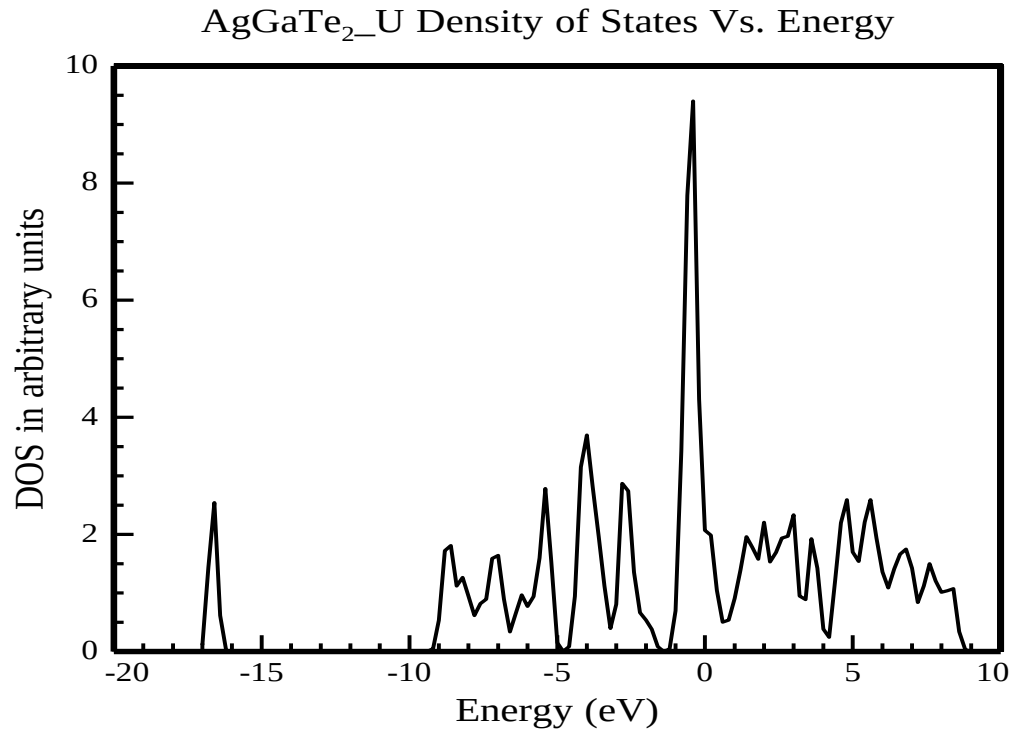
AgGaTe2_U Density of States Vs. Energy
DOS in arbitrary units
10
8
6
4
2
0
-20
-15
-10
-5
0
5
10
Energy (eV)

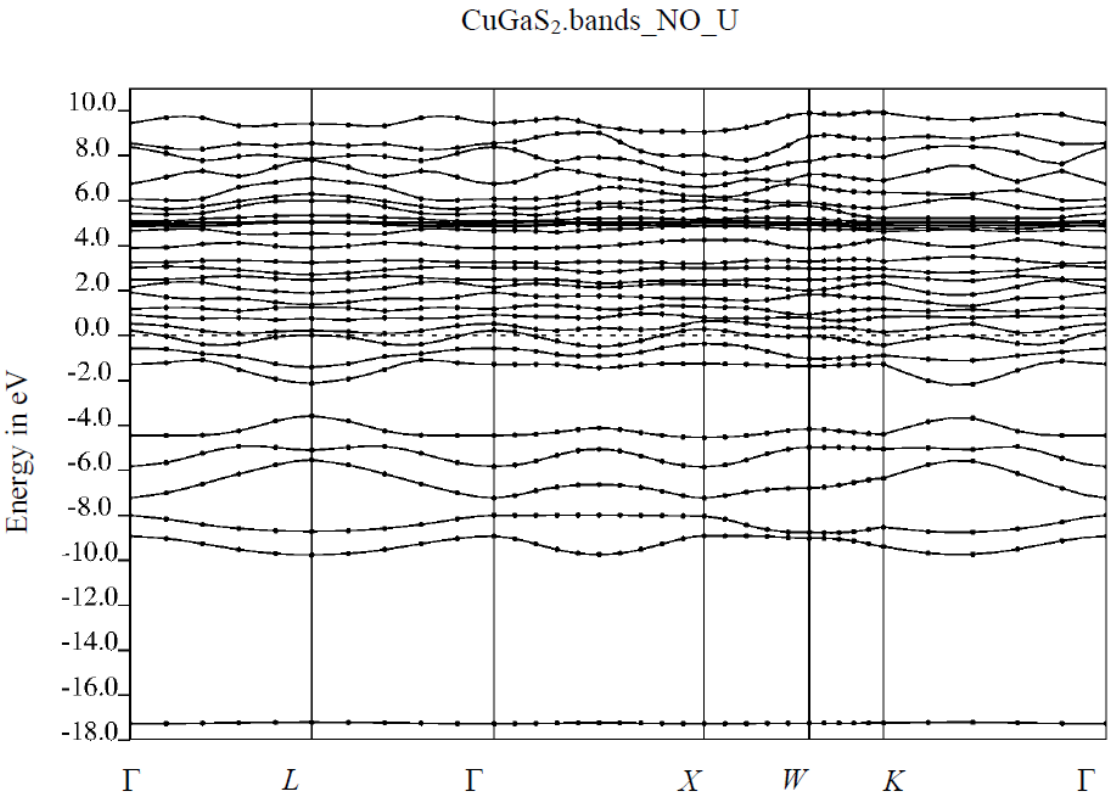
CuGaS2.bands_NO_U
Energy in eV
10.0
8.0
6.0
4.0
2.0
0.0
-2.0
-4.0
-6.0
-8.0
-10.0
-12.0
-14.0
-16.0
-18.0
Γ
L
Γ
X
W
K
Γ

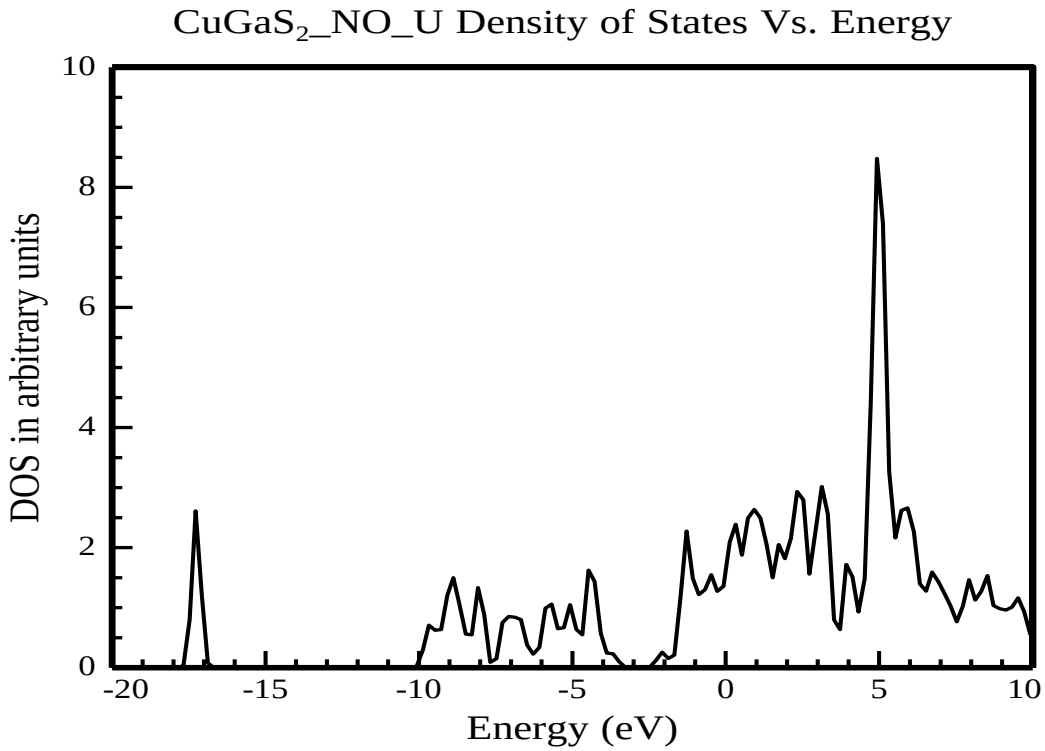
CuGaS2_NO_U Density of States Vs. Energy
DOS in arbitrary units
0
2
4
6
8
10
-20
-15
-10
-5
0
5
10
Energy (eV)

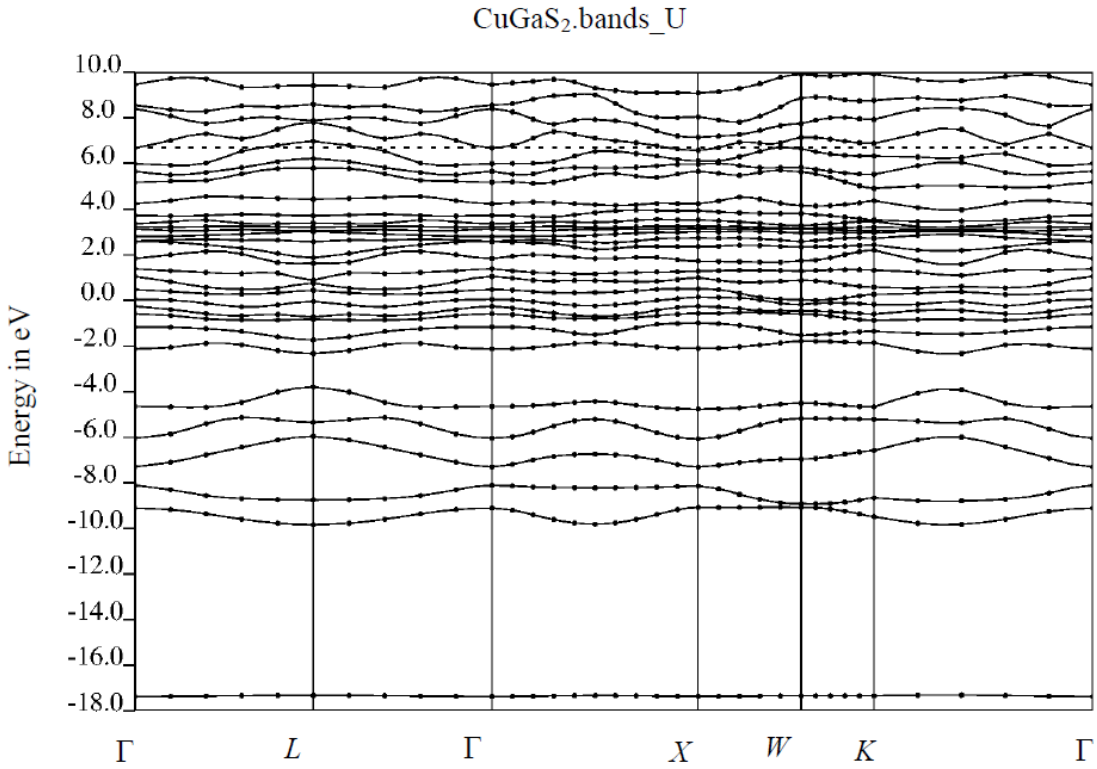
CuGaS2.bands_U
Energy in eV
10.0
8.0
6.0
4.0
2.0
0.0
-2.0
-4.0
-6.0
-8.0
-10.0
-12.0
-14.0
-16.0
-18.0
Γ
L
Γ
X
W
K
Γ

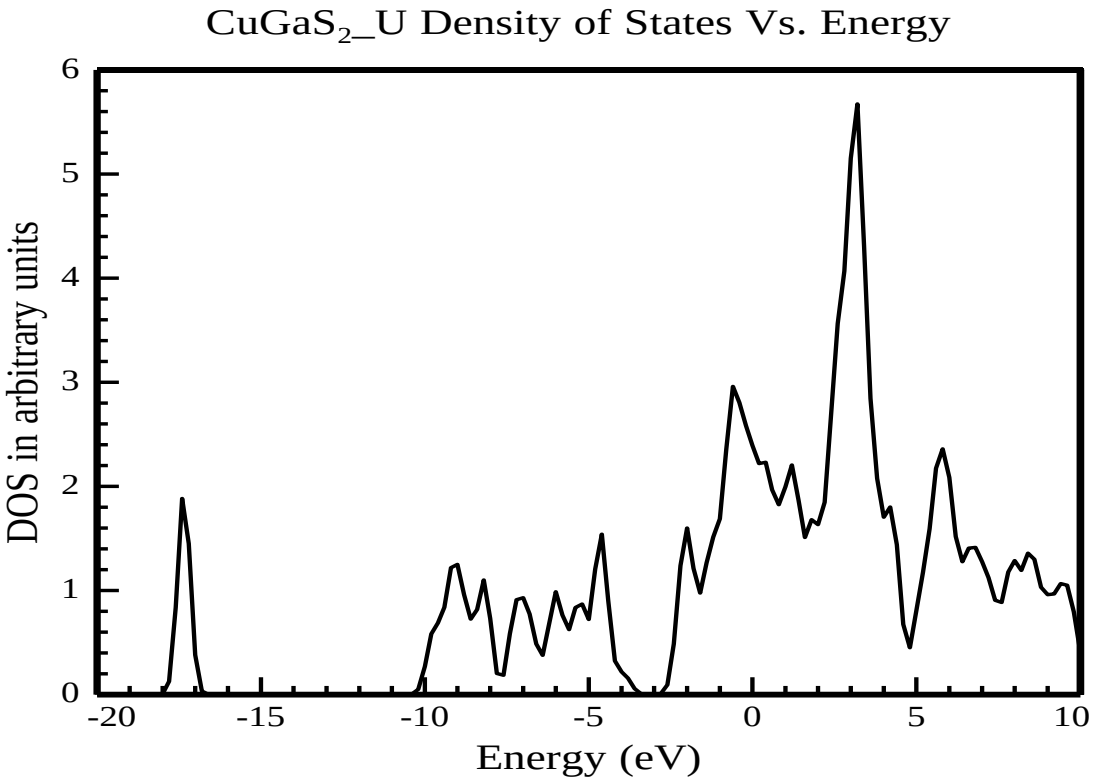
CuGaS2_U Density of States Vs. Energy
DOS in arbitrary units
0
1
2
3
4
5
6
-20
-15
-10
-5
0
5
10
Energy (eV)

$CuInS_2$.bands_NO_U

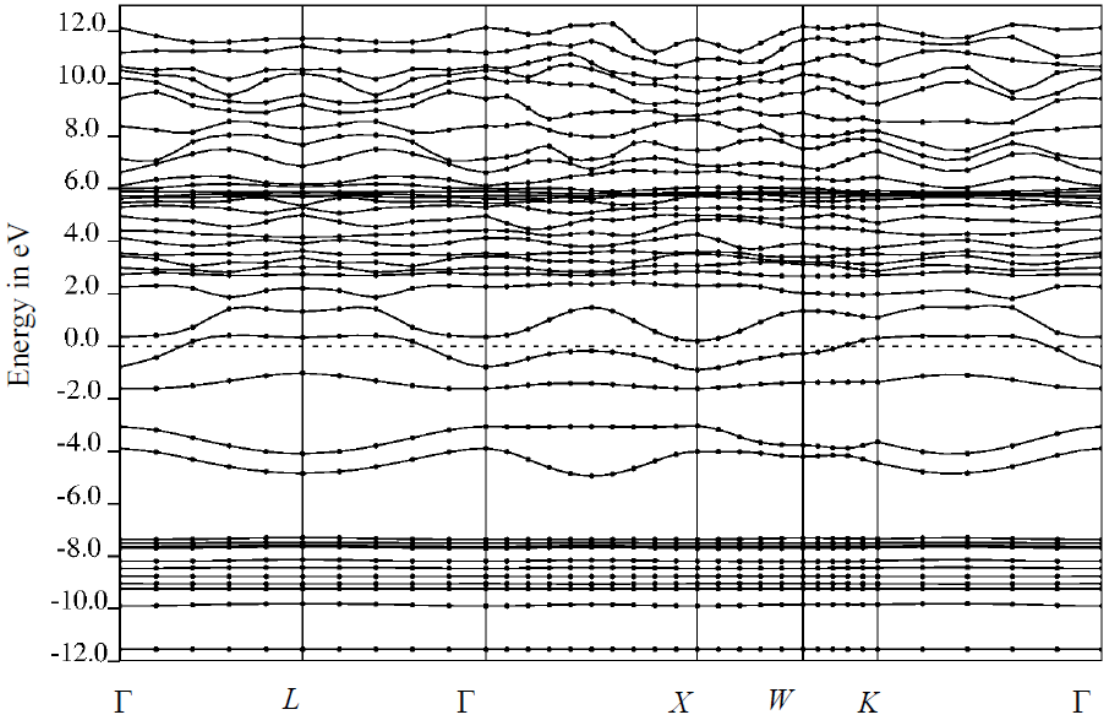

$CuInS_{2\_U}$

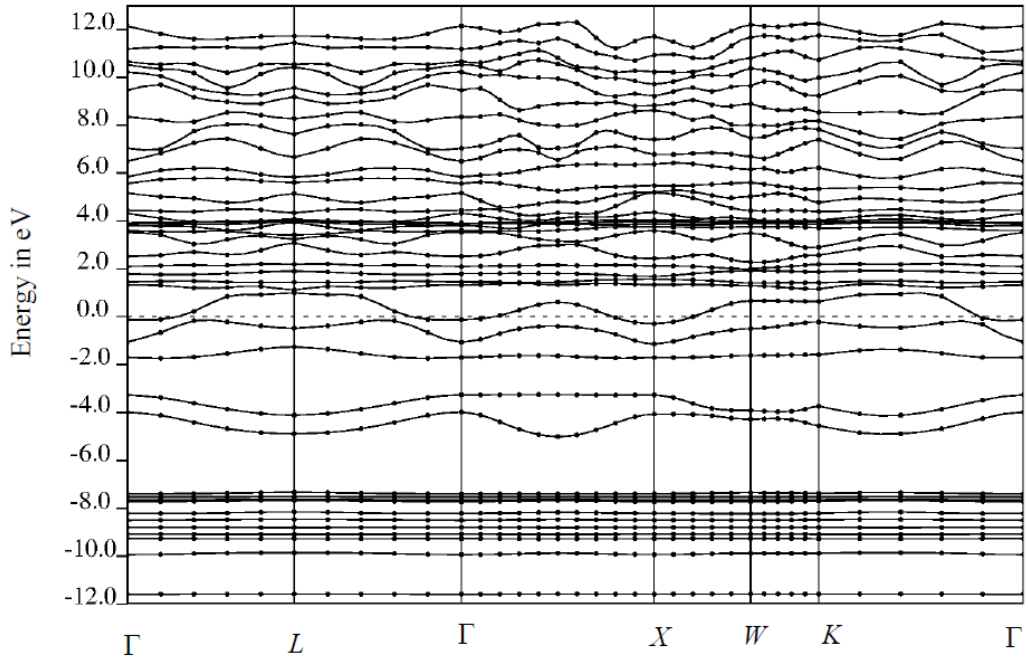

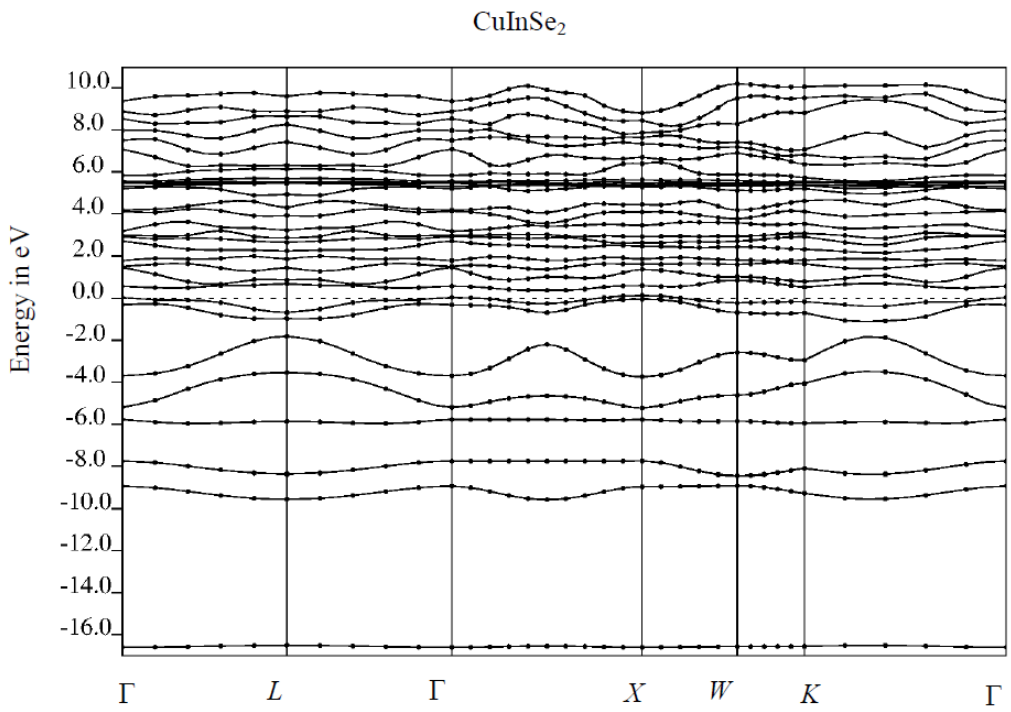
CuInSe2
Energy in eV
10.0
8.0
6.0
4.0
2.0
0.0
-2.0
-4.0
-6.0
-8.0
-10.0
-12.0
-14.0
-16.0
Γ
L
Γ
X
W
K
Γ

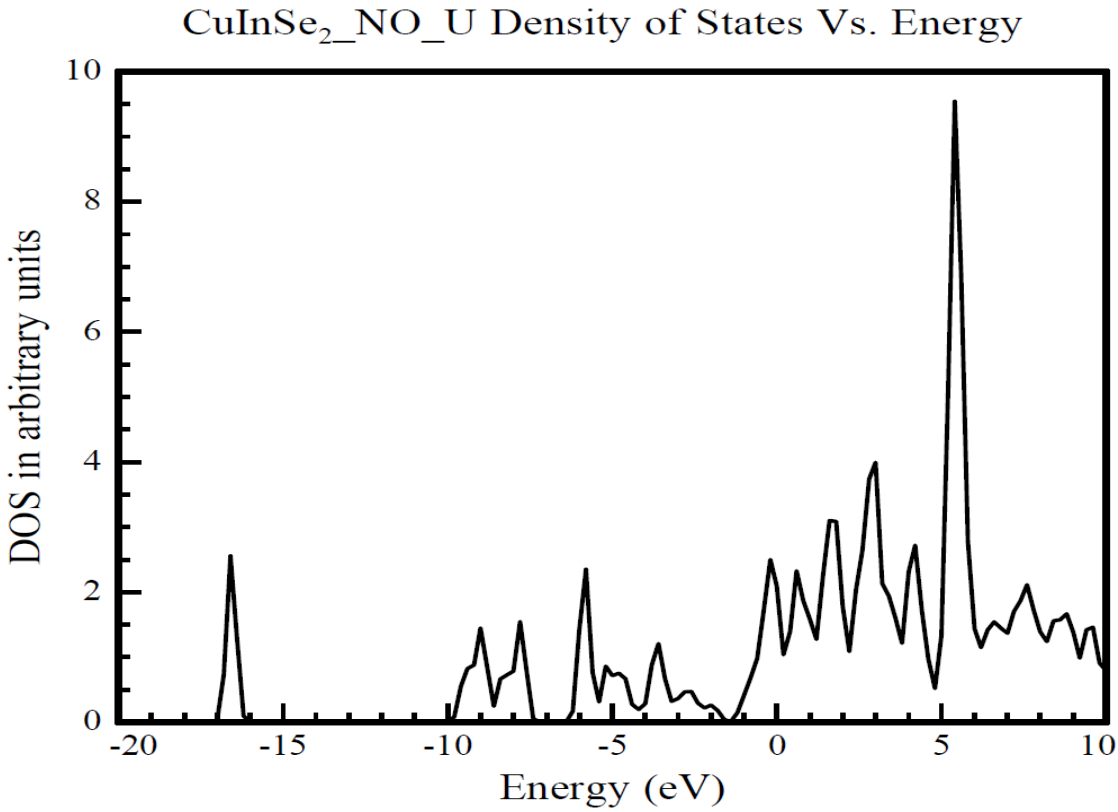
CuInSe2_NO_U Density of States Vs. Energy
DOS in arbitrary units
10
8
6
4
2
0
-20
-15
-10
-5
0
5
10
Energy (eV)

$CuInSe_{2\_U}$

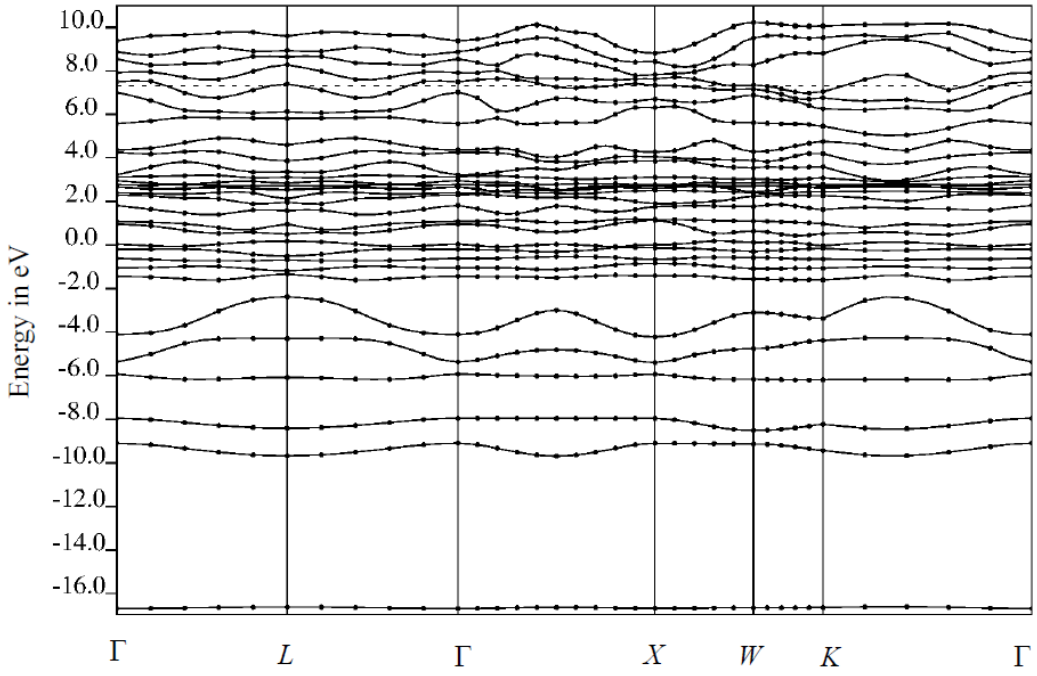
Energy in eV
10.0
8.0
6.0
4.0
2.0
0.0
-2.0
-4.0
-6.0
-8.0
-10.0
-12.0
-14.0
-16.0
Γ
L
Γ
X
W
K
Γ

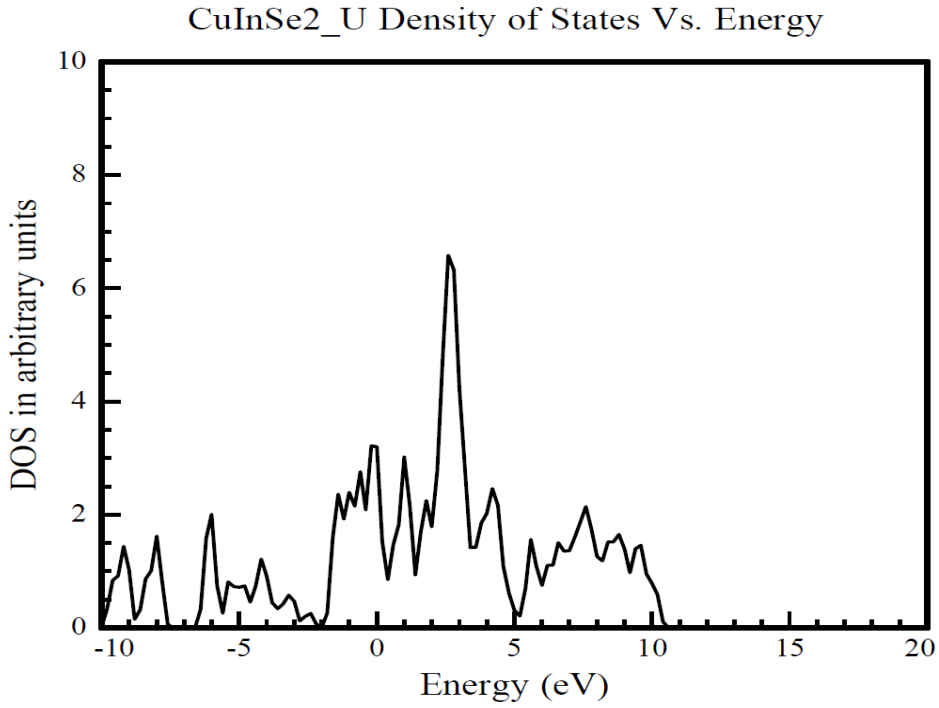
CuInSe2_U Density of States Vs. Energy
DOS in arbitrary units
0
2
4
6
8
10
-10
-5
0
5
10
15
20
Energy (eV)

$ZnSiAs_{2\_NO\_U}$ Band

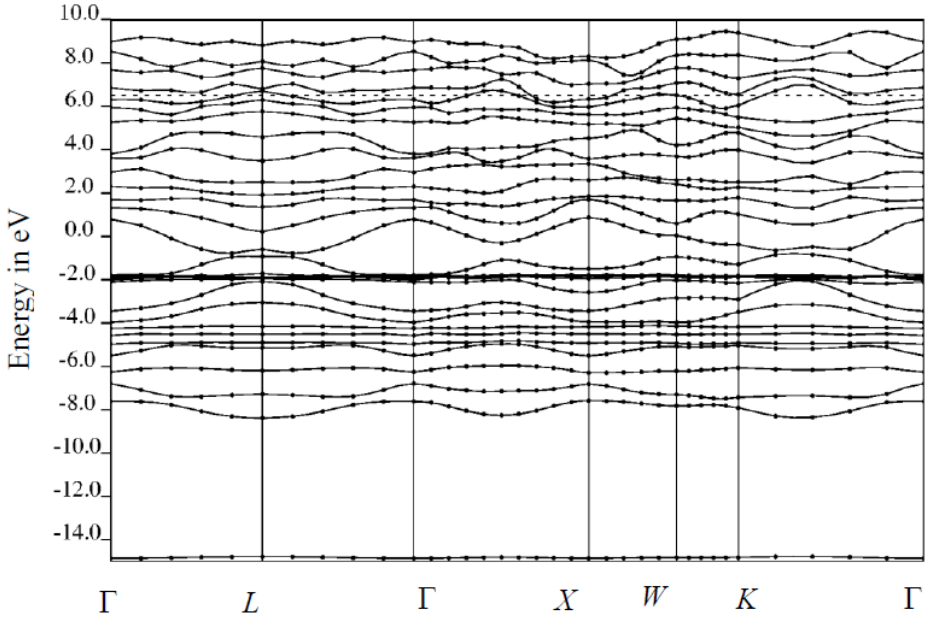

$ZnSiAs_2$ Density of States Vs. Energy

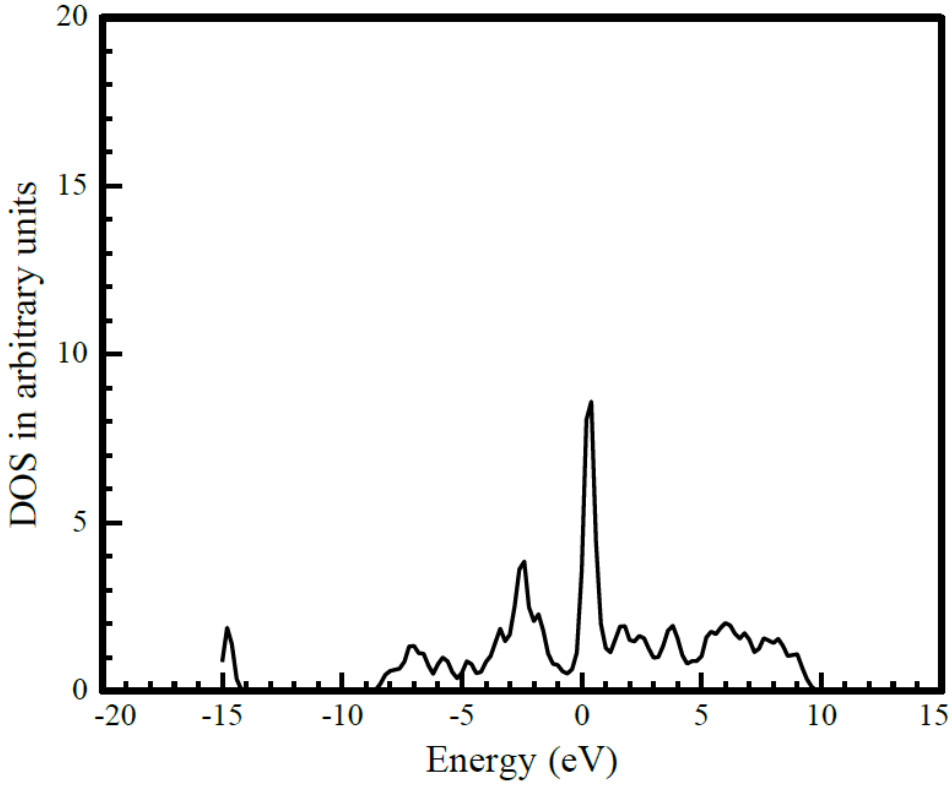

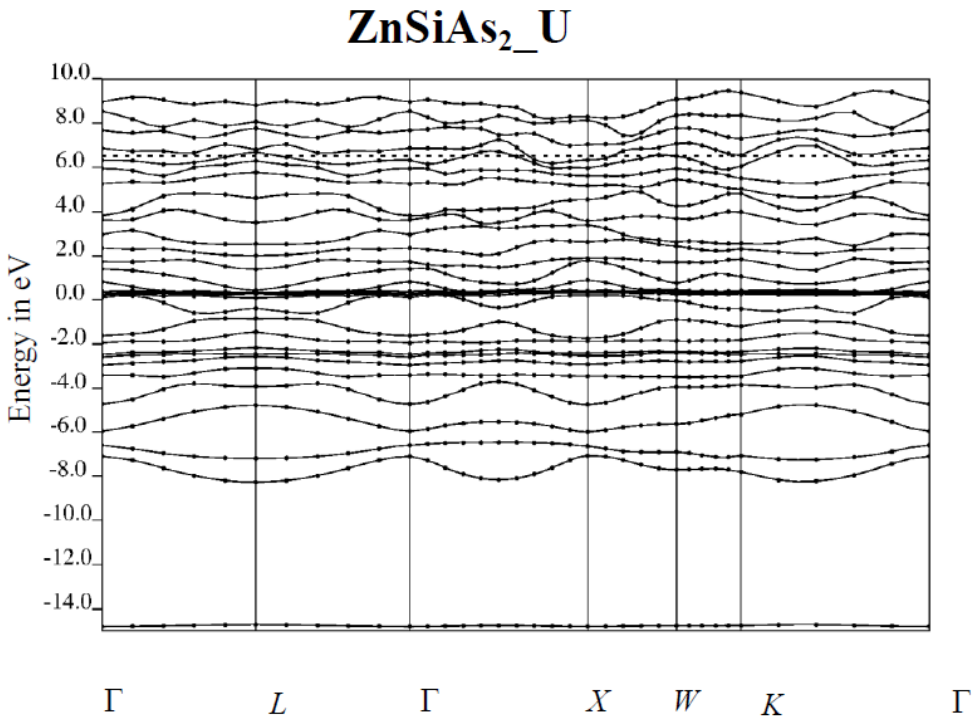
ZnSiAs2_U
Energy in eV
10.0
8.0
6.0
4.0
2.0
0.0
-2.0
-4.0
-6.0
-8.0
-10.0
-12.0
-14.0
Γ
L
Γ
X
W
K
Γ

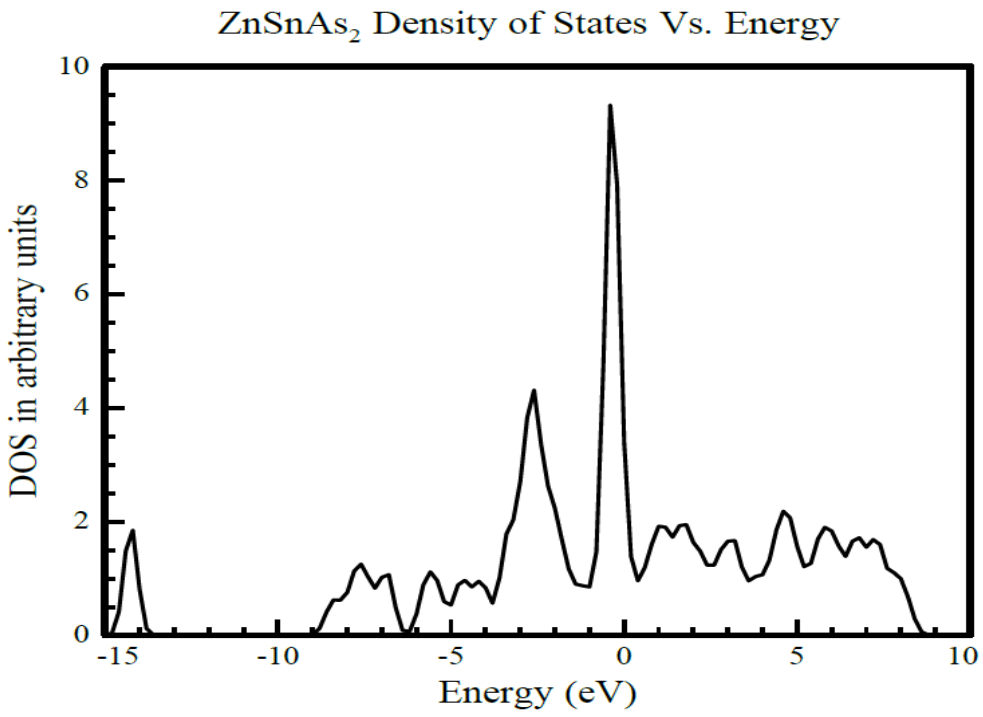
ZnSnAs2 Density of States Vs. Energy
DOS in arbitrary units
10
8
6
4
2
0
-15
-10
-5
0
5
10
Energy (eV)

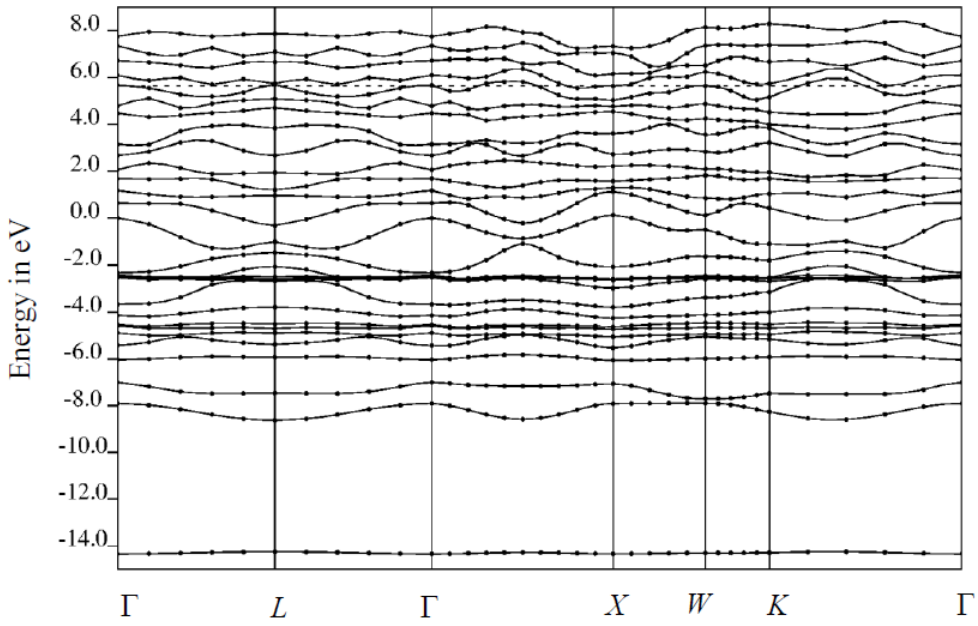

$ZnSnAs_2$ with Hubbard U

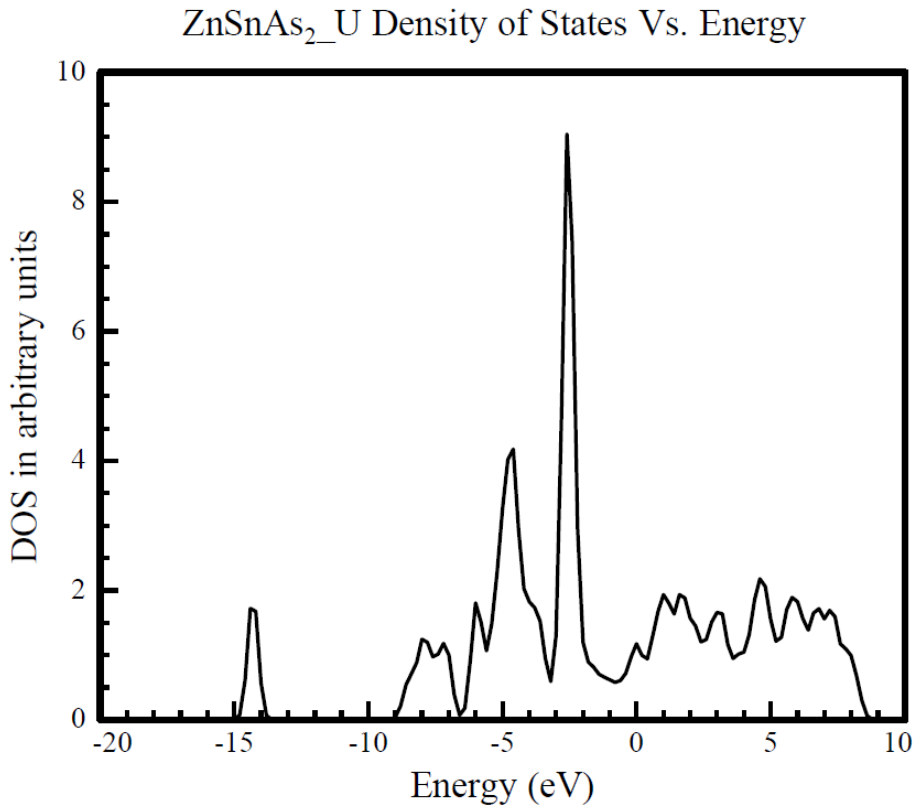

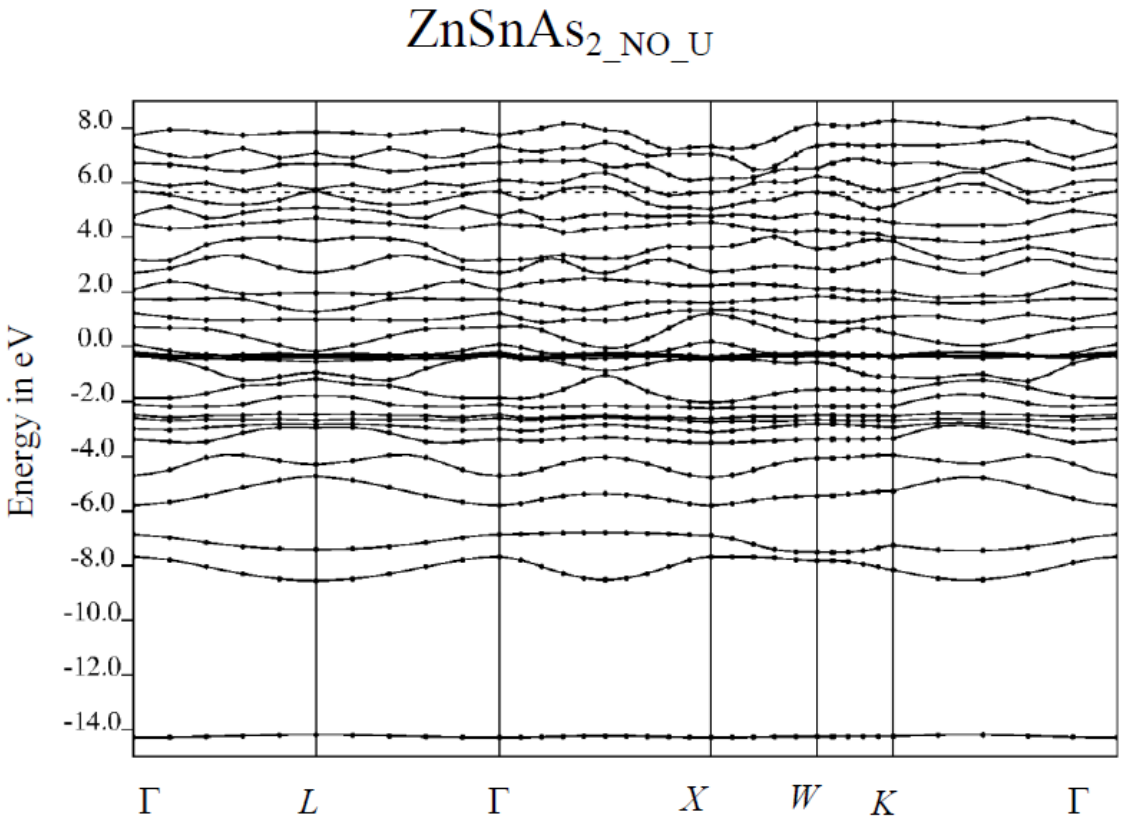
ZnSnAs2_NO_U
Energy in eV
8.0
6.0
4.0
2.0
0.0
-2.0
-4.0
-6.0
-8.0
-10.0
-12.0
-14.0
Γ
L
Γ
X
W
K
Γ

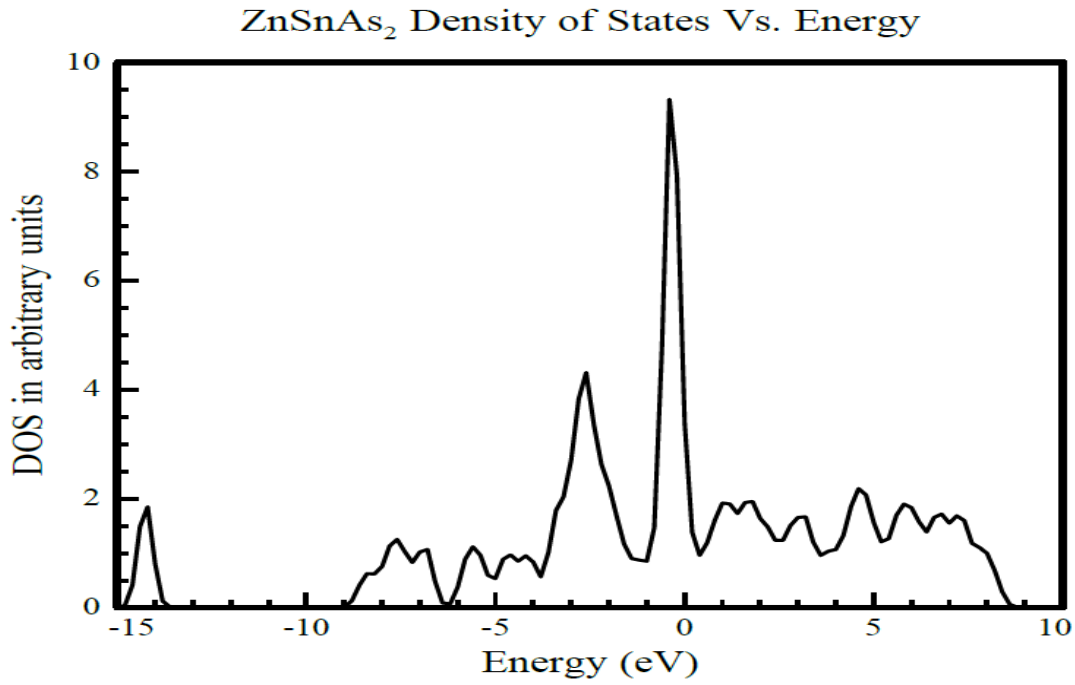
ZnSnAs2 Density of States Vs. Energy
DOS in arbitrary units
10
8
6
4
2
0
-15
-10
-5
0
5
10
Energy (eV)

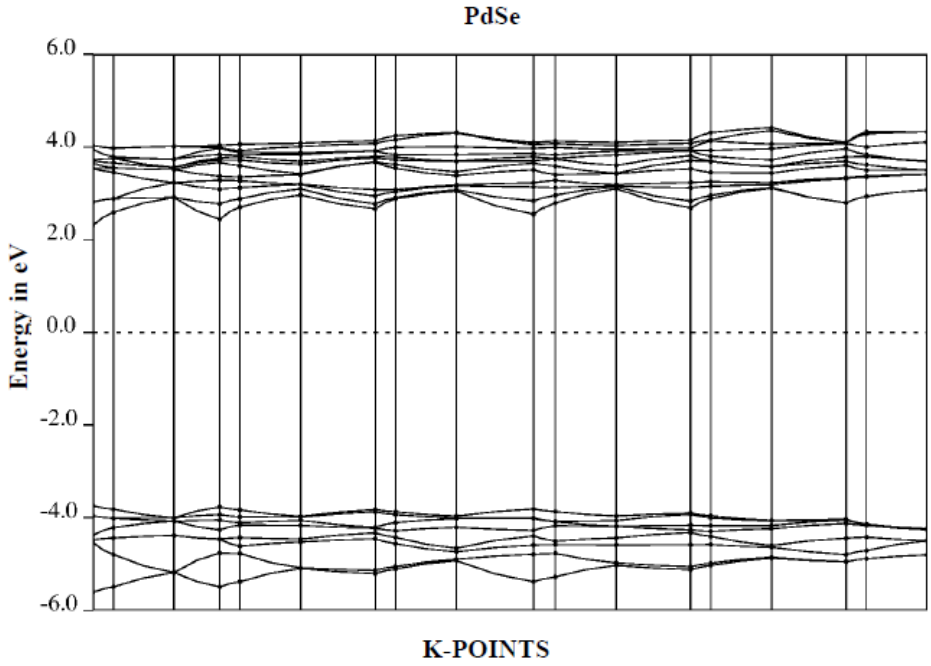
PdSe
6.0
4.0
2.0
0.0
-2.0
-4.0
-6.0
Energy in eV
K-POINTS

APPENDIX C

ENERGY OF FORMATION CALCULATIONS

$AgGaSe_2$

Total Energy from $AgGaSe_2$.SCF.OUT = -221.845Ry

Total Energy from $AgGaSe_2$-V (unrelaxed 1st) = -149.4807Ry (-149.4892Ry)

Total Energy from $AgGaSe_2$ –V (relaxed last) = -157.6650Ry (-157.6717Ry)

Total Energy from $AgGaSe_2$ –Cu doped (unrelaxed) =-237.05Ry

Total Energy from $AgGaSe_2$ – Cu doped (relaxed) = -245.49Ry

$AgGaS_2$

Total Energy $AgGaS_2$.out = -231.38Ry

Total Energy $AgGaS_2$ –V (unrelaxed 1st) =-159.04Ry

Total Energy $AgGaS_2$ –V (relaxed) = -163.51Ry

Total Energy $AgGaS_2$-d.out (unrelaxed) = -159.78Ry

Total Energy $AgGaS_2$-d.out (relaxed) = -164.38Ry

$CuGaS_2$-defects

Total Energy for $CuGaS_2$.out = -263.77Ry

Total Energy for $CuGaS_2$-V.out (unrelaxed) = -176.18Ry

Total Energy for $CuGaS_{2\text{-V.out}}$ (relaxed) =-178.93Ry

Total Energy for $CuGaS_2$-d.out = (unrelaxed) = -176.95Ry

Total Energy of $CuGaS_{2\text{-d.out}}$ (relaxed) = -176.76Ry

$CuInS_2$

Total Energy for $CuInS_2$ .out =-324.49Ry

Total Energy for $CuInS_2$-V.out (unrelaxed) = -236.87Ry

Total Energy for $CuInS_2$-V .out (relaxed) =-237.68Ry

Total Energy for $CuInS_2$-d.out (unrelaxed) =-309.16Ry

Total Energy for $CuInS_2$-d.out (relaxed) =310.21Ry

$CuInSe_2$

Total Energy for $CuInSe_2$.out = -316.76

Total Energy for $CuInSe_2$-V.out (unrelaxed) = -230.30Ry

Total Energy for $CuInSe_2$-V.out (relaxed) =-231.81Ry

Total Energy for $CuInSe_2$-doped (unrelaxed) =-302.47Ry

Total Energy for $CuInSe_2$-doped (relaxed) = -304.30Ry

$ZnSiAs_2$

Total Energy of $ZnSiAs_2$ = -282.06Ry

Total Energy of $ZnSiAs_2$ –V.out (unrelaxed) = -172.61Ry

Total Energy of $ZnSiAs_2$-V.out (relaxed) = -176.37Ry

Total Energy of $ZnSiAs_2$-doped (unrelaxed) = -174.74Ry

Total Energy of $ZnSiAs_2$-doped (relaxed) = -178.64Ry

$ZnSnAs_2$

Total Energy of $ZnSiAs_2$ .SCF.out = -282.049

Total Energy of $ZnSnAs_2$-V (unrelaxed) = -172.71Ry

Total Energy of $ZnSnAs_2$-V (relaxed) =-174.85Ry

Total Energy of $ZnSnAs_2$-doped (unrelaxed) = -174.81Ry

Total Energy of $ZnSnAs_2$-doped (relaxed) =-177.12Ry

APPENDIX D

LDA+U INPUT FILES

AgGaSe2.band.david.in

```
&control
   calculation='bands'
   pseudo_dir = '/home/dennis/pseudo/',
   outdir='/home/dennis/silungweldau/tmp1/',
   prefix='aggase2'
 /
 &system
   ibrav=  7, celldm(1) = 11.282, celldm(3)=1.82, nat=  8, ntyp= 3,
   ecutwfc =50.0, ecutrho = 360,nbnd=40,
   starting_magnetization(1)= 0.0,

   !occupations='smearing',
   !smearing='gauss',
   !degauss=0.01,
   nspin=1,
   lda_plus_u=.true.,
   Hubbard_U(1)=4.2,
   Hubbard_alpha(1)=-0.08
 /
 &electrons
   diagonalization='david'
    mixing_mode = 'plain'
   mixing_beta = 0.7
   conv_thr =  1.0d-8
 /


ATOMIC_SPECIES
 Ag 107.8682 Ag.pz-mt_fhi.UPF
 Ga 69.723 Ga.pz-mt_fhi.UPF
 Se 78.96 Se.pz-mt_fhi.UPF
ATOMIC_POSITIONS
 Ag 0.00 0.00 0.00
 Ag 0.00 0.50 0.50
 Ga 0.50 0.50 0.00
 Ga 0.50 0.00 0.25
 Se 0.301 0.25 0.125
 Se 0.301 0.75 0.125
 Se 0.75 0.301 0.875
 Se 0.25 0.301 0.875
```

```
K_POINTS
 36
   0.0 0.0 0.0 1.0
   0.1 0.1 0.1 1.0
   0.2 0.2 0.2 1.0
   0.3 0.3 0.3 1.0
   0.4 0.4 0.4 1.0
   0.5 0.5 0.5 1.0
   0.4 0.4 0.4 1.0
   0.3 0.3 0.3 1.0
   0.2 0.2 0.2 1.0
   0.1 0.1 0.1 1.0
   0.0 0.0 0.0 1.0
   0.0 0.1 0.0 1.0
   0.0 0.2 0.0 1.0
   0.0 0.3 0.0 1.0
   0.0 0.4 0.0 1.0
   0.0 0.5 0.0 1.0
   0.0 0.6 0.0 1.0
   0.0 0.7 0.0 1.0
   0.0 0.8 0.0 1.0
   0.0 0.9 0.0 1.0
   0.0 1.0 0.0 1.0
   0.1 1.0 0.0 1.0
   0.2 1.0 0.0 1.0
   0.3 1.0 0.0 1.0
   0.4 1.0 0.0 1.0
   0.5 1.0 0.0 1.0
   0.55 0.95 0.0 1.0
   0.60 0.90 0.0 1.0
   0.65 0.85 0.0 1.0
   0.70 0.80 0.0 1.0
   0.75 0.75 0.0 1.0
   0.60 0.60 0.0 1.0
   0.45 0.45 0.0 1.0
   0.30 0.30 0.0 1.0
   0.15 0.15 0.0 1.0
   0.0 0.0 0.0 1.0
```

AgGaSe2.bands.in

```
&inputpp
    prefix='aggase2',
    outdir='/home/dennis/silungweldau/tmp1/'
```

```
   filband='aggase2.band'
   lsym=.true.,
/
```

AgGaSe2.pdos.in

```
&inputpp
   outdir='/home/dennis/silungweldau/tmp1/'
   prefix='aggase2'
   Emin=-21.0, Emax=15.0, DeltaE=0.2
 /
```

AgGaSe2.scf.david.in

```
&control
   calculation = 'scf'
   restart_mode='from_scratch',
   prefix='aggase2',
   tstress = .true.
   tprnfor = .true.
   pseudo_dir = '/home/dennis/pseudo/',
   outdir='/home/dennis/silungweldau/tmp1/'
 /
 &system
   ibrav=  7, celldm(1) =11.282, celldm(3)=1.82, nat=  8, ntyp= 3,
   ecutwfc =50.0,ecutrho = 360,nbnd=40,
   starting_magnetization(1)= 0.0,

   occupations='smearing',
   smearing='gauss',
   degauss=0.01,
   nspin=1,
   lda_plus_u=.true.,  Hubbard_U(1)=4.2,
   Hubbard_alpha(1)=-0.08
 /
 &electrons
   diagonalization='david'
   mixing_mode = 'plain'
   mixing_beta = 0.7
   conv_thr =  1.0d-8
 /
ATOMIC_SPECIES
 Ag 107.8682 Ag.pz-mt_fhi.UPF
 Ga 69.723 Ga.pz-mt_fhi.UPF
 Se 78.96 Se.pz-mt_fhi.UPF
```

```
ATOMIC_POSITIONS

 Ag 0.00 0.00 0.00
 Ag 0.00 0.50 0.50
 Ga 0.50 0.50 0.00
 Ga 0.50 0.00 0.25
 Se 0.301 0.25 0.125
 Se 0.301 0.75 0.125
 Se 0.75 0.301 0.875
 Se 0.25 0.301 0.875

K_POINTS
  10
   0.1250000  0.1250000  0.1250000   1.00
   0.1250000  0.1250000  0.3750000   3.00
   0.1250000  0.1250000  0.6250000   3.00
   0.1250000  0.1250000  0.8750000   3.00
   0.1250000  0.3750000  0.3750000   3.00
   0.1250000  0.3750000  0.6250000   6.00
   0.1250000  0.3750000  0.8750000   6.00
   0.1250000  0.6250000  0.6250000   3.00
   0.3750000  0.3750000  0.3750000   1.00
   0.3750000  0.3750000  0.6250000   3.00
```

AgGaS2.band.david.in

```
 &control
    calculation='bands'
    pseudo_dir = '/home/dennis/pseudo/',
    outdir='/home/dennis/silungweldau/tmp1/',
    prefix='aggas2'
 /
 &system
    ibrav=  7, celldm(1) = 10.847, celldm(3)=1.78, nat=  8, ntyp= 3,
    ecutwfc =50.0, ecutrho = 360,nbnd=40,
    starting_magnetization(1)= 0.0,
    !occupations='smearing',
    !smearing='fd',
    !degauss=0.01,
    nspin=1,
    lda_plus_u=.true.,
    Hubbard_U(1)=5.0,
    Hubbard_alpha(1)=-0.08
 /
```

```
 &electrons
    diagonalization='david'
     mixing_mode = 'plain'
    mixing_beta = 0.7
    conv_thr =  1.0d-8

 /
ATOMIC_SPECIES
 Ag 107.8682 Ag.pz-mt_fhi.UPF
 Ga  69.723  Ga.pz-mt_fhi.UPF
 S   32.065   S.pz-mt_fhi.UPF

ATOMIC_POSITIONS
 Ag 0.00 0.00 0.00
 Ag 0.00 0.50 0.50
 Ga 0.50 0.50 0.00
 Ga 0.50 0.00 0.25
 S 0.309 0.25 0.125
 S 0.309 0.75 0.125
 S 0.75 0.309 0.875
 S 0.25 0.309 0.875

K_POINTS
 36
   0.0 0.0 0.0 1.0
   0.1 0.1 0.1 1.0
   0.2 0.2 0.2 1.0
   0.3 0.3 0.3 1.0
   0.4 0.4 0.4 1.0
   0.5 0.5 0.5 1.0
   0.4 0.4 0.4 1.0
   0.3 0.3 0.3 1.0
   0.2 0.2 0.2 1.0
   0.1 0.1 0.1 1.0
   0.0 0.0 0.0 1.0
   0.0 0.1 0.0 1.0
   0.0 0.2 0.0 1.0
   0.0 0.3 0.0 1.0
   0.0 0.4 0.0 1.0
   0.0 0.5 0.0 1.0
   0.0 0.6 0.0 1.0
   0.0 0.7 0.0 1.0
   0.0 0.8 0.0 1.0
   0.0 0.9 0.0 1.0
   0.0 1.0 0.0 1.0
   0.1 1.0 0.0 1.0
```

```
  0.2 1.0 0.0 1.0
  0.3 1.0 0.0 1.0
  0.4 1.0 0.0 1.0
  0.5 1.0 0.0 1.0
  0.55 0.95 0.0 1.0
  0.60 0.90 0.0 1.0
  0.65 0.85 0.0 1.0
  0.70 0.80 0.0 1.0
  0.75 0.75 0.0 1.0
  0.60 0.60 0.0 1.0
  0.45 0.45 0.0 1.0
  0.30 0.30 0.0 1.0
  0.15 0.15 0.0 1.0
  0.0 0.0 0.0 1.0
```

AgGaS2.bands.in

```
 &inputpp
    prefix='aggas2',
    outdir='/home/dennis/silungweldau/tmp1/'
    filband='aggas2.band'
    lsym=.true.,
/
```

AgGaS2.pdos.in

```
&inputpp
    outdir='/home/dennis/silungweldau/tmp1/'
    prefix='aggas2'
    Emin=-17.0, Emax=15.0, DeltaE=0.2
 /
```

AgGaS2.scf.david.in

```
 &control
    calculation = 'scf'
    restart_mode='from_scratch',
    prefix='aggas2',
    tstress = .true.
    tprnfor = .true.
    pseudo_dir = '/home/dennis/pseudo/',
    outdir='/home/dennis/silungweldau/tmp1/'
 /
```

```
 &system
    ibrav=  7, celldm(1) =12.2, celldm(3)=1.78, nat=  8, ntyp= 3,
    ecutwfc =50.0,ecutrho = 360,nbnd=40,
    starting_magnetization(1)= 0.0,
    !occupations='smearing',
    !smearing='gauss',
    !degauss=0.01,
    nspin=1,
    lda_plus_u=.true.,
    Hubbard_U(1)=5.0,
    Hubbard_alpha(1)=-0.08
 /
 &electrons
    diagonalization='david'
    mixing_mode = 'plain'
    mixing_beta = 0.7
    conv_thr =  1.0d-8
 /
ATOMIC_SPECIES
 Ag 107.8682 Ag.pz-mt_fhi.UPF
 Ga 69.723 Ga.pz-mt_fhi.UPF
 S  32.065 S.pz-mt_fhi.UPF

ATOMIC_POSITIONS
 Ag 0.00 0.00 0.00
 Ag 0.00 0.50 0.50
 Ga 0.50 0.50 0.00
 Ga 0.50 0.00 0.25
 S 0.309 0.25 0.125
 S 0.309 0.75 0.125
 S 0.75 0.309 0.875
 S 0.25 0.309 0.875


K_POINTS
  10
   0.1250000  0.1250000  0.1250000   1.00
   0.1250000  0.1250000  0.3750000   3.00
   0.1250000  0.1250000  0.6250000   3.00
   0.1250000  0.1250000  0.8750000   3.00
   0.1250000  0.3750000  0.3750000   3.00
   0.1250000  0.3750000  0.6250000   6.00
   0.1250000  0.3750000  0.8750000   6.00
   0.1250000  0.6250000  0.6250000   3.00
   0.3750000  0.3750000  0.3750000   1.00
   0.3750000  0.3750000  0.6250000   3.00
```

AgGaTe2.band.david.in

```
&control
   calculation='bands'
   pseudo_dir = '/home/dennis/pseudo/',
   outdir='/home/dennis/silungweldau/tmp1/',
   prefix='aggate2'
/

 &system
   ibrav=  7, celldm(1) = 11.867, celldm(3)=1.895, nat=  8, ntyp= 3,
   ecutwfc =50.0, nbnd = 30,
   starting_magnetization(1)= 0.0,
   occupations='smearing',
   smearing='gauss',
   degauss=0.01,
   nspin=1,
   lda_plus_u=.true.,
   Hubbard_U(1)=5.2,
   Hubbard_alpha(1)=0

 /
 &electrons
   diagonalization='david'
   mixing_mode = 'plain'
   mixing_beta = 0.7
   conv_thr =  1.0d-8
 /

ATOMIC_SPECIES
 Ag 107.8682 Ag.pz-mt_fhi.UPF
 Ga 69.723 Ga.pz-mt_fhi.UPF
 Te 127.60 Te.pz-mt_fhi.UPF

ATOMIC_POSITIONS
 Ag 0.00 0.00 0.00
 Ag 0.00 0.50 0.50
 Ga 0.50 0.50 0.00
 Ga 0.50 0.00 0.25
 Te 0.277 0.25 0.125
 Te 0.277 0.75 0.125
 Te 0.75 0.277 0.875
 Te 0.25 0.277 0.875
```

```
K_POINTS
 36
   0.0 0.0 0.0 1.0
   0.1 0.1 0.1 1.0
   0.2 0.2 0.2 1.0
   0.3 0.3 0.3 1.0
   0.4 0.4 0.4 1.0
   0.5 0.5 0.5 1.0
   0.4 0.4 0.4 1.0
   0.3 0.3 0.3 1.0
   0.2 0.2 0.2 1.0
   0.1 0.1 0.1 1.0
   0.0 0.0 0.0 1.0
   0.0 0.1 0.0 1.0
   0.0 0.2 0.0 1.0
   0.0 0.3 0.0 1.0
   0.0 0.4 0.0 1.0
   0.0 0.5 0.0 1.0
   0.0 0.6 0.0 1.0
   0.0 0.7 0.0 1.0
   0.0 0.8 0.0 1.0
   0.0 0.9 0.0 1.0
   0.0 1.0 0.0 1.0
   0.1 1.0 0.0 1.0
   0.2 1.0 0.0 1.0
   0.3 1.0 0.0 1.0
   0.4 1.0 0.0 1.0
   0.5 1.0 0.0 1.0
   0.55 0.95 0.0 1.0
   0.60 0.90 0.0 1.0
   0.65 0.85 0.0 1.0
   0.70 0.80 0.0 1.0
   0.75 0.75 0.0 1.0
   0.60 0.60 0.0 1.0
   0.45 0.45 0.0 1.0
   0.30 0.30 0.0 1.0
   0.15 0.15 0.0 1.0
   0.0 0.0 0.0 1.0
```

AgGaTe2.bands.in

```
 &inputpp
    prefix='aggate2',
    outdir='/home/dennis/silungweldau/tmp1/'
    filband='aggate2.band'
    lsym=.true., /
```

AgGaTe2.pdos.in

```
&inputpp
   outdir='/home/dennis/silungweldau/tmp1/'
   prefix='aggate2'
   Emin=-17.0, Emax=9.0, DeltaE=0.2 /
```

AgGaTe2.scf.david.in

```
&control
   calculation = 'scf'
   restart_mode='from_scratch',
   prefix='aggate2',
   tstress = .true.
   tprnfor = .true.
   pseudo_dir = '/home/dennis/pseudo/',
   outdir='/home/dennis/silungweldau/tmp1/'
/
&system
   ibrav=  7, celldm(1) =12.2, celldm(3)=1.895, nat=  8, ntyp= 3,
   ecutwfc =50.0,nbnd=30,
   starting_magnetization(1)= 0.0,
   occupations='smearing',
   smearing='gauss',
   degauss=0.01,
   nspin=1,
   lda_plus_u=.true.,
   Hubbard_U(1)=5.2,
   Hubbard_alpha(1)=0
/
&electrons
   diagonalization='david'
   mixing_mode = 'plain'
   mixing_beta = 0.7
   conv_thr =  1.0d-8
/

ATOMIC_SPECIES
 Ag 107.8682 Ag.pz-mt_fhi.UPF
 Ga 69.723 Ga.pz-mt_fhi.UPF
 Te 127.60 Te.pz-mt_fhi.UPF

ATOMIC_POSITIONS
 Ag 0.00 0.00 0.00
 Ag 0.00 0.50 0.50
 Ga 0.50 0.50 0.00
 Ga 0.50 0.00 0.25
```

```
Te 0.277 0.25 0.125
Te 0.277 0.75 0.125
Te 0.75 0.277 0.875
Te 0.25 0.277 0.875


K_POINTS
 10
  0.1250000  0.1250000  0.1250000   1.00
  0.1250000  0.1250000  0.3750000   3.00
  0.1250000  0.1250000  0.6250000   3.00
  0.1250000  0.1250000  0.8750000   3.00
  0.1250000  0.3750000  0.3750000   3.00
  0.1250000  0.3750000  0.6250000   6.00
  0.1250000  0.3750000  0.8750000   6.00
  0.1250000  0.6250000  0.6250000   3.00
  0.3750000  0.3750000  0.3750000   1.00
  0.3750000  0.3750000  0.6250000   3.00
```

CuGaS2.bands.david.in

```
 &control
    calculation='bands'
    pseudo_dir = '/home/dennis/pseudo/',
    outdir='/home/dennis/silungweldau/tmp2/',
    prefix='cugas2'
 /

 &system
    ibrav=  7, celldm(1) = 10.121, celldm(3)=2.064, nat=  8, ntyp= 3,
    ecutwfc =50.0, ecutrho = 300, nbnd=30,
    starting_magnetization(1)=0.0
    !occupations='smearing',
    !smearing='gauss', !degauss=0.02
    lda_plus_u=.true.,
    Hubbard_U(1)=4.6,
    Hubbard_alpha(1)=0,
    nspin=1,
 /

 &electrons
    diagonalization='david'
    mixing_mode = 'plain'
    mixing_beta = 0.7
    conv_thr =  1.0d-8
```

```
 /
ATOMIC_SPECIES
 Cu 63.546 Cu.pz-mt_fhi.UPF
 Ga 69.723 Ga.pz-mt_fhi.UPF
 S 32.065  S.pz-mt_fhi.UPF


ATOMIC_POSITIONS
 Cu 0.00 0.00 0.00
 Cu 0.00 0.50 0.50
 Ga 0.50 0.50 0.00
 Ga 0.50 0.00 0.25
 S 0.262 0.25 0.125
 S 0.262 0.75 0.125
 S 0.75 0.262 0.875
 S 0.25 0.262 0.875

K_POINTS
 36
   0.0 0.0 0.0 1.0
   0.1 0.1 0.1 1.0
   0.2 0.2 0.2 1.0
   0.3 0.3 0.3 1.0
   0.4 0.4 0.4 1.0
   0.5 0.5 0.5 1.0
   0.4 0.4 0.4 1.0
   0.3 0.3 0.3 1.0
   0.2 0.2 0.2 1.0
   0.1 0.1 0.1 1.0
   0.0 0.0 0.0 1.0
   0.0 0.1 0.0 1.0
   0.0 0.2 0.0 1.0
   0.0 0.3 0.0 1.0
   0.0 0.4 0.0 1.0
   0.0 0.5 0.0 1.0
   0.0 0.6 0.0 1.0
   0.0 0.7 0.0 1.0
   0.0 0.8 0.0 1.0
   0.0 0.9 0.0 1.0
   0.0 1.0 0.0 1.0
   0.1 1.0 0.0 1.0
   0.2 1.0 0.0 1.0
   0.3 1.0 0.0 1.0
   0.4 1.0 0.0 1.0
   0.5 1.0 0.0 1.0
   0.55 0.95 0.0 1.0
```

```
  0.60 0.90 0.0 1.0
  0.65 0.85 0.0 1.0
  0.70 0.80 0.0 1.0
  0.75 0.75 0.0 1.0
  0.60 0.60 0.0 1.0
  0.45 0.45 0.0 1.0
  0.30 0.30 0.0 1.0
  0.15 0.15 0.0 1.0
  0.0 0.0 0.0 1.0
```

CuGaS2.bands.in

```
 &inputpp
    prefix='cugas2',
    outdir='/home/dennis/silungweldau/tmp2/'
    filband='cugas2.band'
    lsym=.true.,
 /
```

CuGaS2.pdos.in

```
&inputpp
    outdir='/home/dennis/silungweldau/tmp2/'
    prefix='cugas2'
    Emin=-18.0, Emax=10.0, DeltaE=0.1
 /
```

CuGaS2.scf.david.in

```
 &control
    calculation = 'scf'
    restart_mode='from_scratch',
    prefix='cugas2',
    tstress = .true.
    tprnfor = .true.
    pseudo_dir = '/home/dennis/pseudo/',
    outdir='/home/dennis/silungweldau/tmp2/'
 /
```

```
 &system
    ibrav=  7, celldm(1) =10.121, celldm(3)=1.953, nat=  8, ntyp= 3,
    ecutwfc =50.0,ecutrho = 300.0, nbnd=30,
    starting_magnetization(1)=0.0
    !occupations='smearing',
    !smearing='gauss',
    !degauss=0.02
    lda_plus_u=.true.,
    Hubbard_U(1)=4.6,
    Hubbard_alpha(1)=0,
    nspin=1,
 /

 &electrons
    diagonalization='david'
    mixing_mode = 'plain'
    mixing_beta = 0.7
    conv_thr =  1.0d-8
 /

ATOMIC_SPECIES
 Cu 63.546 Cu.pz-mt_fhi.UPF
 Ga 69.723 Ga.pz-mt_fhi.UPF
 S 32.065  S.pz-mt_fhi.UPF
ATOMIC_POSITIONS
 Cu 0.00 0.00 0.00
 Cu 0.00 0.50 0.50
 Ga 0.50 0.50 0.00
 Ga 0.50 0.00 0.25
 S 0.262 0.25 0.125
 S 0.262 0.75 0.125
 S 0.75 0.262 0.875
 S 0.25 0.262 0.875

K_POINTS
  10
   0.1250000  0.1250000  0.1250000   1.00
   0.1250000  0.1250000  0.3750000   3.00
   0.1250000  0.1250000  0.6250000   3.00
   0.1250000  0.1250000  0.8750000   3.00
   0.1250000  0.3750000  0.3750000   3.00
   0.1250000  0.3750000  0.6250000   6.00
   0.1250000  0.3750000  0.8750000   6.00
   0.1250000  0.6250000  0.6250000   3.00
   0.3750000  0.3750000  0.3750000   1.00
   0.3750000  0.3750000  0.6250000   3.00
```

CuInSeu2.band.david.in

```
 &control
    calculation='bands'
    pseudo_dir = '/home/ubuntu/pseudo/',
    outdir='/home/ubuntu/silungwelda/tmp1/'
    prefix='cuinseu2'
 /

 &system
    ibrav=  7, celldm(1) = 10.375, celldm(3)=2.064, nat=  8, ntyp= 3,
    ecutwfc =50.0,ecutrho = 360,nbnd=30,
    starting_magnetization(1)= 0.0,

    !occupations='smearing',
    ! smearing='gauss',
    !degauss=0.01,
    nspin=1,
    lda_plus_u=.true.,
    Hubbard_U(1)=6.3,
    Hubbard_alpha(1)=0
 /

 &electrons
    diagonalization='david'
    mixing_mode = 'plain'
    mixing_beta = 0.7
    conv_thr =  1.0d-8
 /

ATOMIC_SPECIES
  Cu 63.546 Cu.pz-mt_fhi.UPF
 In 114.818 In.pz-mt_fhi.UPF
 Se 78.96 Se.pz-mt_fhi.UPF

ATOMIC_POSITIONS
 Cu 0.00 0.00 0.00
 Cu 0.00 0.50 0.50
 In 0.50 0.50 0.00
 In 0.50 0.00 0.25
 Se 0.23 0.25 0.125
 Se 0.23 0.75 0.125
 Se 0.75 0.23 0.875
 Se 0.25 0.23 0.875
```

```
K_POINTS
36
  0.0 0.0 0.0 1.0
  0.1 0.1 0.1 1.0
  0.2 0.2 0.2 1.0
  0.3 0.3 0.3 1.0
  0.4 0.4 0.4 1.0
  0.5 0.5 0.5 1.0
  0.4 0.4 0.4 1.0
  0.3 0.3 0.3 1.0
  0.2 0.2 0.2 1.0
  0.1 0.1 0.1 1.0
  0.0 0.0 0.0 1.0
  0.0 0.1 0.0 1.0
  0.0 0.2 0.0 1.0
  0.0 0.3 0.0 1.0
  0.0 0.4 0.0 1.0
  0.0 0.5 0.0 1.0
  0.0 0.6 0.0 1.0
  0.0 0.7 0.0 1.0
  0.0 0.8 0.0 1.0
  0.0 0.9 0.0 1.0
  0.0 1.0 0.0 1.0
  0.1 1.0 0.0 1.0
  0.2 1.0 0.0 1.0
  0.3 1.0 0.0 1.0
  0.4 1.0 0.0 1.0
  0.5 1.0 0.0 1.0
  0.55 0.95 0.0 1.0
  0.60 0.90 0.0 1.0
  0.65 0.85 0.0 1.0
  0.70 0.80 0.0 1.0
  0.75 0.75 0.0 1.0
  0.60 0.60 0.0 1.0
  0.45 0.45 0.0 1.0
  0.30 0.30 0.0 1.0
  0.15 0.15 0.0 1.0
  0.0 0.0 0.0 1.0
```

CuInSeu2.bands.in

```
 &inputpp
    prefix='cuinseu2',
    outdir='/home/ubuntu/silungwelda/tmp1/'
    filband='cuinseu2.band'
    lsym=.true., /
```

CuInSeu.pdos.in

```
 &inputpp
    outdir='/home/ubuntu/silungwelda/tmp1/'
    prefix='cuinseu2'
    Emin=-17, Emax=11.0, DeltaE=0.2
 /
```

CuInSeu2.scf.david.in

```
&control
    calculation = 'scf'
    restart_mode='from_scratch',
    prefix='cuinseu2',
    tstress = .true.
    tprnfor = .true.
   pseudo_dir = '/home/ubuntu/pseudo/',
    outdir='/home/ubuntu/silungwelda/tmp1/'
/

 &system
    ibrav=  7, celldm(1) =10.375, celldm(3)=2.064, nat=8, ntyp= 3,
    ecutwfc =50.0,ecutrho = 500.0,nbnd=30,
    starting_magnetization(1)= 0.0,
    !occupations='smearing',
    ! smearing='gauss',
    !degauss=0.01,
    nspin=1,
    lda_plus_u=.true.,
    Hubbard_U(1)=6.3,
    Hubbard_alpha(1)=0
     /

 &electrons
     diagonalization='david'
    mixing_mode = 'plain'
    mixing_beta = 0.7
    conv_thr =  1.0d-8

 /
ATOMIC_SPECIES
 Cu 63.546 Cu.pz-mt_fhi.UPF
 In 114.818 In.pz-mt_fhi.UPF
 Se 78.96 Se.pz-mt_fhi.UPF
```

```
ATOMIC_POSITIONS
 Cu 0.00 0.00 0.00
 Cu 0.00 0.50 0.50
 In 0.50 0.50 0.00
 In 0.50 0.00 0.25
 Se 0.234 0.25 0.125
 Se 0.234 0.75 0.125
 Se 0.75 0.234 0.875
 Se 0.25 0.234 0.875

K_POINTS
10
  0.1250000  0.1250000  0.1250000   1.00
  0.1250000  0.1250000  0.3750000   3.00
  0.1250000  0.1250000  0.6250000   3.00
  0.1250000  0.1250000  0.8750000   3.00
  0.1250000  0.3750000  0.3750000   3.00
  0.1250000  0.3750000  0.6250000   6.00
  0.1250000  0.3750000  0.8750000   6.00
  0.1250000  0.6250000  0.6250000   3.00
  0.3750000  0.3750000  0.3750000   1.00
  0.3750000  0.3750000  0.6250000   3.00
```

CuInS2.band.david.in

```
 &control
    calculation='bands'
    pseudo_dir = '/home/dennis/pseudo/',
    outdir='/home/dennis/silungweldau/tmp1/',
    prefix='cuins2'
 /

 &system
    ibrav=  7, celldm(1) = 10.433, celldm(3)=2.064, nat=  8, ntyp= 3,
    ecutwfc =50.0,  ecutrho = 360,nbnd=40,
    starting_magnetization(1)= 0.0,
    !occupations='smearing',
    !smearing='fd', !degauss=0.01,
    !nspin=1,
    !lda_plus_u=.true.,
    !Hubbard_U(1)=4.6,
    !Hubbard_alpha(1)=0
 /
```

```
 &electrons
    diagonalization='david'
    mixing_mode = 'plain'
    mixing_beta = 0.7
    conv_thr =  1.0d-8
 /

ATOMIC_SPECIES
 Cu 63.546 Cu.pz-dn-rrkjus_psl.0.2.UPF
 In 114.818 In.pz-dn-rrkjus_psl.0.2.2.UPF
 Se 78.96 Se.pz-n-rrkjus_psl.0.2.UPF



ATOMIC_POSITIONS
 Cu 0.00 0.00 0.00
 Cu 0.00 0.50 0.50
 In 0.50 0.50 0.00
 In 0.50 0.00 0.25
 Se 0.23 0.25 0.125
 Se 0.23 0.75 0.125
 Se 0.75 0.23 0.875
 Se 0.25 0.23 0.875


K_POINTS
 36
   0.0 0.0 0.0 1.0
   0.1 0.1 0.1 1.0
   0.2 0.2 0.2 1.0
   0.3 0.3 0.3 1.0
   0.4 0.4 0.4 1.0
   0.5 0.5 0.5 1.0
   0.4 0.4 0.4 1.0
   0.3 0.3 0.3 1.0
   0.2 0.2 0.2 1.0
   0.1 0.1 0.1 1.0
   0.0 0.0 0.0 1.0
   0.0 0.1 0.0 1.0
   0.0 0.2 0.0 1.0
   0.0 0.3 0.0 1.0
   0.0 0.4 0.0 1.0
   0.0 0.5 0.0 1.0
   0.0 0.6 0.0 1.0
   0.0 0.7 0.0 1.0
   0.0 0.8 0.0 1.0
```

0.0 0.9 0.0 1.0
0.0 1.0 0.0 1.0
0.1 1.0 0.0 1.0
0.2 1.0 0.0 1.0
0.3 1.0 0.0 1.0
0.4 1.0 0.0 1.0
0.5 1.0 0.0 1.0
0.55 0.95 0.0 1.0
0.60 0.90 0.0 1.0
0.65 0.85 0.0 1.0
0.70 0.80 0.0 1.0
0.75 0.75 0.0 1.0
0.60 0.60 0.0 1.0
0.45 0.45 0.0 1.0
0.30 0.30 0.0 1.0
0.15 0.15 0.0 1.0
0.0 0.0 0.0 1.0

CuInS2.bands.in

```
 &inputpp
    prefix='cuins2',
    outdir='/home/dennis/silungweldau/tmp1/'
    filband='cuins2.band'
    lsym=.true.,
 /
```

CuInS2.pdos.in

```
 &inputpp
    outdir='/home/dennis/silungweldau/tmp1/'
    prefix='cuins2'
    Emin=-16.0,
    Emax=11.0,
    DeltaE=0.2
 /
```

CuInS2.scf.david.in

```
 &control
    calculation = 'scf'
    restart_mode='from_scratch',
    prefix='cuins2',
    tstress = .true.
    tprnfor = .true.
    pseudo_dir = '/home/dennis/pseudo/',
    outdir='/home/dennis/silungweldau/tmp1/'
```

```
/
 &system
   ibrav=  7, celldm(1) =10.433, celldm(3)=2.014, nat=  8, ntyp= 3,
   ecutwfc =50.0,ecutrho = 360,nbnd=40,
   starting_magnetization(1)= 0.0,
   !occupations='smearing',
   !smearing='fd',
   !degauss=0.01,
   !nspin=1,
   !lda_plus_u=.true.,
   !Hubbard_U(1)=4.6,
   !Hubbard_alpha(1)=0
 /
 &electrons
   diagonalization='david'
   mixing_mode = 'plain'
   mixing_beta = 0.7
   conv_thr =  1.0d-8
 /

ATOMIC_SPECIES
 Cu 63.546 Cu.pz-dn-rrkjus_psl.0.2.UPF
 In 114.818 In.pz-dn-rrkjus_psl.0.2.2.UPF
 S 32.065  S.pz-n-rrkjus_psl.0.1.UPF

ATOMIC_POSITIONS
 Cu 0.00 0.00 0.00
 Cu 0.00 0.50 0.50
 In 0.50 0.50 0.00
 In 0.50 0.00 0.25
 S 0.246 0.25 0.125
 S 0.246 0.75 0.125
 S 0.75 0.246 0.875
 S 0.25 0.246 0.875


K_POINTS
  10
   0.1250000  0.1250000  0.1250000   1.00
   0.1250000  0.1250000  0.3750000   3.00
   0.1250000  0.1250000  0.6250000   3.00
   0.1250000  0.1250000  0.8750000   3.00
   0.1250000  0.3750000  0.3750000   3.00
   0.1250000  0.3750000  0.6250000   6.00
   0.1250000  0.3750000  0.8750000   6.00
   0.1250000  0.6250000  0.6250000   3.00
```

```
  0.3750000  0.3750000  0.3750000   1.00
  0.3750000  0.3750000  0.6250000   3.00
```

ZnSiAs2.band.david.in

```
&control
   calculation='bands'
   pseudo_dir = '/home/dennis/pseudo/',
   outdir='/home/dennis/silungweldau/tmp1/',
   prefix='znsias2'
 /

 &system
   ibrav=  7, celldm(1) = 10.594, celldm(3)=1.943, nat=  8, ntyp= 3,
   ecutwfc =50.0, ecutrho = 360.0, nbnd=30,
   starting_magnetization(1)=0.0
   !occupations='smearing',
   !smearing='gauss',
   !degauss=0.02
   lda_plus_u=.true.,
   Hubbard_U(1)=4.0,
   Hubbard_alpha(1)=0,
   nspin=1,
 /

 &electrons
   diagonalization='david'
    mixing_mode = 'plain'
   mixing_beta = 0.7
   conv_thr =  1.0d-8
 /

ATOMIC_SPECIES
 Zn 65.38 Zn.pz-mt_fhi.UPF
 Si 28.0855 Si.pz-mt_fhi.UPF
 As 74.92160 As.pz-mt_fhi.UPF
ATOMIC_POSITIONS
 Zn 0.00 0.00 0.00
 Zn 0.00 0.50 0.50
 Si 0.50 0.50 0.00
 Si 0.50 0.00 0.25
 As 0.265 0.25 0.125
 As 0.265 0.75 0.125
 As 0.75 0.265 0.875
 As 0.25 0.265 0.875
```

```
K_POINTS
 36
   0.0 0.0 0.0 1.0
   0.1 0.1 0.1 1.0
   0.2 0.2 0.2 1.0
   0.3 0.3 0.3 1.0
   0.4 0.4 0.4 1.0
   0.5 0.5 0.5 1.0
   0.4 0.4 0.4 1.0
   0.3 0.3 0.3 1.0
   0.2 0.2 0.2 1.0
   0.1 0.1 0.1 1.0
   0.0 0.0 0.0 1.0
   0.0 0.1 0.0 1.0
   0.0 0.2 0.0 1.0
   0.0 0.3 0.0 1.0
   0.0 0.4 0.0 1.0
   0.0 0.5 0.0 1.0
   0.0 0.6 0.0 1.0
   0.0 0.7 0.0 1.0
   0.0 0.8 0.0 1.0
   0.0 0.9 0.0 1.0
   0.0 1.0 0.0 1.0
   0.1 1.0 0.0 1.0
   0.2 1.0 0.0 1.0
   0.3 1.0 0.0 1.0
   0.4 1.0 0.0 1.0
   0.5 1.0 0.0 1.0
   0.55 0.95 0.0 1.0
   0.60 0.90 0.0 1.0
   0.65 0.85 0.0 1.0
   0.70 0.80 0.0 1.0
   0.75 0.75 0.0 1.0
   0.60 0.60 0.0 1.0
   0.45 0.45 0.0 1.0
   0.30 0.30 0.0 1.0
   0.15 0.15 0.0 1.0
   0.0 0.0 0.0 1.0
```

ZnSiAs2.bands.in

```
 prefix='znsias2',
    outdir='/home/dennis/silungweldau/tmp1/'
    filband='znsias2.band'
    lsym=.true.,
```

```
/
```

ZnSiAs2.pdos.in

```
&inputpp
   outdir='/home/dennis/silungweldau/tmp1/'
   prefix='znsias2'
   Emin=-15.0, Emax=10.0, DeltaE=0.2
/
```

ZnSiAs2.scf.david.in

```
&control
   calculation = 'scf'
   restart_mode='from_scratch',
   prefix='znsias2',
   tstress = .true.
   tprnfor = .true.
   pseudo_dir = '/home/dennis/pseudo/',
   outdir='/home/dennis/silungweldau/tmp1/'
/

 &system
   ibrav=  7, celldm(1) =10.594, celldm(3)=1.943, nat=  8, ntyp= 3,
   ecutwfc =50.0,ecutrho = 360.0, nbnd=30,
   starting_magnetization(1)=0.0
   !occupations='smearing',
   !smearing='gauss',
   !degauss=0.02
   lda_plus_u=.true.,
   Hubbard_U(1)=4.0,
   Hubbard_alpha(1)=0,
   nspin=1,
/

 &electrons
   diagonalization='david'
   mixing_mode = 'plain'
   mixing_beta = 0.7
   conv_thr =  1.0d-8
/


ATOMIC_SPECIES
 Zn 65.38 Zn.pz-mt_fhi.UPF
```

```
 Si 28.0855 Si.pz-mt_fhi.UPF
 As 74.92160 As.pz-mt_fhi.UPF

ATOMIC_POSITIONS
 Zn 0.00 0.00 0.00
 Zn 0.00 0.50 0.50
 Si 0.50 0.50 0.00
 Si 0.50 0.00 0.25
 As 0.265 0.25 0.125
 As 0.265 0.75 0.125
 As 0.75 0.265 0.875
 As 0.25 0.265 0.875

K_POINTS
  10
   0.1250000  0.1250000  0.1250000   1.00
   0.1250000  0.1250000  0.3750000   3.00
   0.1250000  0.1250000  0.6250000   3.00
   0.1250000  0.1250000  0.8750000   3.00
   0.1250000  0.3750000  0.3750000   3.00
   0.1250000  0.3750000  0.6250000   6.00
   0.1250000  0.3750000  0.8750000   6.00
   0.1250000  0.6250000  0.6250000   3.00
   0.3750000  0.3750000  0.3750000   1.00
   0.3750000  0.3750000  0.6250000   3.00
```

ZnSnAs.band.david.in

```
 &control
    calculation='bands'
    pseudo_dir = '/home/dennis/pseudo/',
    outdir='/home/dennis/silungwelda/tmp2/',
    prefix='znsnas'
 /

 &system
    ibrav=  7, celldm(1) = 11.059, celldm(3)=2.00, nat=  8, ntyp= 3,
    ecutwfc =50.0, ecutrho = 360.0, nbnd=30,
    starting_magnetization(1)=0.0
    occupations='smearing', smearing='gauss', degauss=0.02
    lda_plus_u=.true., Hubbard_U(1)=4.6, Hubbard_alpha(1)=0,
    nspin=1,
 /

 &electrons
    diagonalization='david'
```

```
   mixing_mode = 'plain'
   mixing_beta = 0.7
   conv_thr =  1.0d-8
 /
ATOMIC_SPECIES
 Zn 65.38 Zn.pz-mt_fhi.UPF
 Sn 118.710 Sn.pz-mt_fhi.UPF
 As 74.92160 As.pz-mt_fhi.UPF

ATOMIC_POSITIONS
 Zn 0.00 0.00 0.00
 Zn 0.00 0.50 0.50
 Sn 0.50 0.50 0.00
 Sn 0.50 0.00 0.25
 As 0.250 0.25 0.125
 As 0.250 0.75 0.125
 As 0.75 0.250 0.875
 As 0.25 0.250 0.875

K_POINTS
 36
   0.0 0.0 0.0 1.0
   0.1 0.1 0.1 1.0
   0.2 0.2 0.2 1.0
   0.3 0.3 0.3 1.0
   0.4 0.4 0.4 1.0
   0.5 0.5 0.5 1.0
   0.4 0.4 0.4 1.0
   0.3 0.3 0.3 1.0
   0.2 0.2 0.2 1.0
   0.1 0.1 0.1 1.0
   0.0 0.0 0.0 1.0
   0.0 0.1 0.0 1.0
   0.0 0.2 0.0 1.0
   0.0 0.3 0.0 1.0
   0.0 0.4 0.0 1.0
   0.0 0.5 0.0 1.0
   0.0 0.6 0.0 1.0
   0.0 0.7 0.0 1.0
   0.0 0.8 0.0 1.0
   0.0 0.9 0.0 1.0
   0.0 1.0 0.0 1.0
   0.1 1.0 0.0 1.0
   0.2 1.0 0.0 1.0
   0.3 1.0 0.0 1.0
   0.4 1.0 0.0 1.0
```

```
  0.5 1.0 0.0 1.0
  0.55 0.95 0.0 1.0
  0.60 0.90 0.0 1.0
  0.65 0.85 0.0 1.0
  0.70 0.80 0.0 1.0
  0.75 0.75 0.0 1.0
  0.60 0.60 0.0 1.0
  0.45 0.45 0.0 1.0
  0.30 0.30 0.0 1.0
  0.15 0.15 0.0 1.0
  0.0 0.0 0.0 1.0
```

ZnSnAs.bands.in

```
 &inputpp
    prefix='znsnas',
    outdir='/home/dennis/silungwelda/tmp2/'
    filband='znsnas.band'
    lsym=.true.,
 /
```

ZnSnAs.pdos.in

```
 &inputpp
    outdir='/home/dennis/silungwelda/tmp2/'
    prefix='znsnas'
    Emin=-15.0, Emax=9.0, DeltaE=0.2
 /
```

ZnSnAs.scf.david.in

```
 &control
    calculation = 'scf'
    restart_mode='from_scratch',
    prefix='znsnas',
    tstress = .true.
    tprnfor = .true.
    pseudo_dir = '/home/dennis/pseudo/',
    outdir='/home/dennis/silungwelda/tmp2/'
 /

 &system
    ibrav=  7, celldm(1) =11.059, celldm(3)=2.00, nat=  8, ntyp= 3,
    ecutwfc =50.0,ecutrho = 360.0, nbnd=30,
    starting_magnetization(1)=0.0
    occupations='smearing', smearing='gauss', degauss=0.02
    lda_plus_u=.true., Hubbard_U(1)=4.6, Hubbard_alpha(1)=0,
    nspin=1,
```

```
/

 &electrons
    diagonalization='david'
    mixing_mode = 'plain'
    mixing_beta = 0.7
    conv_thr =  1.0d-8
/

ATOMIC_SPECIES
 Zn 65.38 Zn.pz-mt_fhi.UPF
 Sn 118.710 Sn.pz-mt_fhi.UPF
 As 74.92160 As.pz-mt_fhi.UPF

ATOMIC_POSITIONS
 Zn 0.00 0.00 0.00
 Zn 0.00 0.50 0.50
 Sn 0.50 0.50 0.00
 Sn 0.50 0.00 0.25
 As 0.250 0.25 0.125
 As 0.250 0.75 0.125
 As 0.75 0.250 0.875
 As 0.25 0.250 0.875

K_POINTS
  10
   0.1250000  0.1250000  0.1250000   1.00
   0.1250000  0.1250000  0.3750000   3.00
   0.1250000  0.1250000  0.6250000   3.00
   0.1250000  0.1250000  0.8750000   3.00
   0.1250000  0.3750000  0.3750000   3.00
   0.1250000  0.3750000  0.6250000   6.00
   0.1250000  0.3750000  0.8750000   6.00
   0.1250000  0.6250000  0.6250000   3.00
   0.3750000  0.3750000  0.3750000   1.00
   0.3750000  0.3750000  0.6250000   3.00
```

BIBLIOGRAPHY

[1] F. Chiker, B. Abbar, A. Tadjer, H. Aourag, B. Khelifa, Materials Science & Engineering B, 98 (2003) 81.

[2] J. L. Shay and J.H. Wernick, Ternary Chalcopyrite Semiconductors: Growth, Electronic Properties and Applications, Pergamon Press, Oxford, (Pergamon, New York) (1975).

[3] B. Panda, Structural and Electronic Properties of Chacopyrite Semiconductors, M.Sc. Dissertation, National Institute of Technology, Roukela (2012).

[4] I. Repins, M.A. Contreras, B. Egaas, C. DeHart, J. Scharf, C. L Perkins, B. To, R. Noufi, Progress in Photovoltaics: Research and applications 16 (3), 235.

[5] T. Dullweber, U. Rau, M. A. Contreas, R. Noufi,H.W.Schock, IEEET Electron Dev., 47(912)(2000) 2249.

[6] R. A. Mickelsen, W. S. Chen, 16th IEEE Photovoltaic Specialists' Conference Vol.781, 16th IEEE Photovoltaic Specialists' Conference, San Diego, CA (USA)(1982).

[7] H. Hahn. *et. al*, Z Anorg. Chem, 271(1953) 153.

[8] C. H. Goodman. *et. al*, Physica, 20(1954) 1107.

[9] F. Hopkins, Laser Focus World,31(1995) 87.

[10] N. Greenwood and A. Earnshaw, Chemistry of Elements 2nd Edn, Oxford: Butterworth-Heinmann(1997).

[11] H. Kyama and T. Iwata.Japan Patent Japanese Patent 08/095,209 (1996).

[12] O. Tanabe.USA Patent US patent 5,030545(1991).

[13] R. Yamamoto.Japan Patent Japanese patent 61/215,661(1986).

[14] J. Emsley, Nature's Building Blocks': An A-Z Guide to the Elements (New ED), New York: Oxford Press(2011).

[15] P. Hohernberg and W. Kohn, Phys. Rev., B136(1964) 864.

[16] W. Kohn and J. Sham, Phys. Rev., A140 (1965) 1133.

[17] W. Kohn and P Hohenberg, Phys Rev.,864B (1964) 136.

[18] Z. Yin, Microscopic mechanisms of Magnetism and SuperconductivityStudied From First Principle Calculations,University of california(2005).

[19] M. Cococcioni, S. de Gironcoli, Phys. Rev., B 71 (2005) 035105

[20] M. Cococcion,Rev. Mineral. Geochem, 147 (2010) 71.

[21] H. Kulik. *et al.*, Phys. Rev. Lett., 97 (2006) 103001.

[22] H. Hsu. *et. al.*, Physics of the Earth and Planetary Interiors,185 (2011) 13.

[23] MichealCo`te`, International School on Numerical methods for Correlated Systems in Condensed matter, Universite` de Montre`al (2008).

[24] C. Kittel, Introduction to Solid State Physics, 6th Ed, New York: Wiley (1986).

[25] J . Faist, Optical Properties of Semiconductors,Eidgenossiche Techniche Hoshshule Zurich (2008).

[26] J. E. Jaffe. *et a.l*, Phys Rev., B 29 (1984) 1882.

[27] A. Shaukat.*et al*., J. Phys. Chem. Solids, 39(1979)1269.

[28] J. L. Shay and I. H. Wernick, Ternary Chalcopyrite Semiconductors: Growth, Electronic Properties and Apllications, New York: Pergamon Press (1975).

[29] S. Mishra,Structural, Electronic and Optical Properties of Chalcopyrite Type Semiconductors,National Institute of Technology, Rourkela (2012).

[30] M. Suzuki. *et al.*, Jpn. J.Appl. Phys., 36 (1997) L1139.

[31] A. Kokalj, Comp. Mater. Sci., 28 (2003) [Online]. Available: http://www.xcrysden.org/.

[32] X. Jiang and W. R. Lambert, Phys Rev., B 69, 035201(2004) 1-6.

[33] Mackinnon, Tables of Numerical Data and Functional Relations in Science and Technology, New series, Group III, Vol.17,pt.h, Berlin: Springer (1985).

[34] M. L. Cohen, Phys. Rev., B3(1985) 7988.

[35] W. Kohn and ,Phys. Rev., 137, A1697 (1964) .

[36] P. Giannozzi, S. Baroni, N. Bonini, M. Calandra, R. Car, C. Cavazzoni, D. Ceresoli, G.I. Chiarotti, M. Cococcioni, I. Dabo, A. Dal Corso, S. de Gironcoli, S. Fabris, G. Fratesi, R. Gebauer, U. Gerstmann, C. Gougoussis, A. Kokalj, M. Lazzeri, I. Martin-Samos, N. Marzari, F. Mauri, R. Mazzarello, S. Paolini, A. Pasquarello, I. Paulatto, C. Sbraccia, S. Scandolo, G. Sclauzero, A.P. Seitsonen, A. Smogunov, P. Umari, R.M. Wentzcovitch, J. Phys.: Condens. Matter 21 (2009) 395502.

[37] A. K. Arora, T. Sakuntala, J. Phys. Chem. Solids, 54 (1993) 381.

[38] R. Asokamamani, R. M. Amirthakumari, R. Rita, C. Ravi, Phys. Stat. Sol (b) 213 (1999) 349

[39] T.Tinoco, A. Polian, D. Gomez, J. P Itie, Physica Status Solid, 198 (1996) 433

[40] M. Hopcroft.*et al.* , Jpournal of Microeletromechanical Systems 19 (2) (2010) 229

[41] S. Kobayashi, T. Ohno, N. Tsuboi, F. Kaneto and T. Maruyama, Jpn.J. Appl.Phys., 28 (1989) 189.

[42] J. Shay, B. Tell, H. Kasper and L. Schiavone, Phys, Rev. B, 5 (1972) 5003.

[43] B. Tell, J. Shay and H. Kasper, Phy. Rev. B, 9 (1974) 5203.

[44] H. H., N. Yamamoto and T. Miyauchi, Jpn. J. Appl. Phys., 17 (1978) 521.

[45] J. Shay, B. Tell, H. Kasper and L. Schiavone, Phys. Rev. B, 7 (1973) 4485.

[46] S. Dey. and V. K. Jain,Platinum Metals Rev., 48 no. 1(2004) 16.

[47] J.P. Perdew, K. Burke, M. Ernezerhof, Phys. Rev.,3865 (1996)77.

[48] J.P. Perdew, K. Burke, M. Ernezerhof, Phys. Rev.,1396 (1997) 78.

[49] H.P Garg and J Prakash, Solar Energy: Fundamentals and Applications, New Delhi, Tata McGraw-Hill (2000).

[50] R.W.G Wyckoff, Crystal Structures, Inter-Science Publishers, New York (1963)

[51] www.fisica.uniud.it/~giannozz/QE-Tutorial_io.pdf

[52] D Vanderbilt, Theory of Pseudopotentials, Bangalore Summer School, 2006

[53] AIMS Workshop on Electronic Structure Theory: Methods and Applications-July 2008

[54] A.Kavitha and M Dhana, Adv Mat. Lett. 255 (2012) **3**

[55] J.L Shay. *et al.*, Phy. Rev. Lett., 1162 (1972) **29**

[56] Robert Hull, Properties of Crystalline Silicon, Stevenage, IET (1999)

[57] Fukushima Accident, World Nuclear Association (2016)

[58] Allessandra Satta Hands-on Tutorial on Quantum Espresso Package, Cagliari, (2005)